TECHNICAL CONSIDERATIONS FOR CO-LOCATING UWB AND GPS RADIOS

by

TYLER H. VAN SLYKE

B.S., Kansas State University, 2006

A THESIS

submitted in partial fulfillment of the

requirements for the degree

MASTER OF SCIENCE

Department of Electrical and Computer Engineering

College of Engineering

KANSAS STATE UNIVERSITY
Manhattan, Kansas

2009

Approved by:

Co-Major Professor
William B. Kuhn

Approved by:

Co-Major Professor
Balasubramaniam Natarjan

ABSTRACT

Excitement about using ultra-wideband (UWB) technology for networking has grown considerably over the last few years. UWB has several strengths, including high data rates, security, and robustness in multipath environments. Despite these benefits, UWB has been scrutinized for its potential to interfere with narrowband technologies like the Global Positioning System (GPS). Until recently, much of the literature about UWB and GPS compatibility has been published on the basis of theoretical analysis alone.

We have investigated the compatibility of UWB and GPS signals using theoretical analysis as well as laboratory measurements with a consumer GPS receiver and a WiMedia UWB device. We conclude from our tests that the UWB device does emit interference in the GPS L1 band, but the interference is low enough that careful antenna and chipset placement could allow UWB and GPS radios to coexist in a single product.

Also, we have evaluated several UWB antennas to determine their fitness for use in a handheld electronic product. We find that the antennas' gain pattern and return loss do not have a significant effect upon the data throughput of the UWB system. Thus, we infer that the indoor environment is highly dispersive and that the UWB system is able to exploit multipath propagation.

Furthermore, we have created a link budget to estimate the distances over which a WiMedia UWB system should be capable of operating. In the lab, the maximum distances over which the UWB device actually operated were about half of what we expected. This suggests that the path loss exponent and standard deviation of fading could be higher than we expected or that the implementation loss of the UWB chipset is quite high.

Currently the market potential of UWB is uncertain. If UWB is embraced by the consumer electronics industry as the wireless platform of choice for Certified Wireless USB and high-speed Bluetooth technology, it could become a ubiquitous networking feature for electronic products such as phones, laptops, cameras, media players, and portable navigation devices. In this thesis, we strive to provide information that would be useful when undertaking a GPS and UWB radio integration project.

TABLE OF CONTENTS

LIST OF FIGURES

LIST OF TABLES

LIST OF ACRONYMS

AWGN ..... Additive White Gaussian Noise

BER ..... Bit Error Rate

BNC ..... Bayonet Neill-Concelman

BPAM ..... Binary Pulse Amplitude Modulation

BPSK ..... Binary Phase Shift Keying

C/A ..... Coarse Acquisition

CDF ..... Cumulative Distribution Function

CM ..... Channel Model

CNR ..... Carrier to Noise Ratio

CP ..... Cyclic Prefix

CW-USB ..... Certified Wireless Universal Serial Bus

DAA ..... Detect and Avoid

DCM ..... Dual Carrier Modulation

DS-UWB ..... Direct Sequence Ultra-Wideband

EIRP ..... Effective Isotropic Radiated Power

FCC ..... Federal Communications Commission

FDMA ..... Frequency Division Multiple Access

FDS ..... Frequency Domain Spreading

FFI ..... Fixed Frequency Interleaving

FFT ..... Fast Fourier Transform

GPS ..... Global Positioning System

GSM ..... Global System for Mobile Communications

IC ..... Integrated Circuit

IEEE ..... Institute of Electrical and Electronics Engineers

IFFT ..... Inverse Fast Fourier Transform

ISO ..... International Organization for Standardization

I-UWB ..... Impulse Ultra-Wideband

LHCP ..... Left-Hand Circularly Polarized

LNA ..... Low Noise Amplifier

LOS ..... Line of Sight

LPDA ..... Log-Periodic Dipole Array

MAC ..... Medium Access Control

MB-OFDM ..... Multi-band Orthogonal Frequency Division Multiplexing

MC-UWB ..... Multi-Carrier Ultra-Wideband

NLOS ..... Non-Line of Sight

NTIA ..... National Telecommunications and Information Administration

OFDM ..... Orthogonal Frequency Division Multiplexing

OOK ..... On/Off Keying

PCB ..... Printed Circuit Board

PDP ..... Power Decay (or Delay) Profile

PER ..... Packet Error Rate

PHY ..... Physical Layer

PND ..... Portable Navigation Device

PPS ..... Precise Positioning Service

PRNG ..... Pseudo-Random Number Generator

QAM ..... Quadrature Amplitude Modulation

QoS ..... Quality of Service

QPSK ..... Quadrature Phase Shift Keying

RF ..... Radio Frequency

RHCP ..... Right-Hand Circularly Polarized

RMS ..... Root-Mean-Squared

RX ..... Receiver

SIG ..... Special Interest Group

SNR ..... Signal to Noise Ratio

SPS ..... Standard Positioning Service

SRAM..... Static Random Access Memory

SSB.....Single Side-Band

SV.....Space Vehicle

TDMA .....Time Division Multiple Access

TDS ..... Time Domain Spreading

TEM ..... Transverse Electric and Magnetic

TFC.....Time-Frequency Code

TFI..... Time-Frequency Interleaving

TG3a.....IEEE 802.15.3a Task Group

TH-UWB ..... Time-Hopping Ultra-Wideband

TX..... Transmitter

USB .....Universal Serial Bus

USB-IF ..... Universal Serial Bus Implementers' Forum

UWB.....Ultra-Wideband

WLAN..... Wireless Local Area Network

WPAN .....Wireless Personal Area Network

ZPS .....Zero Padded Suffix

ACKNOWLEDGMENTS

It would be a mistake to not recognize those around me who have made it possible to complete this research. Some of them have provided technical guidance, some have provided encouragement, and others have provided both. It was with help from these key people that I have been able to address the little details of this project while simultaneously keeping the big picture in mind.

The members of my advisory committee have been sources of valuable inspiration throughout my collegiate career. I would like to thank Professor Bill Kuhn for encouraging me to get into the lab and "try it out." For me, nothing solidifies classroom learning like real-world tinkering with antennas, filters, amplifiers, network analyzers, and a healthy dose of patience. Furthermore, I am grateful that Professor Bala Natarajan has challenged me to understand the theory behind communication systems. It would be difficult for me to comprehend what happens in the invisible realm of radio waves without the solid foundation of math that he provided in his classes. Additionally, I appreciate Professor Don Gruenbacher's encouragement to balance academics and home life. He has patiently helped me understand tough engineering concepts during office hours, and he has reminded me that I should always make my family a priority. Sincere thanks are due to all of the members of my committee for reviewing this thesis and providing feedback.

I would also like to express gratitude to Garmin International for providing me two summer internships and for sponsoring this project, all of which made it financially possible for me to attend graduate school. Several people at Garmin have offered valuable technical guidance over the last few years, namely Mike Wiegers, Steve

Phillips, and Mike Cunning. They have communicated to me Garmin's emphasis upon solid engineering as the only way to meet and exceed the expectations of consumers in the electronics market.

I am especially thankful to my family for its prayers, encouragement, and support. My wife Kami has been the faithful friend who has shared with me the joys and trials of starting a family while finishing graduate school. What a strong and virtuous woman she is! Thanks also to my son Truett for giving me big smiles and fun play breaks when I needed them. Also, the support from my parents has been fundamental to my success. Throughout my life, they have encouraged me to work hard, finish what I started, serve others, and keep focused on the things that truly matter.

Most importantly, I thank my Lord Jesus Christ for strengthening me to run the race that is set before me. His grace has been sufficient in every challenge. All credit and honor belong to Him alone!

Chapter 1

Introduction

A promising, new radio technology called UWB has been developed to create short-range WPANs. UWB offers many advantages over existing wireless technologies, including higher data rates, greater security, and more robust performance in the multipath environments. Each of these is needed as the consumer electronics industry creates smaller, more-connected portable devices.

Despite UWB's strengths, however, it has been slow to penetrate the market for several reasons. 1) The frequency spectrum for UWB has been available in the United States since 2002 [1], but the electronics industry has needed time to agree upon implementation standards and to refine the technology; 2) Current UWB chipsets consume too much power to be used in handheld devices. Future chipsets are expected to use as little as half the power of current chipsets [2]; 3) It has been reported that prices for UWB chipsets are still too high [3]; 4) Spectrum regulators around the world have been concerned that UWB will interfere with local narrowband systems, so they have

disallowed UWB operation in certain frequency bands; and 5) the average consumer already relies upon various wireless platforms such as Bluetooth and the IEEE 802.11 family for networking, and demand for the features of UWB is simply not strong enough yet.

A few products with UWB have been available since early 2007 in the United States, but that number of products has not grown significantly since then. The first products to feature UWB were wireless USB hubs. While substantially faster than the previous "rogue" wireless USB systems operating at 2.4 GHz, these high speed UWB hubs were and still are unable to reach the full potential data rates offered by UWB due to limits of the wired USB protocol [2]. At this time, a small number of high-end laptops include UWB, but few peripherals also use UWB. An embedded UWB controller will not be perceived as needed by the consumer until the peripherals also adopt the technology. Appendix B contains a list of known UWB products at the time of this writing. The "killer-app" for UWB might be high-rate, streaming connectivity between audio/video devices, but few such products have sprung yet for UWB.

UWB still has market potential, though. In 2006, the USB Implementers' Forum selected a type of UWB developed by an industry group called the WiMedia Alliance as the radio platform that will support CW-USB [2], [4]. Also, it is believed that high-speed Bluetooth technology will eventually utilize WiMedia UWB as its PHY [2]. If the large number of Bluetooth- and wired USB-enabled devices—mobile phones, laptop computers, media players, digital cameras, and PNDs—that exist currently is any indication regarding the success that CW-USB or next-generation Bluetooth will achieve, then UWB has a bright future once the power consumption of the chipsets is reduced.

Compared to the single-carrier and spread-spectrum systems that are common today, UWB is quite novel. UWB introduces a new kind of spectral sharing in which signals are allowed overlap in frequency. UWB spreads signal energy at a very low power level across a wide frequency band instead of concentrating signal energy within a narrow band. This allows UWB to operate harmoniously, in principle, across the bands of incumbent wireless systems. The ability of radios to share the frequency spectrum will be particularly important as greater numbers of wireless devices are deployed.

1.1 Motivation

It is the overlapping nature of UWB signals that concerns some people. They worry that UWB emissions will raise the noise floor and cause significant problems for sensitive communication signals like those used in GPS, air traffic control, and mobile phone networks. Civilians and military personnel around the world rely on these critical systems to perform their duties safely, and even slight performance degradation in certain situations could have disastrous consequences [5], [6], [7], [8].

The concern is not only the effect that a single UWB device might have but the aggregate effect caused by potentially millions of UWB emitters [5]. Several researchers at Stanford predict "that UWB will become such a widespread utility that there will some day be as many as ten UWB devices per person" [6]. Other researchers are not concerned about the impact of UWB on GPS [9], [10]. Regardless, once a new technology like UWB has flooded the electronics market, it will be difficult to retract. We should carefully consider the effects of UWB emissions on sensitive systems like GPS before UWB technology is dispersed. Although UWB has potential to cause large-scale interference problems, many experts are unsure regarding the extent [5], [6], [7], [8]. This

project is mostly concerned with interference on a small scale, however, such as the kind that might be experienced when a UWB device is operated in close proximity to a GPS device. If the interference to GPS is low enough, perhaps a UWB radio could be integrated into a product such as a PND. From our research, we believe it is possible.

Many UWB schemes have been proposed, but the flavor that has been standardized by the WiMedia Alliance has gained the widest industry support—at least for WPANs. Membership in the alliance includes many leaders in both the hardware and software markets [11]. Although the number of WiMedia consumer products has not grown substantially in the past few years, most of the few UWB chipsets are WiMedia-certified. A list of WiMedia chipsets is provided in Appendix B.

If WiMedia UWB eventually becomes the standard WPAN for mobile phones, computers, media players, and other accessories, then adding UWB capability to a PND will probably make good business sense. GPS manufacturers already include Bluetooth (for phone connectivity) in some of their automotive devices. The first step toward this integration goal is to carefully investigate UWB and ensure that its interference will not have a deleterious effect on GPS performance. The next step is to evaluate the technical requirements to implement UWB and understand the performance it can offer in terms of data throughput and link distance.

1.2 Research Contributions

GPS is a mature technology for which a healthy amount of research has been conducted. A fair amount of research has considered GPS interference from pulse-based UWB signals [5], [6], [7], [8], [9], [12], [13], [14], [15], [16], [17]. However, very little research has been published about GPS interference produced by a WiMedia UWB

emitter. Because WiMedia UWB has the potential to become a popular WPAN implementation in consumer electronic devices, its compatibility with GPS should be assessed. In January 2008, we published a paper [18] that contained interference measurements from a WiMedia UWB chipset in the GPS L1 band (1,575 MHz). This thesis contains more detailed results, plus it reports the performance of a GPS receiver in the presence of a WiMedia UWB emitter. At the time of this writing, we are still unaware of any other published research attempts to quantify the effect of WiMedia UWB on a GPS receiver.

For the particular UWB system we evaluated, we found that most of the interference it generates at GPS L1 is radiated from its circuitry, not the RF output. Fortunately this type of interference can likely be controlled through careful PCB layout and the use of adequate shielding. We believe that the interference is low enough that conscientious placement of antennas and ICs could allow GPS and UWB radios to coexist in one device.

Later in this thesis, we compare the characteristics of several chip-type UWB antennas that could be used in a handheld product. Their performance with a WiMedia UWB device in a typical indoor environment is evaluated. Our measurements indicate that an antenna's orientation has little effect on the maximum data throughput of the UWB system. This is likely due to the ability of the WiMedia PHY to utilize rich multipath content.

In an effort to estimate the distances over which a WiMedia UWB device should be able to operate, we have constructed a theoretical link budget. Some of the widely-cited papers about UWB channel sounding report very low values for the path loss

exponent and standard deviation of fading in the indoor environment. Our lab tests with the UWB system suggest that these reported values may be optimistically too low for our laboratory, because the maximum distances that we measured for the system were much lower than those expected from theory. Alternatively, the results could mean that the implementation loss in the UWB product is far from optimal.

1.3 Thesis Organization

Following this introduction chapter, Chapter 2 presents the basics of GPS and UWB operation along with a brief theoretical analysis of the GPS jamming issue. Chapter 3 contains quantitative emissions measurements from a WiMedia UWB device in the GPS L1 band. In Chapter 4, we discuss the antenna characteristics that are needed for good UWB performance, and then we provide the measured characteristics of several chip-type UWB antennas. Chapter 5 returns to theory as we discuss the fundamentals of indoor UWB channel modeling, and Chapter 6 presents test results of the WiMedia UWB system with each of the evaluated antennas in a typical indoor environment. We concentrate on the throughput data rate and distance performance of the device, comparing the results to theory and to the data taken for the antennas evaluated in Chapter 4. Then, in Chapter 7, we give technical recommendations for GPS and UWB coexistence in a single product based on the interference, antenna, and channel performance measurements presented in the previous four chapters. Finally, Chapter 8 provides a summary of the research project and points out areas which merit further exploration.

Chapter 2

Background Information

In this chapter, we present the fundamental concepts of GPS and UWB. To begin, we review the technical aspects of GPS and emphasize the importance of protecting GPS receivers from interference. Then, we present a brief history of UWB communications and technical details about UWB's two most prominent, modern implementation architectures. Next, we consider the worldwide regulations of frequency spectrum and the restrictions they impose on the operation of UWB radios. Finally, we discuss the concerns raised by the technical community regarding the co-existence of GPS and UWB radios and provide our own theoretical analysis of the subject.

2.1 The Global Positioning System

The NAVSTAR Global Positioning System was developed and deployed by the United States military to provide positioning and timing data anywhere in the world. The system's greatest accuracy is reserved for use by the US government and other approved

entities. This exclusive service is called the Precise Positioning Service (PPS). Civilians can access the Standard Positioning System (SPS)—a free, unencrypted version of the GPS signal that provides location information that is 90% accurate to ten meters [19].

Navigation signals are provided to GPS users by a constellation of at least 24 satellites, or space vehicles (SVs), in six orbital planes. The US military usually operates several spare SVs in the constellation. A GPS receiver needs signals from at least four GPS satellites to calculate a location and time fix. Depending on the geometry of the SV constellation, receiving signals from more than four satellites usually provides greater receiver accuracy—except in the case of multipath..

Each of the current, second-generation (Block II, IIA, IIR and IIF) satellites operates one S-band and two L-band transponders. Two of the three bands are reserved for US government use: the L2 band at 1227.6 MHz and S band at 2227.5 MHz. The third band, L1, at 1575.42 MHz, carries the SPS signal that can be processed by civilian GPS receivers.

The SPS L1 signal from each SV is actually composed of three parts: the navigation message, the Coarse Acquisition (C/A) code, and the sinusoidal carrier. The navigation message has a predefined length of 37,500 bits and broadcast rate of 50 bps, so it repeats every 12.5 minutes. It contains ephemeris data about the satellite's location in the sky and almanac data about the status of the entire system. The C/A code, also known as the L1 code, is a 1023-bit pseudorandom sequence that is broadcast at a chip rate of 1.023 MHz. This code spreads the power of the navigation message to allow for precise receiver timing and provide some resistance to jamming. Although the sidelobes in the frequency domain theoretically extend ad infinitum, most of the signal's useable

energy is contained within a 2 MHz bandwidth. The C/A code of each SV is pseudo-orthogonal to the others, and all SPS signals are broadcast at the same L1 frequency.

To create the SPS signal, the navigation message and C/A code are combined by modulo-2 addition prior to being modulated via binary phase shift keying (BPSK) on the carrier at 1575.42 MHz. The block diagram in Figure 2-1 shows the transmitter's conceptual parts, and Figure 2-2 shows a representation of C/A code #1 in the frequency domain.

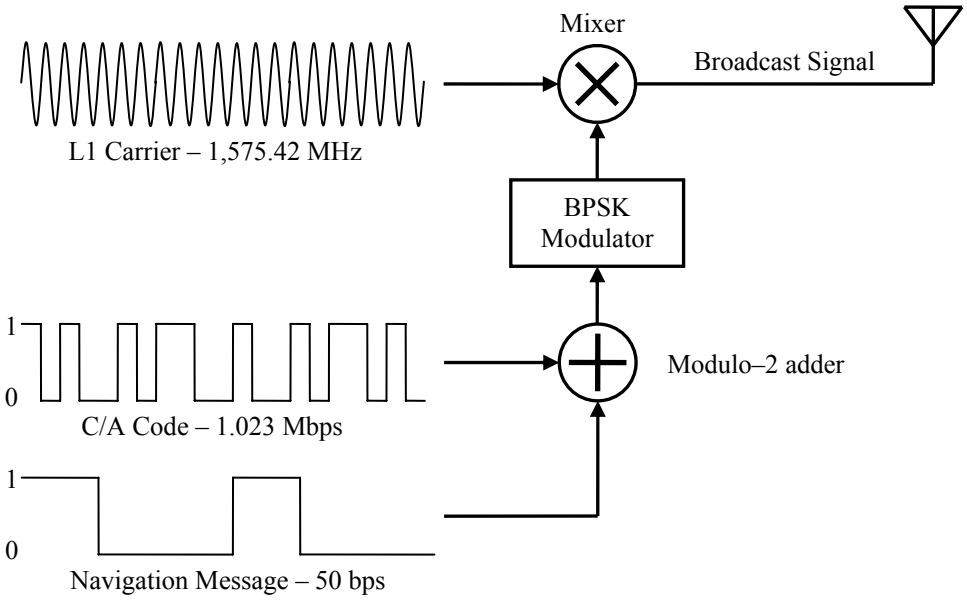

Figure 2-1: The three components of the SPS signal.

Once the signals from at least four SVs have been successfully acquired using digital signal processing techniques, the user's position can be determined. Many modern GPS receivers can process at least 12 satellite signals in parallel. A four-dimensional time and position fix is calculated by estimating the pseudorange, or distance, from the user to each satellite. This is accomplished by comparing the timing in which signals are received. To enhance the accuracy of the pseudorange estimates, the pseudoranges are

modified to account for additional delay as the GPS signals pass through the ionosphere and troposphere. The estimation is further refined by considering relativistic effects due to the velocities of the satellites and the earth along with differences in the earth's gravitational field.

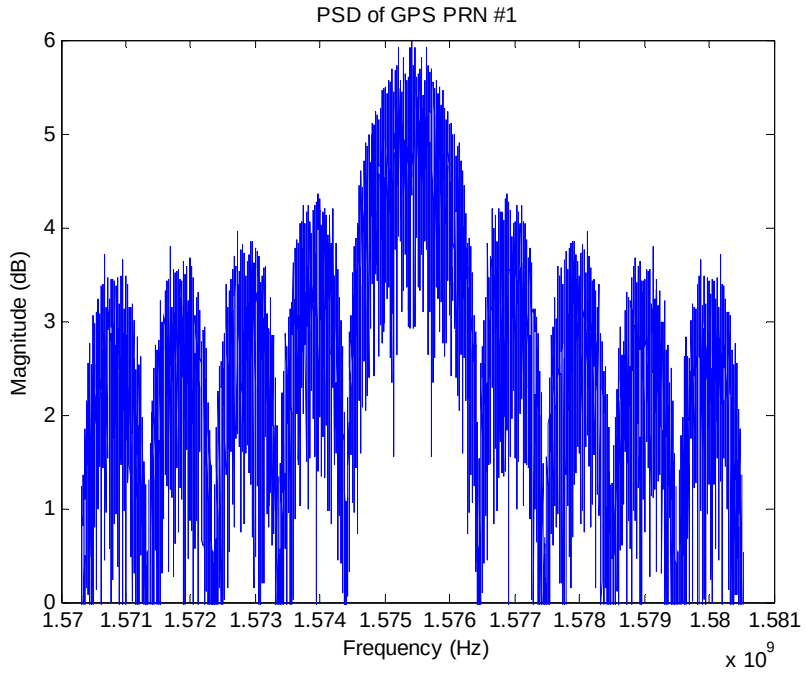

Figure 2-2: Power spectral density plot of C/A code #1. Only main lobe and four sidelobes are shown.

Providing useful GPS signals to the earthbound user is a challenge, because the satellites orbit the earth at an altitude of roughly 20,200 km. The limited broadcast power of each SV is focused using a planar helix array into a conical beam that covers the portion of earth that is visible from the satellite. The specified relative strength of the GPS signal is shown in Figure 2-3. On Earth, the specified minimum power level for the received GPS signal is -130 dBm through an unobstructed view of the sky [19]. Obstructions such as buildings, canyons, and trees can degrade the accuracy of the position solution by attenuating the signals or reflecting them (multipath). Since the

amount of received GPS signal energy is very low, a GPS receiver is vulnerable to interference and jamming signals.

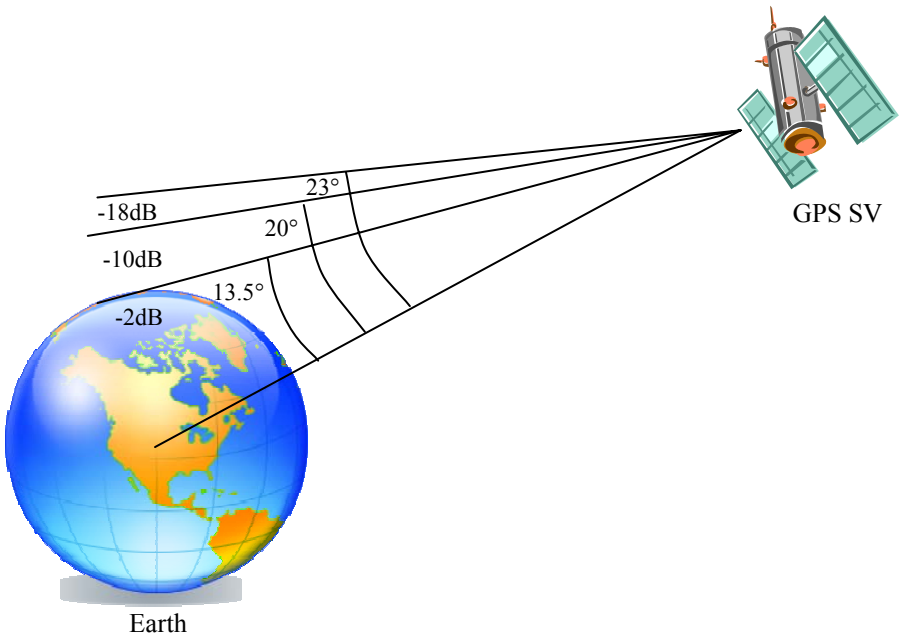

Figure 2-3: Beam pattern of broadcast GPS signal. [19]

Jamming has symptoms which can be easily noticed by the user of a GPS receiver. One symptom is that the device may take a long time to—or may never—acquire a satellite lock. Another symptom is that the position fix may appear to jump around excessively or the unit may report degraded positional accuracy. Both symptoms are irritating to users, so care must be taken to prevent self-jamming by the device and to harden it against interference from nearby sources. One of the main goals of this research project is to determine whether a certain UWB emitter creates appreciable interference to a GPS receiver in an effort to provide a preliminary assessment of the compatibility of UWB and GPS radios.

2.2 Ultra-Wideband Signals

The idea of communicating using wide bandwidths has existed for many years. The well-known Shannon-Hartley theorem establishes a theoretical upper bound on channel capacity for a relatively error-free communication system and is expressed as

$$C = B\log_2(1 + SNR) \tag{2-1}$$

where the channel capacity C, in bits per second, is linearly proportional to the bandwidth of the channel B, in hertz, and logarithmically proportional to the signal-to-noise ratio SNR. It can be implied from this relationship that increasing channel bandwidth B is more effective at increasing channel capacity C than is increasing SNR. So enters the concept of UWB communications.

The spark gap transmitters built by Tesla, Marconi and others at the beginning of the twentieth century were actually primitive types of UWB transmitters. Those experimenters did not intend to create wide-band radios for the purpose of increasing data rates; they used spark gaps simply because the technology for tunable, narrowband radios had not yet been invented. The problem with spark gap signals was that their wide bandwidths severely limited the technology's number of potential users. It was not until the development of narrow-band, tunable radios that many people could share the wireless spectrum. The FCC was created in 1934 to allocate radio spectrum and regulate the growing wireless community.

Since 1934, radio technology has progressed substantially to bring us the sophisticated wireless networks upon which our mobile phones and computers communicate today. Many modern systems are still narrow-band in nature, but an increasing number of systems are being implemented using spread-spectrum techniques

to improve data rates, security, and the number of potential users. While spread-spectrum typically provides better performance than narrow-band, its performance seems low compared to that of UWB in theory. The main factors limiting widespread use of UWB have been primarily the limited power of digital signal processors and the insufficient quality of wideband filters and antennas. Within the last decade, however, processors, microwave antennas, and filtering techniques have advanced significantly.

The swath of spectrum from 3.1 to 10.6 GHz that has been established in the United States for UWB was officially opened by the FCC in 2002 [1]. UWB is defined an antenna transmission with a bandwidth greater than 500 MHz or a fractional bandwidth greater than 20% [20]. The FCC recognizes three general types of UWB devices: 1) imaging systems, including ground penetrating radars and wall, through-wall, surveillance, and medical imaging devices; 2) vehicular radar systems (22-29 GHz); and 3) communications and measurement systems. Radiation limits are imposed per Title 47 of the Code of Federal Regulations, Part 15, Subpart F [20]. A GPS device with UWB capability would fall into the Handheld profile. Additional masks for indoor use and other UWB device types are provided in Appendix A. A portable UWB device used in a WPAN must operate below the limits shown in Figure 2-4. The limits are specified in terms of frequency and EIRP. It is important to note that the solid line in the figure below shows the EIRP limits for *intentional* UWB emissions such as those that emanate from the antenna. The limits for *unintentional* emissions from the circuitry, etc. are more relaxed, allowing EIRP levels up to the standard limit of -41.3 dBm/MHz even in the GPS band.

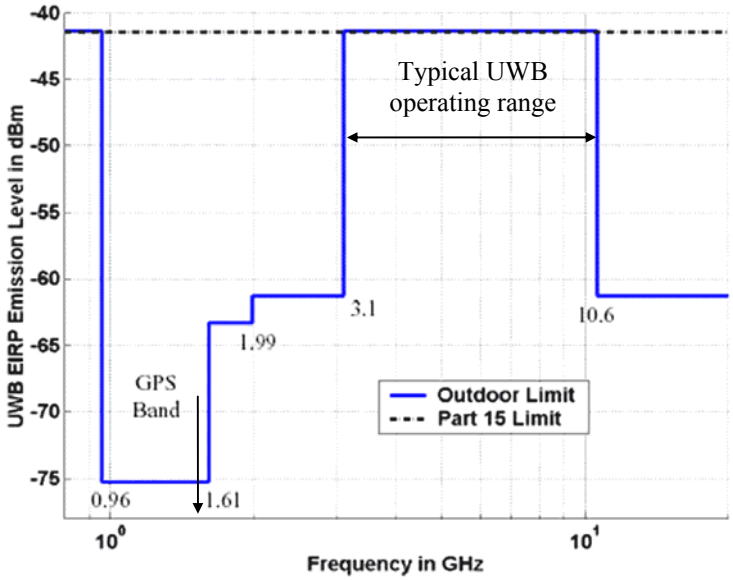

Figure 2-4: Handheld UWB spectral mask (USA).

Using a UWB signal has several advantages over using a traditional single carrier—or even spread spectrum—technique. The first, and perhaps most obvious, is that the larger bandwidth provides higher data rates (for a given SNR). Existing WPAN standards such as Bluetooth 2.1 support maximum data rates of only a few megabits per second (Mbps), while the current WiMedia UWB standard supports raw data rates up to 480 Mbps, depending on the distance between the transmitter and receiver [4]. Furthermore, UWB resists interception, jamming, and detection due to the low transmitted power that is spread over a wide bandwidth [21]. In theory, UWB operates across already-allocated channels without causing significant interference, since UWB power levels are limited to the same levels that have been imposed for unintentional radiation, as shown in Figure 2-5.

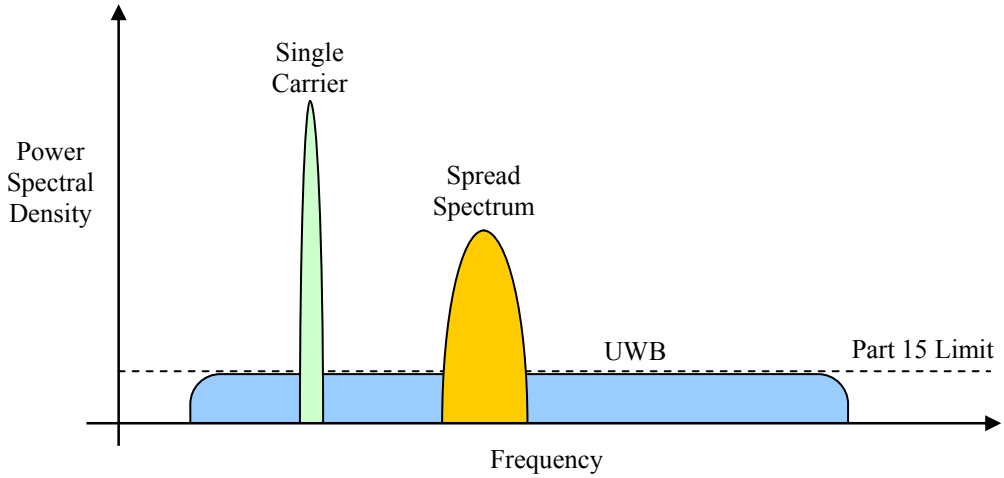

Figure 2-5: Power density comparisons of UWB and narrowband systems (not to scale).

The guidelines for UWB transmissions are fairly general. Provided the EIRP stays below the spectral limits and the signal has a bandwidth of at least 500 MHz or fractional bandwidth greater than 20%, the FCC makes no further stipulations. This allows system designers to choose a modulation scheme that works best for their application.

2.2.1 Dueling Architectures

After the FCC opened the UWB airwaves, IEEE 802.15.3a Task Group (TG3a) was established to develop a UWB standard for high-speed WPANs. TG3a received more than 20 different proposals which generally fell into two categories: impulse UWB (I-UWB) and multi-carrier UWB (MC-UWB). I-UWB is based in the time domain, and it includes approaches such as direct-sequence UWB (DS-UWB) and time-hopping UWB (TH-UWB). MC-UWB is based in the frequency domain, and its most prominent approach is multi-band orthogonal frequency division multiplexing (MB-OFDM). TG3a meticulously narrowed the proposals down to a single I-UWB scheme and a single MB-

OFDM scheme, but it was unable to obtain the 75% consensus needed to approve either scheme for the 802.15.3a standard.

To build support for I-UWB, a group called the UWB Forum was established by Freescale Semiconductor in February 2004. The UWB Forum did not endorse any single form of UWB, but its members tended to favor impulse radio schemes. At the same time, another group called the MultiBand OFDM Alliance was fighting to steer 802.15.3a toward MB-OFDM. Intense debate over the architectures continued more than two years.

While TG3a was deliberating, the MultiBand OFDM Alliance asked ECMA International to draft a standard for MB-OFDM. It also merged with a group called the WiMedia Alliance, which was focused on MAC implementation. In December 2005, ECMA released ECMA-368 and ECMA-369, which became the WiMedia MB-OFDM standards for UWB PHY and MAC layers, respectively. WiMedia then submitted ECMA-368 to the ISO, which later released it worldwide as ISO/IEC 26907:2007.

In January 2006, the UWB Forum and WiMedia Alliance recognized that 802.15.3a was deadlocked, and they both agreed to support dissolution of the task group without conclusion. The UWB Forum then continued to pursue various types of I-UWB but never drafted an official standard. Eventually, many members of the UWB Forum quietly withdrew and joined WiMedia.

At the time of this writing, WiMedia's MB-OFDM UWB scheme appears to have gained the most industry support for communication systems. Although it still has not yet been deployed widespread, it has officially been selected as the radio platform for CW-USB, and it is also expected to serve as the PHY implementation for the Seattle release of

Bluetooth technology [2]. (The Bluetooth 3.0 standard was split into two pieces, with the first piece, released in April 2009, utilizing 802.11 technology.)

I-UWB is still used for certain applications such as imaging systems and radars, but it appears to have been abandoned for high data rate consumer communication systems. We are unaware of any high data rate WPAN products using the impulse radio approach. Since our goal has been to investigate the possibility of adding UWB to a consumer GPS receiver, this thesis concentrates mostly on the MB-OFDM method. For completeness, however, we first present the basics of impulse radio.

2.2.2 The Impulse Radio Approach

Although UWB has become a buzz term in recent years, wide-band radios have actually existed for more than a century. During the 1890s, Marconi, Tesla, and other experimenters tinkered with spark-gap transmitters to send pulses of Morse code through the then-supposed "luminiferous aether." Those early transmitters spread signal energy over such large bandwidths that it was difficult for multiple users in the same geographic area to access the wireless channel simultaneously without interference. Very little was known at that time about tunable circuits. Later, carrier-based radios were developed that could occupy fixed frequency bands, allowing many users to share the wireless spectrum. The US government recognized the need to manage spectral usage, so it created the FCC in 1934.

Many of UWB's early applications were military-related. Short electromagnetic pulses were used to help defeat enemy torpedoes during World War II [21]. Radar systems worked by sending out short radio pulses, waiting for them to echo off a remote object, and translating the echo's delay into an estimated distance. As the technology

progressed, systems became more sophisticated. Implementations of I-UWB have provided radar and communication systems with security and low probability of detection—a necessity for clandestine operations. Recent applications such as the DRACO and ORION radio systems described in [21] were designed to offer networking capability for troops' mobile voice, data, and video transmission needs. Other applications for I-UWB include systems for determining the location of assets on a battlefield and ground penetrating radars to detect buried landmines.

Outside of radar applications, the use of I-UWB in the civilian world has been somewhat limited. Interest in UWB was piqued in 1998 when the FCC issued a Notice of Inquiry to investigate the how UWB could share the spectrum. Later, in February 2002, it formally opened the airwaves for license-free operation [1]. Since then, researching I-UWB for communication systems has gained significant interest. Impulse radio systems are often called carrier-less systems, because they do not need a carrier to modulate data to frequencies that are conducive to wireless propagation. Perhaps the greatest reason why impulse radio has received so much attention is the novel way that it differs from traditional radio. In typical communication systems, a main goal is to minimize spectral spreading while maximizing data throughput. In I-UWB, the ultra-wide bandwidths of short pulses are exploited to provide radically higher data rates than traditional systems can provide for a given output power level.

To modulate data wirelessly, I-UWB transmitters produce rapid patterns of pulses in the time domain. We can easily understand from linear transform theory that extremely short pulses in the time domain produce extremely wide bandwidths in the frequency domain. Significant effort has been made to minimize the amount of spectral "waste" in

I-UWB by carefully selecting the pulse shapes. The most common pulse shapes are derived from the Gaussian monopulses (or monocycles), shown in Figure 2-6.

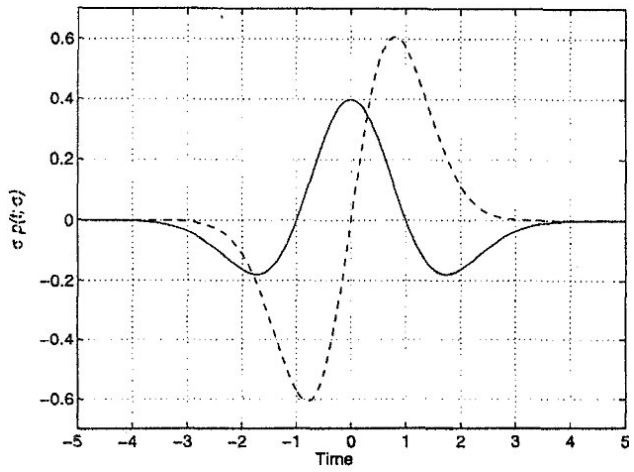

Figure 2-6: Normalized Gaussian (solid) and Rayleigh (dotted) monopulses [22].

2.2.2.1 I-UWB Modulation Schemes

Three prominent pulse modulation schemes exist for I-UWB: position modulation, amplitude modulation, and phase modulation. An example of each is shown in Figure 2-7. The position method works by altering the time period between subsequent pulses. For the amplitude scheme, either binary pulse amplitude modulation (BPAM) or on/off keying (OOK) can be used. The phase modulation approach simply inverts the pulses according to the input data. For all three types of modulation schemes, the resulting spectra are typically quite jagged due to the fundamental pulse repetition rate. Randomly dithering the pulse train in time can smooth its frequency spectrum, which can minimize interference to narrowband systems (Figure 2-8) [12], [23].

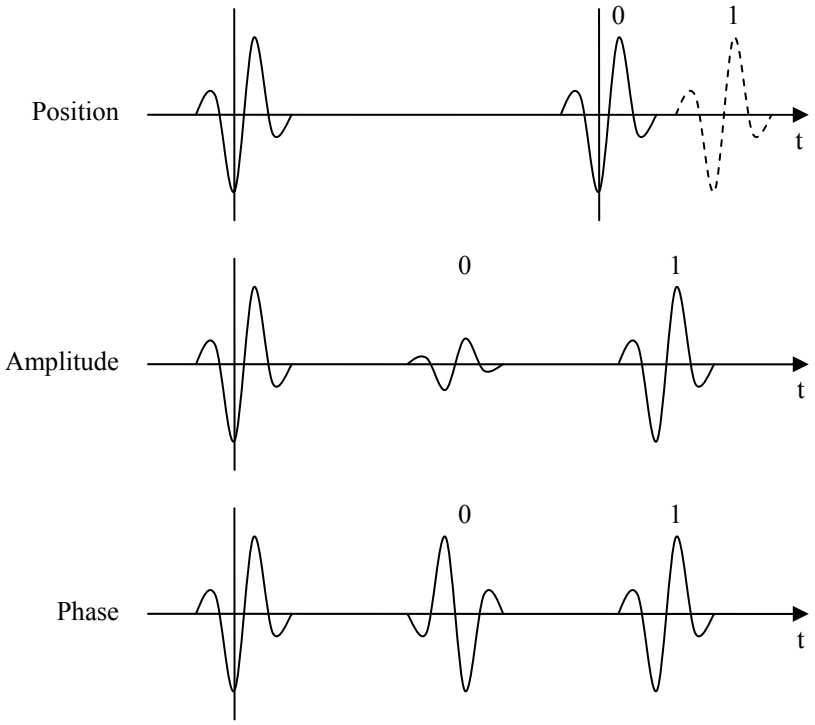

Figure 2-7: Three I-UWB pulse modulation methods. Adapted from [24].

Even with timing randomization, it can be challenging to control the spectrum. The consumer electronics market is a global market, and easily adapting to local spectrum regulations is critical for the success of any UWB system. Filtering I-UWB pulses to accomplish this goal is usually undesirable, since it distorts the pulse shape and introduces non-linear phase dispersion [25].

I-UWB has challenges in the time domain, too. Due to the brevity of the pulses, precise synchronization between the transmitter and receiver is required. Multipath propagation in indoor environments further complicates reception, necessitating the use of a receiver with a RAKE architecture [26]. (More on the subject of channel modeling is discussed in Chapter 5.) Although I-UWB is a novel way to modulate data wirelessly,

successfully implementing impulse radio for high data rate applications in practice requires a substantial amount of processing capability.

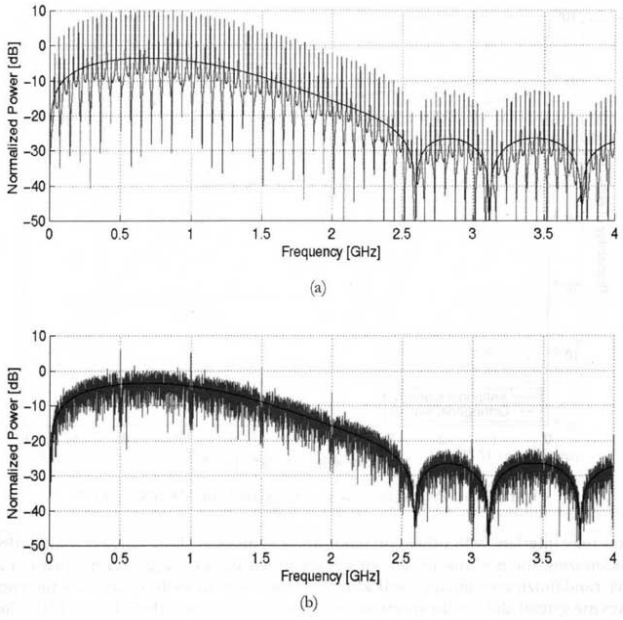

Figure 2-8: Spectrum of UWB pulse train without (a) and with (b) randomizing techniques [23].

2.2.3 The WiMedia Approach

While I-UWB uses repeated pulses in the time domain to achieve a wide bandwidth, MC-UWB uses many narrowband carriers to satisfy the FCC bandwidth criterion. As mentioned previously, a prominent form of MC-UWB is defined by ECMA-368, the WiMedia MB-OFDM PHY standard [4]. In WiMedia, the entire UWB spectrum from 3.1 GHz to 10.6 GHz is divided into 14 bands. MB-OFDM uses these 14 bands to allow as many as 43 users to access UWB spectrum in the same physical area by combining time division and frequency-division multiple access (TDMA and FDMA) techniques.

2.2.3.1 Band Organization

The WiMedia PHY standard (version 1.2) organizes the fourteen bands into six band groups. Figure 2-9 shows the organization of the bands and band groups. Band Groups 1 through 4 contain three bands each, and the fifth band group contains the remaining two bands. Band Group 6 was defined after the initial release of the WiMedia standard to promote worldwide compatibility, and it is discussed in greater detail in Section 2.2.4.

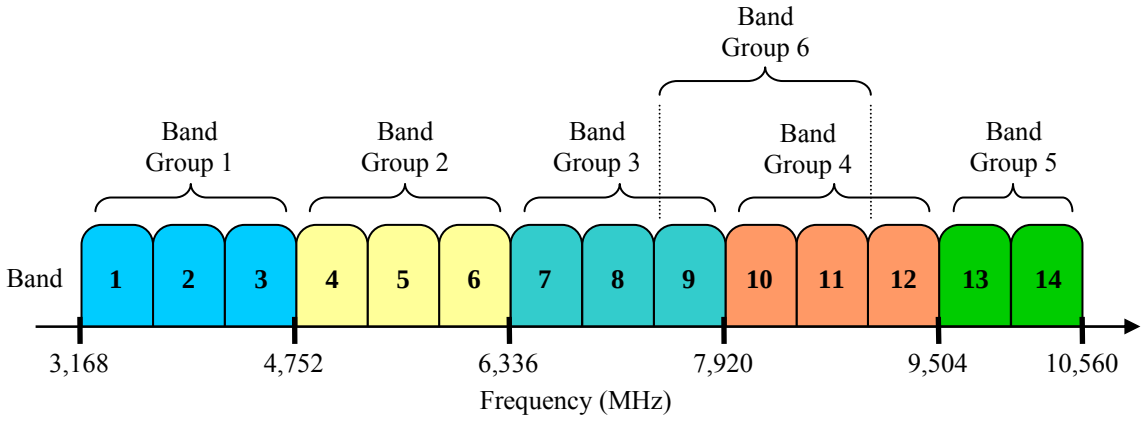

Figure 2-9: WiMedia band group organization [4].

Each band is 528 MHz wide, and the center frequency f_C of each band can be found in MHz using

$$f_C(MHz) = 2904 + 528 \cdot n_b \tag{2-2}$$

where n_b is the band number from 1 to 14. Table 2-1 lists the start, center, and stop frequencies of each band.

Table 2-1: WiMedia band allocations [4].

Band Number	Start Frequency (MHz)	Center Frequency (MHz)	Stop Frequency (MHz)
1	3,168	3,432	3,696
2	3,696	3,960	4,224
3	4,224	4,488	4,752
4	4,752	5,016	5,280
5	5,280	5,544	5,808
6	5,808	6,072	6,336
7	6,336	6,600	6,864
8	6,864	7,128	7,392
9	7,392	7,656	7,920
10	7,920	8,184	8,448
11	8,448	8,712	8,976
12	8,976	9,240	9,504
13	9,504	9,768	10,032
14	10,032	10,296	10,560

2.2.3.2 Band Hopping Patterns

Within each band group, multiple access is achieved by hopping in patterns called time-frequency codes (TFCs). A TFC defines the band hopping sequence during a data frame. For each band group except Band Group 5, a user is assigned one of ten possible TFCs. All ten TFCs for Band Group 1 are listed in Table 2-2. The TFCs for subsequent band groups follow this same pattern.

Two types of TFCs are specified: time-frequency interleaving (TFI) and fixed-frequency interleaving (FFI). In TFI, the user hops from band to band within the band group. An example of band hopping using TFC #1 is shown in Figure 2-10. In FFI, the user stays on a single band. Except in Band Group 5, each band group has seven TFCs that are TFI and three TFCs that are FFI. Band Group 5 has three total TFCs; one is TFI and two are FFI. Band Group 6 has ten TFCs, but they cannot be used when all the TFCs

of Band Groups 3 and 4 are used, due to the overlap of the band groups. Thus, the total number of unique TFCs across the entire UWB band is 43. The TFCs are designed to minimize the number of collisions across each data frame for multiple, non-synchronous transmissions in the same physical area.

Table 2-2: Time-frequency codes for Band Group 1 [4]

TFC Number	Hoppinng Sequence						TFC Type
1	1	2	3	1	2	3	TFI
2	1	3	2	1	3	2	TFI
3	1	1	2	2	3	3	TFI
4	1	1	3	3	2	2	TFI
5	1	1	1	1	1	1	FFI
6	2	2	2	2	2	2	FFI
7	3	3	3	3	3	3	FFI
8	1	2	1	2	1	2	TFI
9	1	3	1	3	1	3	TFI
10	2	3	2	3	2	3	TFI

2.2.3.3 WiMedia Data Frame

The WiMedia data frame is composed of six symbols. Each symbol has duration of 312.5 nanoseconds. Within the symbol, the IFFT output has a period of 242.42 nanoseconds. A zero-padded suffix (ZPS) lasting 70.08 nanoseconds precedes the next IFFT output to help minimize inter-symbol interference (ISI) due to multipath. This time period also allows the frequency synthesizer to jump to and stabilize at the center frequency of the next band in the hopping pattern. Overall, the duration of the data frame is 1.875 microseconds [4].

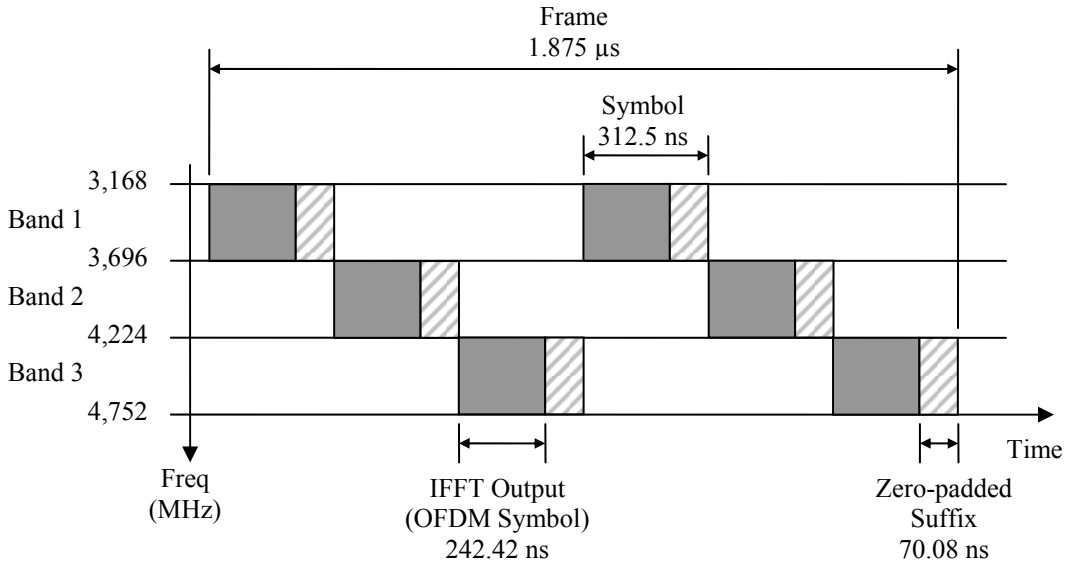

Figure 2-10: Example realization of a transmitted RF signal using three bands and TFC #1. Adapted from [4]

2.2.3.4 ODFM Tones

Each OFDM band is composed of 128 orthogonal tones which are generated and recovered using a 128-point FFT/IFFT. Orthogonal spreading sequences allow the carriers to overlap in frequency and still be recoverable, as shown in Figure 2-11. Within the context of each 4.125 MHz-wide tone, the wireless channel can be considered flat (see section 5.4 for more information). This reduces sensitivity to variations in the channel without needing complex equalization. Additionally, the transmitted spectrum can be controlled easily to help the transmitter adapt to worldwide spectrum regulations and avoid interfering with existing narrowband systems [22]. If certain frequencies are disallowed or are already in use, the OFDM controller can simply notch out the applicable tones.

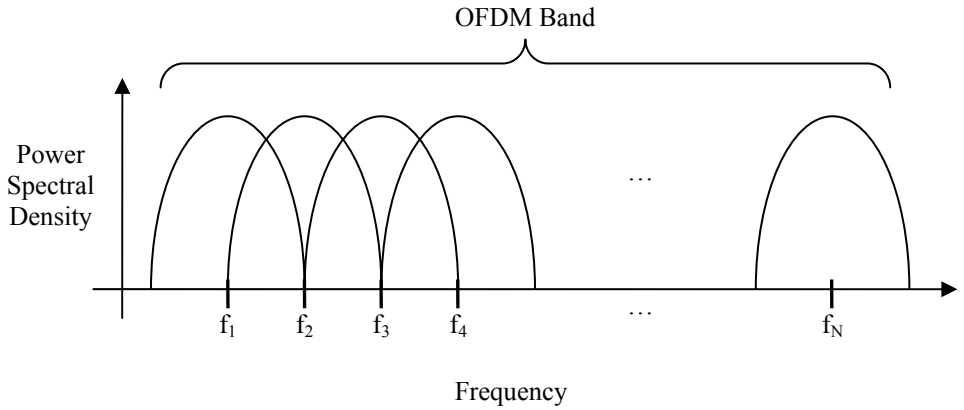

Figure 2-11: Carriers f_1, f_2, … f_N are orthogonal for OFDM.

Not all of the 128 tones are used to transmit payload data; only 100 carriers actually do this. Figure 2-12 shows the relative locations of the carriers within the band. Twelve pilot carriers are spread across the band to provide channel estimation. Once the quality of the link has been estimated, the system decides which data rates can be supported. At the edges of the band, fifteen null carriers and guard carriers help reduce interference to and from adjacent bands. The 122 active carriers occupy a bandwidth of 503.25 MHz—enough to satisfy the FCC definition of UWB.

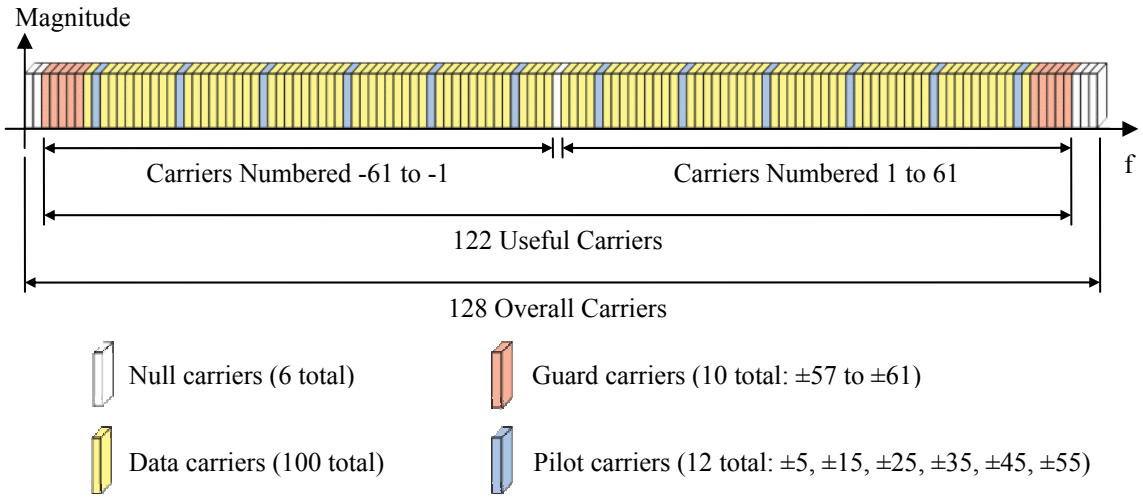

Figure 2-12: OFDM carrier assignments. Adapted from [27].

2.2.3.5 Data Rate Profiles

WiMedia UWB provides eight payload data rate profiles: 53.3, 80, 106.7, 160, 200, 240, 320, and 480 Mbps. During operation, the maximum data rate that can be supported is determined by the WiMedia PHY based on the condition of the channel. As the link quality deteriorates, the payload data rate must be decreased to provide sufficient error resilience. A block diagram of the encoding process is shown in Figure 2-13.

Figure 2-13: Block diagram of the data encoding process.

Before any coding redundancy is added to the signal, however, the data bits are whitened using a scrambler. The scrambler is implemented by a pseudo-random number generator (PRNG), given as

$$g(D) = 1 + D^{14} + D^{15} \tag{2-3}$$

where D represents a single bit delay element. Thus, the bit stream $x[n]$ is generated as

$$x[n] = x[n-14] \oplus x[n-15], n = 0,1,2,... \tag{2-4}$$

Once the data stream has been scrambled, it passes through the heart of the error correction scheme: the convolutional coder shown in Figure 2-14. It has constraint length $K = 7$ and "mother" rate $R = 1/3$. The various data rates are later derived by puncturing the code and adding redundancy in the time and frequency domains.

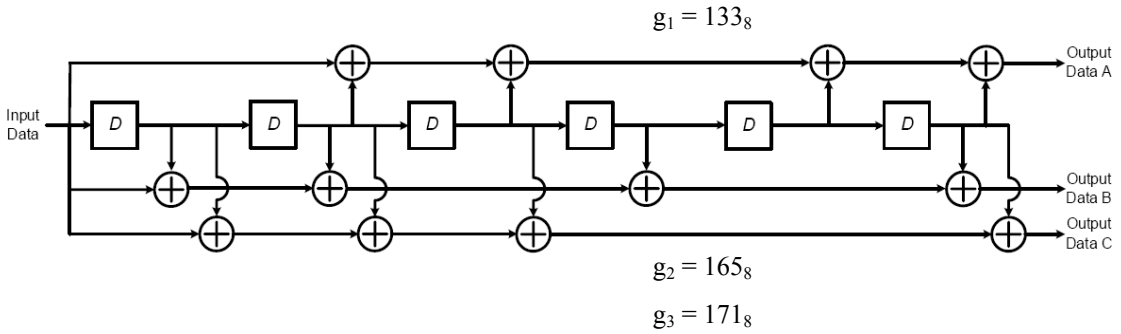

Figure 2-14: WiMedia convolutional channel coder. *K* = 7, *R* = 1/3 [4].

During the code puncturing process, some bits are removed from the sequence, and the remaining bits are transmitted. At the receiver, dummy bits are reintroduced to the sequence at the locations where bits were previously stolen. Redundancy added by the convolutional coding allows the original data to be recovered using the Viterbi algorithm. The ratio of the number of stolen bits to the number of total bits changes according to the selected data rate. Figure 2-15 illustrates the code puncturing process.

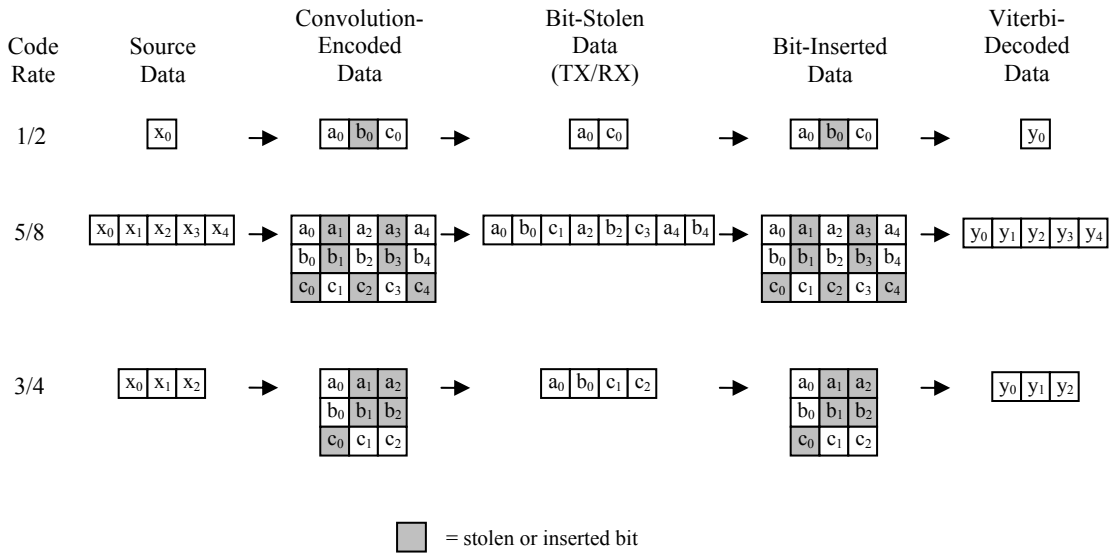

Figure 2-15: Examples of code puncturing. Adapted from [4]

The actual channel bit rate for all of the profiles is 640 Mbps. Varying the amount of redundancy in the coded, time, and frequency domain provides the various payload data rates. A technique called frequency domain spreading (FDS) halves the data rate by transmitting the same data on two separate carriers within an OFDM symbol. This can improve bit-error rate (BER) performance in environments where narrow-band interferers are present. Another way to modify the data rate is to transmit the same data across two consecutive OFDM symbols. This technique is called time-domain spreading (TDS), and it also cuts the effective data rate in half. Combinations of code puncturing, FDS, and TDS provide the eight possible data rates shown in Table 2-3. The lowest data rate, 53.3 Mbps, uses redundancy in the coded, time, and frequency domains to provide the most robust connection. In contrast, the 480 Mbps profile uses only a small amount of coding redundancy to provide the fastest link, assuming that the condition of the channel allows it.

Table 2-3: WiMedia PHY service data rate-dependent parameters [4]

Data Rate (Mbps)	Modulation Scheme	Coding Rate (*R*)	FDS	TDS	Spreading Gain	Coded Bits per Frame	Info Bits per Frame
53.3	QPSK	1/3	Yes	Yes	4	300	100
80	QPSK	1/2	Yes	Yes	4	300	150
106.7	QPSK	1/3	No	Yes	2	600	200
160	QPSK	1/2	No	Yes	2	600	300
200	QPSK	5/8	No	Yes	2	600	375
320	DCM	1/2	No	No	1	1,200	600
400	DCM	5/8	No	No	1	1,200	750
480	DCM	3/4	No	No	1	1,200	900

The actual throughput of each data rate profile is lower due to frame overhead—namely the preamble and header. A standard preamble requires five frames, but a special burst-mode preamble consists of three. Burst mode is only available for the data rates of

320 Mbps and above. After the preamble, the header takes two frames. Then the payload data and a small pad follow. The standard payload length can be up to 4,096 bytes, while the burst mode length is restricted to 4,045 bytes. The number of frames required to carry the payload data varies according to the data rate profile. Figure 2-16 compares the frame elements for both modes.

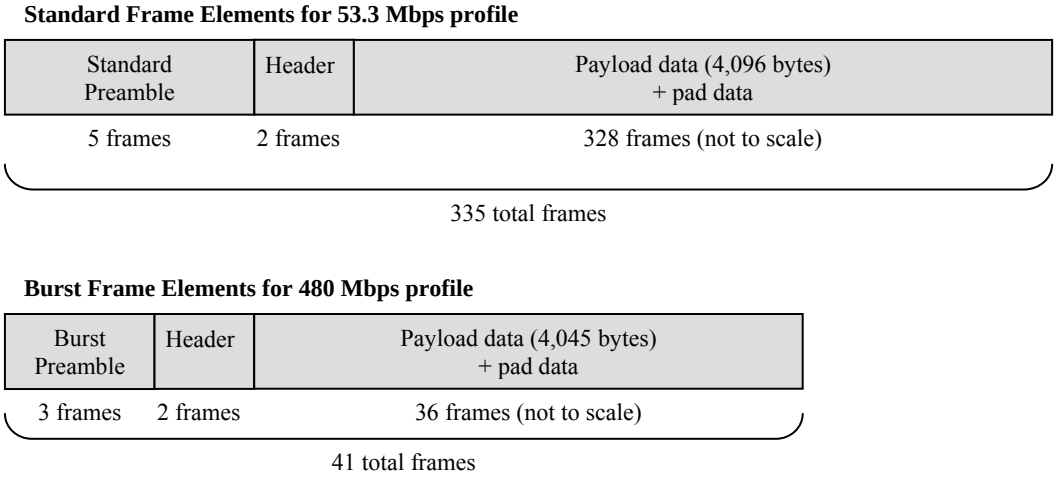

Figure 2-16: Frame elements for 53.3 Mbps (standard mode) and 480 Mbps (burst mode).

We can calculate the PHY efficiency by dividing the number of frames for the payload data by the total number of frames. A more accurate calculation would take into account the length of the pad data, but for our purposes we can lump it with the payload data. For the 53.3 Mbps profile, the PHY efficiency is about 98%. For the 480 Mbps profile in standard mode, the PHY efficiency is about 84%. In burst mode, the PHY efficiency jumps up to about 88%. Shortening the preamble by two frames makes a significant difference as the payload data rate increases.

There is additional overhead at the MAC layer due to the presence of beacon periods. The number of required beacon periods increases as the number of WiMedia

receivers located in the same physical area increases. At best, the MAC efficiency is about 99%, and it is about 94% at worst [28]. Multiplying the efficiency of the PHY and MAC layers allows us to calculate the best and worst case WiMedia protocol efficiency and, ultimately, the theoretical maximum throughput of the system. The estimates in Table 2-4 are made assuming that channel conditions permit a negligibly-low packet error rate (PER) at the receiver. Judging by the throughput rates, the WiMedia protocol offers a remarkable level of efficiency that suits it well for streaming media such as high-definition video compressed using H.264 [2].

Table 2-4: Maximum throughput estimates for 53.3 and 480 Mbps profiles.

Data Rate Profile (Mbps)	Best-Case Throughput (Mbps)	Worst-Case Throughput (Mbps)
53.3	49	52
480	395	418

2.2.3.6 Data Interleaving Process

After passing through the convolutional coder and puncturer, the data stream is interleaved in three stages [4]. The first stage permutes bits across six consecutive OFDM symbols. Then, the second stage permutes the bits across the carriers of each OFDM symbol. Finally, the third stage cyclically shifts the bits in successive OFDM symbols. The bit interleaver is designed to provide robustness against narrow-band interferers and burst errors, especially in modes using TDS and FFI.

2.2.3.7 Constellation Mapping

For the data rates of 200 Mbps and below, quadrature phase shift keying (QPSK) is used. QPSK is a common modulation scheme that uses the baseband data to modulate

the phases of the carrier in π/2 (90°) increments. The four possible symbols can be represented using two orthogonal basis functions—typically sine and cosine. Mapping is achieved by assigning two bits of baseband data to a single QPSK symbol (a complex number) as shown in Figure 2-17. QPSK is fairly straightforward to implement at both the transmitter and receiver, and it offers good performance for lower SNRs. Compared to its simpler relative, binary phase shift keying (BPSK), QPSK offers twice the bandwidth efficiency for the same energy efficiency [52].

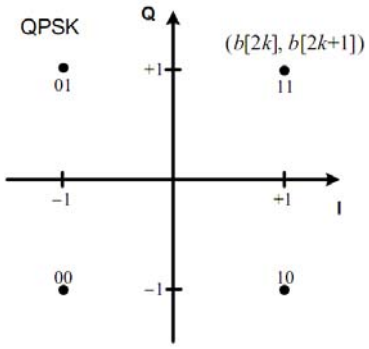

Figure 2-17: QPSK constellation used for WiMedia data rates of 200 Mbps and below [4].

For short transmitter/receiver separation distances (less than three or four meters LOS), the SNR is typically large enough to support a more complicated mapping scheme that has greater bandwidth efficiency than QPSK. The data rates of 320 Mbps and higher are mapped using a four-dimensional technique called dual-carrier modulation (DCM). In DCM as described by ECMA-368 [4], two unique 16-QAM constellations are created that employ Gray coding to maximize error resilience. The baseband data arriving from the bit interleaver are grouped into chunks of 200 bits. These chunks are further separated into 50 groups containing four bits each. For the bits $b[i]$ with $i \in [0, 199]$, the groups are constructed as

$$group(k) = \{b[g(k)],\ b[g(k)+1],\ b[g(k+50)],\ b[g(k+51)]\} \text{ with}$$

$$g(k) = \begin{cases} 2k & k \in [0, 24] \\ 2k+50 & k \in [25, 49] \end{cases} \quad \text{(2-5)}$$

This yields groups 0 to 49 as follows:

$$group(0) = \{b[0],\ b[1],\ b[50],\ b[51]\},$$

$$group(1) = \{b[2],\ b[3],\ b[52],\ b[53]\},\ \ldots$$

$$group(49) = \{b[148],\ b[149],\ b[198],\ b[199]\}.$$

Each $group(k)$ is mapped to the DCM constellation in Figure 2-18. Then, the resulting $\{d_I[k],\ d_Q[k],\ d_I[k+50],\ d_Q[k+50]\}$ values are normalized to $1/\sqrt{10}$. Because each group is mapped to two 16-QAM constellations, it will be represented in the frequency domain in two places. Indices k and $k + 50$ provide about 200 MHz spacing between the two frequency domain representations of the input group bits. The probability that the both parallel tones will both experience a deep fade at the receiver is small, so some performance gain is realized [29].

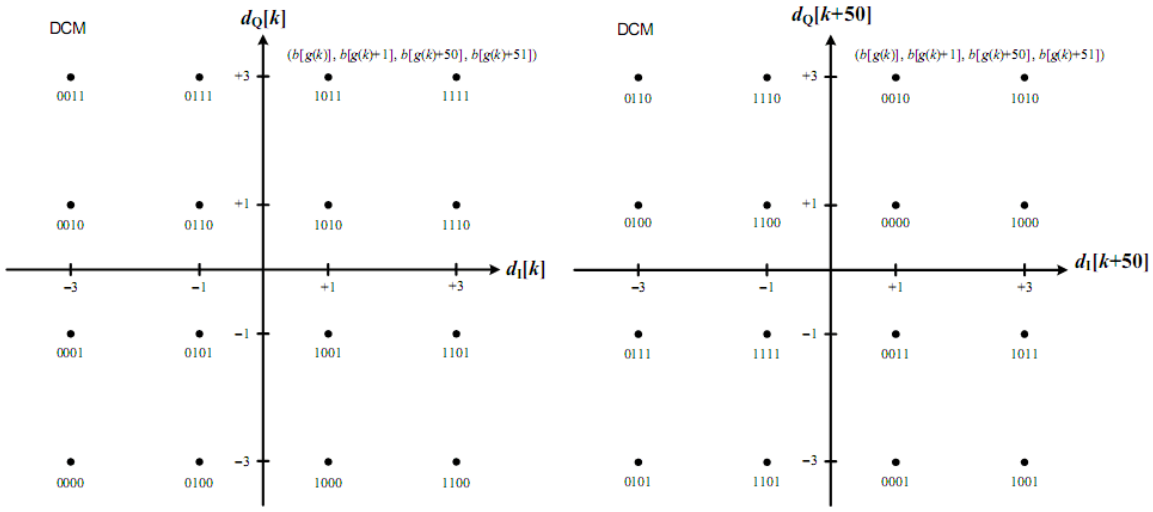

Figure 2-18: Dual 16-QAM constellations used in DCM [4].

2.2.3.8 OFDM Modulator

Next, 100 symbols produced by the QPSK or DCM mappers, along with 28 pilot and guard carriers, are applied to a 128-point IFFT device to produce an OFDM time-domain symbol. The frequency-domain carriers are assigned are as shown in Figure 2-12. The OFDM symbol has duration 242.42 ns and is appended by the ZPS of 70.28 ns. The sampling frequency is 528 MHz, so the OFDM output and ZPS last 128 periods and 37 periods, respectively. Overall, the symbol has duration 312.5 ns, yielding a rate of 3.2 MHz.

Before the IFFT output is applied to the DAC and then the antenna, it is mixed with the center frequency of the current band. The center frequency is specified by the band hopping sequence of the TFC. To successfully implement the hopping sequence, a synthesizer is needed that can switch frequencies and stabilize within the time allotment of the ZPS.

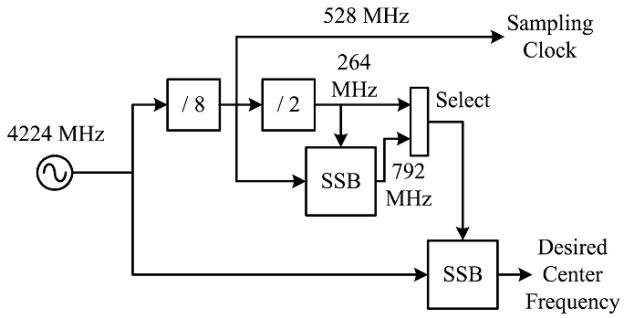

Figure 2-19: Example synthesizer architecture for Band Group 1 that can switch between frequencies within a few nanoseconds [30].

An example architecture of such a synthesizer for Band Group 1 operation is shown in Figure 2-19. Batra et al. report that a simulated switching time of 2 ns has been observed for this synthesizer [30]. It produces the 528 MHz sampling clock for the IFFT

and the center frequencies for bands 1, 2, and 3 using a 4,224 MHz oscillator. For band 1, the center frequency of 3,432 MHz is obtained by mixing 4,224 MHz with 792 MHz. For bands 2 and 3, the center frequencies of 3,960 MHz and 4,488 MHz, respectively, are obtained by beating 4,224 MHz with 264 MHz. Although not described in the paper, further frequency selection is necessary to separate the 3,960 MHz and 4,488 MHz frequencies for use and to attenuate spurious tones from the SSB mixer [31]. Another synthesizer design is described in [31].

2.2.3.9 Receiver Sensitivity

The WiMedia UWB standard says very little about the implementation of the receiver. It does specify the minimum receiver sensitivity level for each data rate profile in an AWGN channel, though. The sensitivity values given in Table 2-5 assume a noise figure of 6.6 dB referenced at the antenna, 2.5 dB implementation loss, and 3 dB margin.

Table 2-5: Minimum receiver sensitivities for WiMedia Band Group 1 [4].

Data Rate (Mbps)	Minimum Receiver Sensitivity (dBm)
53.3	-80.8
80	-78.9
106.7	-77.8
160	-75.9
200	-74.5
320	-72.8
400	-71.5
480	-70.4

Compared to narrowband systems, UWB requires very little margin [32], [33]. It is common to encounter margins of 20-30 dB in narrowband systems in order to combat frequency-selective fading [34]. A disadvantage of having a large margin is that transmit

power is wasted during the times it is not needed. The wideband nature of UWB helps it resist the ill effects of fading [32], [35], [36]. Therefore, it requires much less margin, and subsequently, less excess transmit power. This allows a greater link distance for a given receiver sensitivity. More on the subject of UWB fading and channel modeling is discussed in Chapter 5.

2.2.4 Worldwide Compliance

The United States led the world in permitting unlicensed UWB operation when the FCC amended the Part 15 rules in 2002 [1]. Other countries have followed suit, however none has allowed the use of the full 3.1 to 10.6 GHz spectrum as the US has. Figure 2-20 shows the availability of WiMedia bands currently in the world. Some of the WiMedia bands are unavailable due to existing services in certain areas, and some bands are allowed as long as the UWB device has detect-and-avoid (DAA) capability, meaning that it is capable of notching out its signal to avoid interfering with existing narrowband services in the band. DAA helps UWB coexist autonomously by operating in the "empty space" around narrowband systems. This type of cognitive-radio technique will likely become more common or even essential in the future as greater numbers of wireless devices must share the frequency spectrum.

As countries allocated spectrum for UWB, it was apparent that none of the original five WiMedia band groups would be fully available worldwide. Having a common band group is important for the success of UWB products. WiMedia devices using the first band group are not allowed to use TFCs using band 1 in Japan and band 1 or 2 in China. WiMedia recognized that defining another band group composed of bands

9, 10, and 11 would provide worldwide compatibility, so it created Band Group 6 in version 1.2 of MB-OFDM.

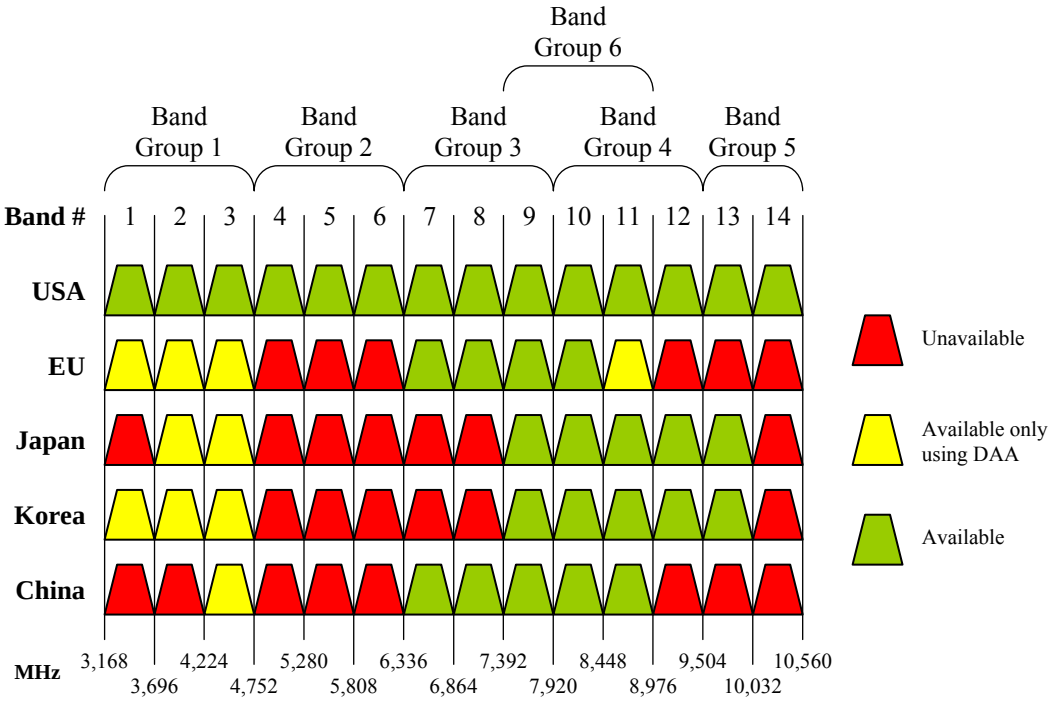

Figure 2-20: Regional availability of WiMedia bands.

2.3 Coexistence Concerns

When the FCC opened the UWB spectrum in 2002, it did not raise the level of permissible unintentional radiation; it simply allowed intentional UWB emissions to be radiated at the same power level that was previously allowed only for unintentional radiation. Outside the UWB operating band, the EIRP limits for intentional emissions were set significantly lower in an effort to protect sensitive systems like GPS, wireless local area networks (WLANs), cellular telephone systems, and WiMax.

Experts are unsure how the widespread use of UWB will affect GPS once it has been widely distributed [5], [6], [7], [8]. An extensive report regarding the coexistence of

UWB and GPS was published by the National Telecommunications and Information Administration (NTIA) in February 2001 [12]. While its conclusion was that the GPS receivers of the time were mostly tolerant of dithered I-UWB signals, the NTIA acknowledged that GPS performance could easily be degraded as the number of nearby UWB sources increased. For some types of UWB, namely those with a pulse repetition frequency that is significantly higher than the bandwidth of the victim GPS receiver, the interference can be modeled as AWGN [6], [37]. Otherwise, modeling the interference is more complicated.

Within the UWB band, FCC rules permit the EIRP of an intentional UWB emission from a handheld device to be no greater than -41.3 dBm per 1 MHz bandwidth [20]. The spectral masks for the other types of UWB devices are provided in Appendix A. Disregarding the duty cycle of the transmission, this translates into a maximum power output of -14.3 dBm across the 122 active carriers in MB-OFDM. In the GPS band, the FCC imposes a stricter limit of -75.3 dBm/MHz, as seen in Table 2-6. Though the power level is significantly reduced, a UWB device can still theoretically erode the margin of a GPS receiver if the antennas are placed too close to each other.

Table 2-6: FCC radiated emission limits for handheld UWB devices [20].

Frequency (MHz)	EIRP (dBm/1 MHz)
960-1,610	-75.3
1,610-1,990	-63.3
1,990-3,100	-61.3
3,100-10,600	-41.3
Above 10,600	-61.3

Let us calculate the power of the interference that might reach the GPS receiver if the two devices are separated by some distance. The Friis equation is commonly used in

narrowband systems when the receiver is located at a known distance, line-of-sight from the transmitter with negligible multipath.

$$P_r = P_t G_r G_t \left(\frac{\lambda}{4\pi R} \right)^2 \tag{2-6}$$

Here, P_r is the incident power in Watts; P_t is the effective isotropic radiated power in Watts; G_r is the gain of the receiving antenna; G_t is the gain of the transmitting antenna; λ is the wavelength in meters; and R is the separation distance in meters. In this case, the GPS unit is the victim receiver, and the UWB source is the offending transmitter. Let us assume that the interference is Gaussian and that both antennas have unity gain for simplicity.

We will also assume that the bandwidth of the GPS receiver is 1 MHz. If the UWB device radiates at a uniform power of -75.3 dBm in the GPS bandwidth, we can calculate the distance between the devices when the incident power equals that of the thermal noise power. We calculate the thermal noise power using

$$P_N = kTB, \tag{2-7}$$

where P_N is the noise power in Watts; k is Boltzmann's constant, 1.38E-23 J / K; T is the absolute temperature in Kelvin; and B is the bandwidth in Hertz. We assume an ambient temperature of 290 Kelvin and a bandwidth of 1 MHz. This yields a noise power of 4.00E-15 Watts, which is -114 dBm. When the incident power of (2-6) equals the noise power of (2-7), the noise floor has risen 3 dB in this bandwidth. It can also be said that the sensitivity of the GPS receiver has been degraded by 3 dB. By solving (2-6) for R, the separation distance between transmitter and receiver can be calculated as 1.3 meters. For any distance less than 1.3 meters, the sensitivity degradation is greater than 3 dB. This

result suggests that a UWB transmitter at the FCC limits would interfere significantly with (jam) a co-located GPS receiver.

Recognizing the sensitivity of GPS and cellular telephone systems, WiMedia suggests even stricter EIRP limits for UWB emissions. Conformance to the limits shown in Table 2-7 is not required to achieve certification, but it is recommended to minimize interference when UWB, GPS, and cellular devices are operated in close proximity. If we repeat our analysis using WiMedia's recommended limit of -84.7 dBm/MHz in the GPS band, we find that the 3 dB jamming distance is reduced from 1.3 meters to 0.44 meters.

Table 2-7: Out-of-band emission limits recommended by WiMedia [4].

Frequency (MHz)	Recommended Emission Limits (dBm/MHz)
869-894	-83.3
925-960	-82.5
1,570-1,581	-84.7
1,805-1,880	-76.8
1,930-1,990	-76.2
2,110-2,170	-75.4

The FCC limit at 1,575 MHz for unintentional emissions remains at -41.3 dBm/MHz, which is 34 dB higher than the limit for intentional UWB emissions. Consequently, unintentional emissions radiated from the UWB circuitry could cause more GPS jamming problems than emissions radiating from the UWB antenna. Any device, UWB or otherwise, with unintentional emissions at the FCC limit of -41.3 dBm/MHz in the GPS band would sufficiently block GPS reception. This is an "old" problem faced by GPS manufacturers who develop devices using microprocessors, Bluetooth radios, and switching power supplies which generate interference. Therefore, we believe that careful circuit board routing is essential to avoid self-jamming when a

UWB radio is co-located with a GPS receiver. In the next chapter, we investigate the intentional and unintentional emissions emanating from a commercially-available WiMedia UWB device and actually measure their impact upon the CNR performance of a consumer GPS receiver in an anechoic chamber.

Chapter 3

Measured Emissions of a Commercial UWB Device

As mentioned previously, the UWB operating band extends from 3.1 GHz to 10.6 GHz. Intentional UWB emissions are limited by the FCC to -41.3 dBm/MHz in this band and even lower levels outside the band, depending on frequency. Emissions are restricted most heavily at 1,575 MHz, the GPS L1 band, to EIRP levels of -75.3 dBm/MHz. While it was intended that these restrictions be sufficient to protect sensitive services like GPS, our analysis shows that a UWB transmitter can theoretically jam a GPS receiver from a distance of 1.3 meters if the power density of its emissions at 1,575 MHz is equal to the FCC limit. Even worse for GPS performance could be the unintentional emissions from the UWB circuitry which can be as strong as -41.3 dBm/MHz. Since circuit board routing has much to do with unintentional emissions, let us assume that unintentional emissions can be limited through careful design of a UWB and GPS product.

Having recognized the potential problem for UWB and GPS coexistence, our next step in this project was to actually measure the emissions of a WiMedia UWB device and then evaluate the impact they had on GPS performance. In this chapter, we present measured emissions data in the GPS L1 band from a commercial UWB device and compare them to emissions from a USB flash drive. The results indicate that the emissions from the UWB device are stronger than those from the flash drive and that unintentional emissions from the processors and digital circuitry are significantly stronger than those emanating from the UWB antenna. Despite relatively low levels of emissions from the antenna, we recognize that they do raise the noise floor at 1,575 MHz and therefore could degrade GPS performance if they were coupled directly into the GPS receiver. Finally, we conclude from GPS testing in an anechoic chamber that the total emissions from a nearby UWB device degrade the sensitivity of the GPS receiver by approximately 1 dB—much less than the theoretical worst-case value of 20 dB.

3.1 Evaluated UWB Device

At the beginning of this project, only one UWB product was commercially available in the United States: the Belkin Cable-Free USB Hub (shown below). We obtained two such devices for testing. Since that time, numerous other UWB products have been released, including some other USB hubs and high-end laptops. Appendix C provides a list of commercial products known to use UWB at the time of this writing.

Figure 3-1: Belkin Cable-Free USB Hub system (purchased March 2007).

The Belkin Cable-Free USB Hub is designed to provide wireless USB 2.0 connectivity from a computer dongle to a remote hub. Figure 3-1 shows the relative sizes of the hub and dongle. A "wall wart" power supply is required by the hub, but it is not pictured. The smaller dongle plugs into a host desktop or laptop computer with USB, and the hub accepts up to four wired USB devices such as disk drives, cameras, media players, and printers.

The dongle and hub communicate wirelessly via the WiMedia Common Radio Platform (described in Section 2.2.3) to create a Hi-Speed USB link between the computer and remote devices. The printed product guide included with the system reports that this system operates only in Band Group 1 and that it can use only five of the ten possible TFCs. Although the WiMedia standard defines five additional band groups, this device and many other early UWB products have likely used only Band Group 1 in order to decrease costs and expedite product deployment.

3.1.1 Selectable Data Rates of the Device

A configuration program included with the hub allows the user to select a PHY data rate or choose an "auto" option that lets the system select the highest data rate for the quality of the link. The system supports all eight of the WiMedia data rate profiles: 53.3, 80, 106.7, 160, 200, 320, 400, and 480 Mbps. According to the printed guide, the highest data rate can be achieved only when the hub and dongle are separated by less than one or two meters. The guide claims that connectivity is possible for distances up to twenty meters, although at reduced data rates.

In operational tests, we were unable to maintain a link beyond about five meters, depending on the environment. Additionally, we found that the maximum throughput of the system is about 20 Mbps and verified that it can only be achieved at close distances with no clutter between the transmitter and receiver. We suspect that implementation limits of the wired USB protocol over UWB contribute to the lower-than-expected rate. The theoretical throughput limit for legacy USB over UWB is about 80 Mbps [2]. For wireless high definition video, a recent report [38] shows that a WiMedia chipset optimized for video streaming can offer excellent performance (over 100 Mbps actual throughput) in real-world tests. More information about our data rate tests is provided in Chapter 6.

3.2 Configuration of Measurement Equipment

To measure the emissions that would be seen by a GPS receiver, we created a special test receiver with a low noise figure. Our test receiver consisted of three parts: 1) an antenna, 2) a low-noise amplifier (LNA) module, and 3) a spectrum analyzer with an internal pre-amp. After assembling the test receiver, we configured the UWB system as

shown in Figure 3-2. A USB 2.0 flash drive was plugged into the UWB hub to serve as a data source/sink. Then we moved the antenna of the test receiver over and around the UWB system, looking for sources of emissions and saving screenshots on the spectrum analyzer.

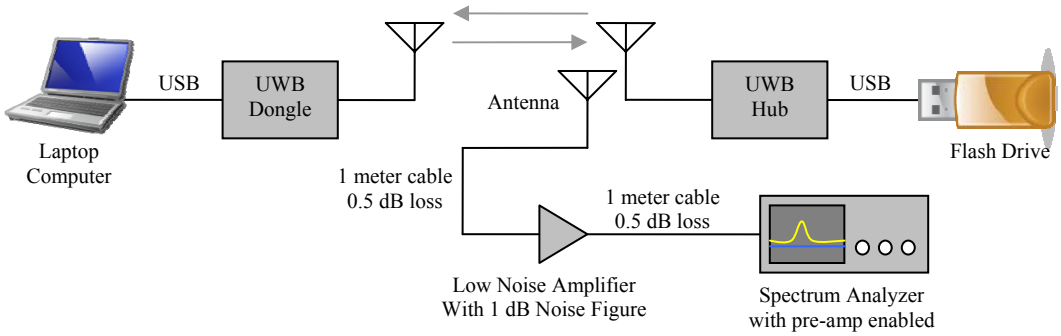

Figure 3-2: Test Configuration.

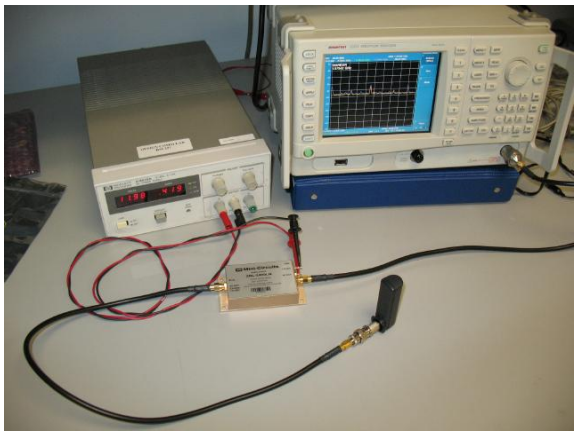

Figure 3-3: Measurement system used in GPS L1 interference measurements.

We used a Mini-Circuits ZRL-2400LN+ LNA as the front end amplifier. The ZRL-2400LN+ has a published noise figure of 1.0 dB and typical gain of 27 dB at 1,575 MHz. The upper frequency limit of the ZRL-2400LN+ is specified at 2,400 MHz, so we did not use this LNA for taking measurements in the UWB operating band. For measurements from 2 to 6 GHz, we used two Mini-Circuits ZX650-6013E+ amplifiers in

a cascade configuration. The ZX650-6013E+ amplifier has a published noise figure of 3.3 dB and typical gain of 12-15 dB across the band.

3.2.1 System Noise Figure

The overall sensitivity and noise figure of the test receiver depends heavily upon the noise figure and gain of the LNA. The LNA must provide gain that is significantly greater than the noise figure of the spectrum analyzer in order to provide meaningful results. Using the hot/cold (Y-Factor) method [39], we verified the published noise figure of the ZRL-2400LN+ amplifier and then calculated the noise figure of the complete test receiver by adding 0.5 dB to account for the loss in the first cable.

The first step was to measure the LNA's gain. Using a network analyzer in S21 mode, we found gain G_1 of the LNA to be 29 dB at 1,575 MHz. We found that the combined loss of the two coaxial cables used in this experiment is about 1 dB, so we reduced G_1 to 28 dB to account for this loss. Turning to the spectrum analyzer, we enabled its input pre-amp, set the attenuator to 0 dB, and set the resolution bandwidth to 1 MHz. We observed the noise power N_{o2} to be -102.5 dBm, (5.62E-14 Watts) when the analyzer's input was terminated with 50 ohms. Next, we powered the LNA with a 12 volt supply and connected it to the spectrum analyzer. The noise power N_{o12} was measured to be -87.6 dBm (1.74E-12 Watts). The difference in the noise levels at the analyzer when we terminated the input and then connected the LNA was about 15 dB. Therefore, we confirmed that the LNA provides enough gain to sufficiently overcome the noise figure of the spectrum analyzer. The noise factor F_2 of the analyzer was computed to be 14.0 using

$$F_2 = \frac{N_{o2}}{kT_0B}, \tag{3-1}$$

where the denominator represents the noise power in Watts; k is Boltzmann's constant, 1.38E-23 J / K; T_0 is the absolute temperature in Kelvin; and B is the bandwidth in Hertz. We assumed an ambient temperature of 290 Kelvin and noise bandwidth of 1 MHz. The noise figure NF_2 of the analyzer was found to be 11.5 dB using

$$NF = 10\log_{10}(F). \tag{3-2}$$

Next, we connected the HP 346B noise source to the input of the LNA as shown in Figure 3-4. While the noise source was off, we measured the "cold" noise power N_C to be -87.6 dBm (1.74E-12 Watts) at the spectrum analyzer. Then we powered up the noise source and measured the "hot" noise power N_H to be -73.5 dBm (4.47E-11 Watts). Using the hot and cold noise power values, we computed the Y factor as

$$Y = \frac{N_H}{N_C} \tag{3-3}$$

with Y being to equal 25.7.

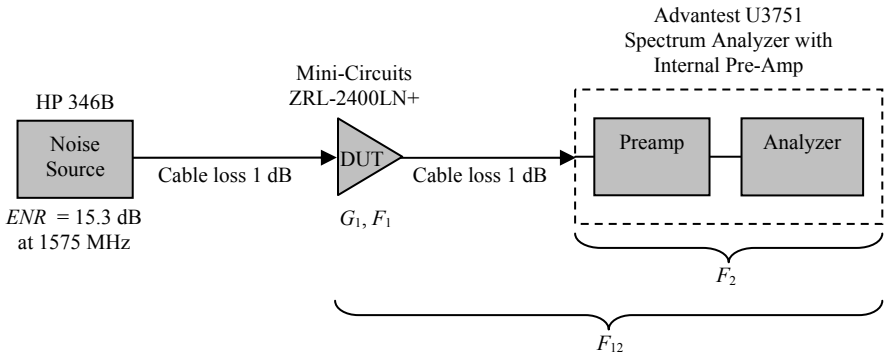

Figure 3-4: Measuring the noise figure of the LNA and the combined system.

Assuming the "cold" temperature of the noise source was equal to the ambient temperature T_0 used in (3-1), we calculated the noise factor F_{12} of the combined system with

$$F_{12} = \frac{ENR - 1}{Y - 1}, \tag{3-4}$$

where Y is the factor calculated in (3-3) and ENR is the excess noise ratio, interpolated as 15.3 dB from data provided on the label of the noise source. F_{12} was found using (3-4) to be 1.27, which corresponds to an overall system noise figure NF_{12} of 1.0 dB. Finally, we solved the classic cascade equation

$$F_{12} = F_1 + \frac{F_2 - 1}{G_1} \tag{3-5}$$

for the noise factor F_1 to obtain a final noise figure value of 1.0 dB for the LNA, which agreed with the datasheet's published value. Overall, we calculate the noise figure of the entire test receiver to 1.5 dB, which would be comparable to that of a very good GPS receiver.

Using the method outlined in this section, we then evaluated the two Mini-Circuits ZX650-6013E+ amplifiers to be used in the 2-6 GHz measurements. We found that their cascaded gain is 25 to 30 dB, depending on frequency, and their cascaded noise figure is 4.0 dB.

3.2.2 Measurement of Antenna Characteristics

Once we had measured the noise figures of the LNAs, we then evaluated three antennas that would be used in the interference measurements. For measurements in the GPS band at 1,575 MHz, we used a quadrifilar helix antenna that is typical of those

antennas found on some consumer GPS receivers (shown in Figure 3-5). For wider measurements spanning from 1 to 2 GHz, we used a log-periodic dipole array (LPDA) antenna that is designed to operate between 900 MHz and 2.6 GHz. For wideband measurements in the 2 to 6 GHz range, where UWB systems transmit, we used a smaller LPDA that is designed to operate from 2 to 11 GHz. Both LPDAs are shown to-scale in Figure 3-6.

Figure 3-5: Quadrifilar helix antenna used for GPS-band interference measurements.

Figure 3-6: LPDAs used in wide-band interference measurements.

3.2.2.1 Quadrifilar Helix Antenna Characterization

To assess the level of interference seen in the GPS band, we used the quad helix antenna. It is designed to receive right-hand circularly polarized (RHCP) GPS signals at 1,575 MHz. The quad helix antenna, the ZRL-2400LN+ LNA, and the spectrum analyzer functioned as our high-sensitivity GPS test receiver.

We measured the approximate frequency response of the quad helix antenna using the large LPDA and a network analyzer. It was previously determined that the response of the large LPDA was roughly flat from 1 to 2 GHz using an S21 measurement of two identical antennas. When using the LPDA to measure the response of the quad helix, the two antennas were pointed at each other and separated by a distance of about 30 centimeters—longer than one wavelength at 1,575 MHz. Then the network analyzer was placed in S21 mode, and the plot of Figure 3-7 was obtained. Assuming that the response of the LPDA is flat from 1 to 2 GHz, the variations in the S21 response can be attributed to the quad helix antenna. The peak response of the quad helix was found to be 1,562 MHz, and the 3 dB bandwidth extended from 1,538 to 1,577 MHz. The measured 3 dB bandwidth can be seen in Figure 3-8.

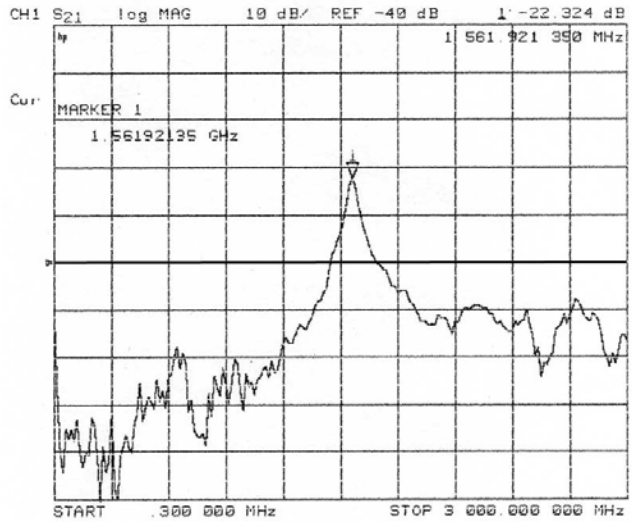

Figure 3-7: Approximate wideband frequency response of quadrifilar helix antenna. S21 measurement made using quad helix antenna and log-periodic antenna with a separation distance of 30 cm. Start: 300 KHz. Stop: 3 GHz.

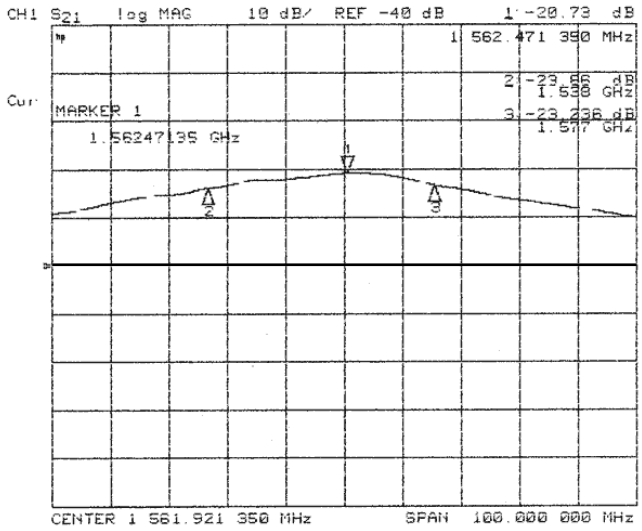

Figure 3-8: Approximate 3 dB bandwidth of quadrifilar helix antenna. S21 measurement made using quad helix antenna and log-periodic antenna with a separation distance of 30 cm. Center: 1,562 MHz. Span: 100 MHz.

Once we had confirmed that the quad helix antenna's response covered the center of the GPS L1 band, we measured its gain pattern in a small anechoic chamber. Figure

3-9 shows the test configuration. The quad helix antenna was placed at one end of the chamber, and a dipole antenna tuned to 1,575 MHz was placed at the other end. The antennas were spaced 30 centimeters apart. The dipole was connected to a signal generator which produced a 1,575 MHz tone, and the quad helix was connected to a spectrum analyzer which displayed the power of the received signal. We rotated the quad helix about its BNC connector in ten-degree increments. After normalizing the received power values to 0 dB, we obtained the gain pattern shown in Figure 3-10.

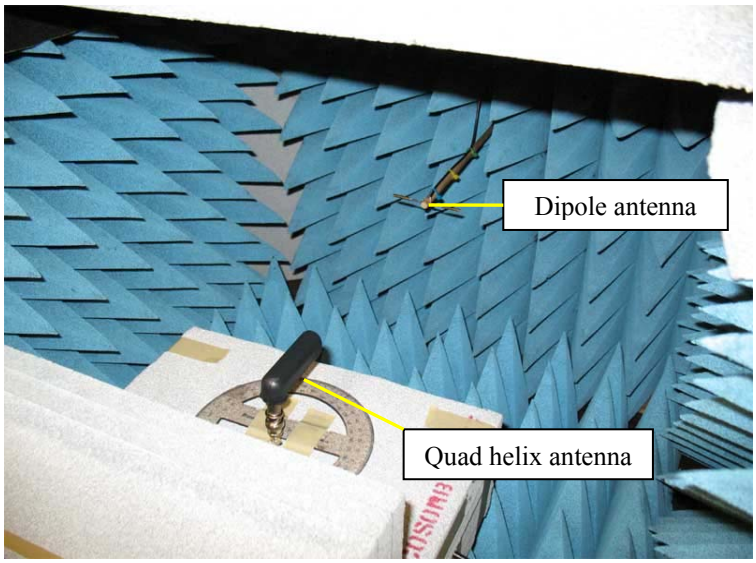

Figure 3-9: Anechoic foam chamber used in gain pattern measurements of quadrifilar helix antenna.

This quad helix antenna has several properties to optimize it for receiving GPS signals. First, it has a fairly wide gain pattern, as seen in the figure below. Its 3 dB beamwidth is approximately 90°, and its 10 dB beamwidth is about 160°. This allows it to receive GPS signals from satellites that are distributed throughout the sky. Second, it has a respectable front-to-back ratio of 16 dB. Assuming that the antenna is oriented upward, it is much more sensitive to signals arriving line-of-sight (LOS) from the

satellites than it is to non-line-of-sight (NLOS) signals bouncing off the ground. Also, its helical construction optimizes it to receive signals that are right-hand circularly polarized (RHCP) but not those that are left-hand circularly polarized (LHCP). LOS GPS signals arrive at the antenna as RHCP, and their polarization is reversed each time they are reflected. Since the signal loses energy each time it is reflected, the first reflection is usually the strongest. We did not expect to receive polarized emissions from the UWB system. Therefore, we did not verify the antenna's sensitivity to polarization.

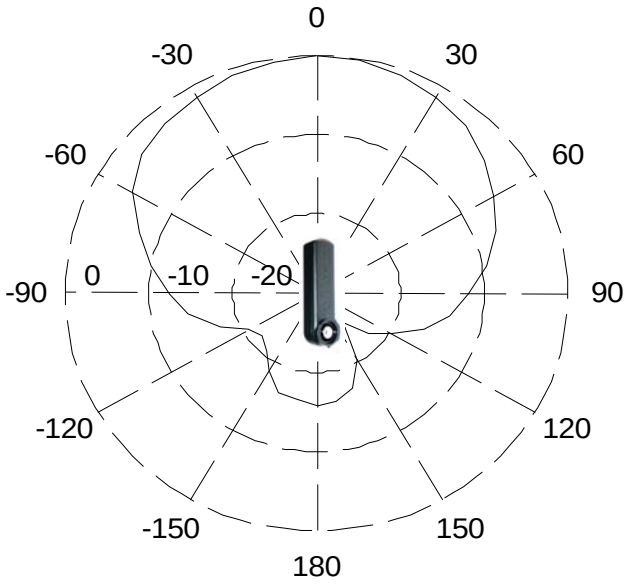

Figure 3-10: Measured gain pattern of the quadrifilar helix antenna used in interference assessments. Pattern measured at 1,575 MHz.

Since the gain pattern of the quad helix antenna is so wide, we determined that emissions measurements would need to be taken in the antenna's near field, close to the signal source. A distance of one centimeter was selected to minimize the contributions from adjacent signal sources.

3.2.2.2 LPDA Characterization

The return loss of each LPDA was measured and found to be 10 dB or better throughout its specified operating range. The larger antenna had an operating range from 1 to 2 GHz, and the smaller antenna had an operating range from 2 to 11 GHz. For narrowband signals, the relevant elements of the LPDA function like a Yagi-Uda antenna that has only a few elements. However, we have conservatively assumed that the gain in the forward direction is 2 dB over the isotropic case, which is like a dipole.

3.3 Measuring Emissions from the UWB System

During preliminary measurements of the UWB system, we noticed that emission levels changed depending on the level of activity by the system. In particular, it was observed that transferring a large file (roughly 109 MB) from a flash drive plugged into the hub to the computer raised the noise floor at 1,575 MHz by several decibels. In order to keep straight the emission levels generated for the different states of the UWB system, several naming conventions were applied. The *baseline state* was considered to be the unpowered state where the only signals received by the measurement system were from the surrounding environment. The baseline level was determined by *kTB*, our 1.5 dB noise figure, and interference from nearby equipment. We did not conduct these measurements in an anechoic chamber, so some interfering tones from nearby equipment can be seen in the spectral plots.

Once the UWB system was connected and powered but not transferring any file data, its state was called the *idle state*. Some spectral activity was observed in this state, as the UWB system likely checks the link quality periodically and the wired USB protocol polls connected devices. When the system actively transferred a file from the

flash drive to the computer, its state was called the *transferring state*. This was the state in which the greatest emission levels were seen. We expected that data flow over USB contributed some of the emissions, so we connected the flash drive directly to the computer to serve as a reference.

Since the FCC differentiates between the emissions from the antenna and the circuitry, we investigated both sources for potential GPS L1 interference. For intentional UWB antenna transmissions, the EIRP limit is -75.3 dBm/MHz in the GPS band. For unintentional emissions coming from the non-RF circuitry, including the UWB MAC chip, the classic Part 15 limit of -41.3 dBm/MHz applies.

3.3.1 Emissions from the USB Cable

Measurements were taken close to the USB cable connecting the computer and the flash drive in order to quantify the emissions levels generated purely by USB data flow (configuration diagram shown in Figure 3-11). For these measurements, the quadrifilar helix antenna was held one centimeter above the USB cable. The baseline measurement was taken with the USB cable unplugged from the computer. The idle measurement was taken with the flash drive connected to the computer but not transferring a file. The transferring measurement was taken while copying a large file from the flash drive to the computer.

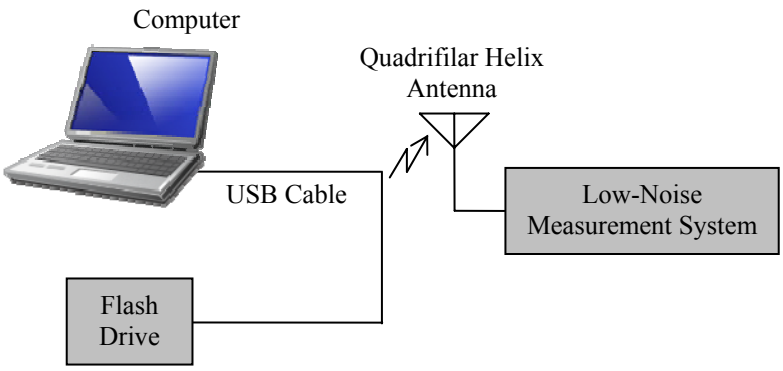

Figure 3-11: Configuration for USB cable emission measurement.

As shown in the spectrum plots of

Figure 3-12, USB data flow caused the noise floor to rise about 4 dB while a file transfer was in progress. This showed that emissions from a USB cable during a Hi-Speed USB data transfer alone could create significant GPS interference.

A) B)

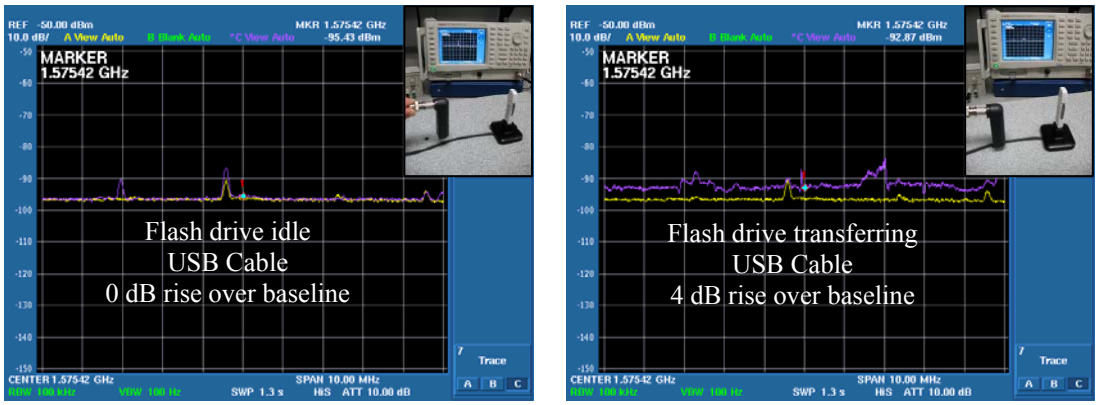

Figure 3-12: Emissions levels from USB cable in idle and transferring states. Bottom trace represents baseline state in both graphics, top/superimposed trace represents idle state in A), and top trace represents active state in B). Antenna height: 1 cm above USB cable. Span: 10 MHz.

3.3.2 Emissions from the Circuitry

Emissions generated by the circuitry of the UWB dongle and hub were investigated and compared to those from a flash drive. In the flash drive measurement, the quad helix antenna was placed one centimeter away from the flash drive at the point of maximum interference.

For the UWB dongle measurement, the quad helix antenna was placed one centimeter above the Wisair 502/531 UWB chipset. For the UWB hub measurement, the quad helix antenna was placed one centimeter above the Wisair 502/531 UWB chipset and the main processor. The baseline state was obtained with the devices unplugged. The idle state was obtained when the devices were plugged in but were not transferring any files. The transferring state was obtained while copying a large file from the flash drive to the computer, whether the flash drive was connected directly to the computer or to the UWB hub.

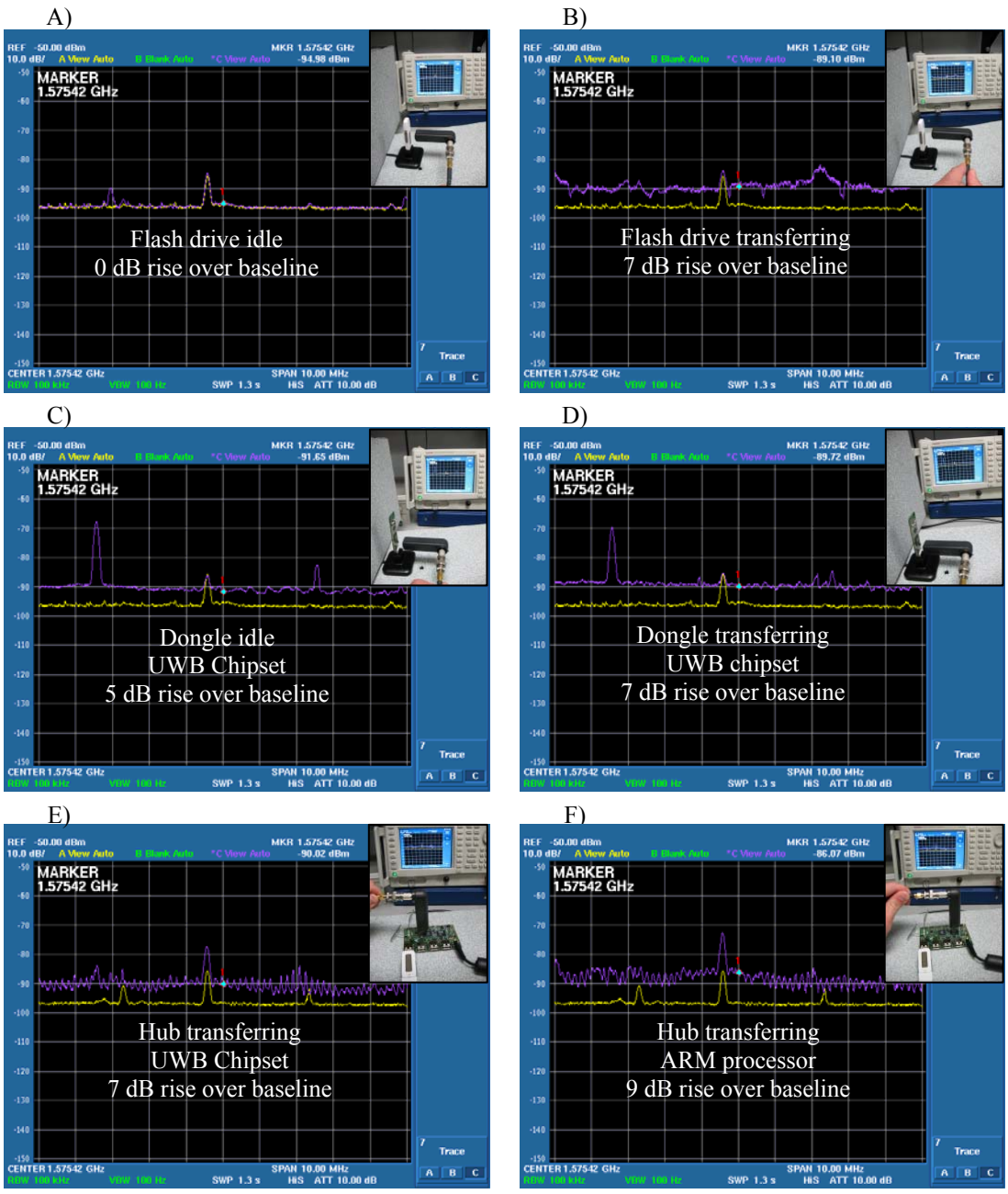

Figure 3-13: Emission levels at GPS L1 created by circuitry of flash drive, dongle, and hub for idle and transferring states. Antenna spacing: 1 cm. Span: 10 MHz.

Figure 3-13 shows the spectrum plots for the flash drive and UWB dongle circuitry in the idle and transferring states. The spiked pattern observed in some of the plots is believed to be the result of the interaction of the pulsed UWB transmissions (OFDM symbol rate of 3.2 MHz) with the sweep time of the spectrum analyzer.

Decreasing the sweep time widened the spikes, and vice versa. In the idle state, the flash drive generated negligible emissions, but emissions from the dongle raised the noise floor by 5 dB. Both devices generated similar emission levels, roughly 7 dB, once the file transfer commenced. Emissions from the circuitry of the UWB hub were measured using the same procedure. Measurements were taken above the hub's UWB chipset and ARM processor as shown in Figure 3-13 E) and F). Results for the measurements were similar to those from the dongle, but levels above the processor during the file transfer were slightly higher at 9 dB.

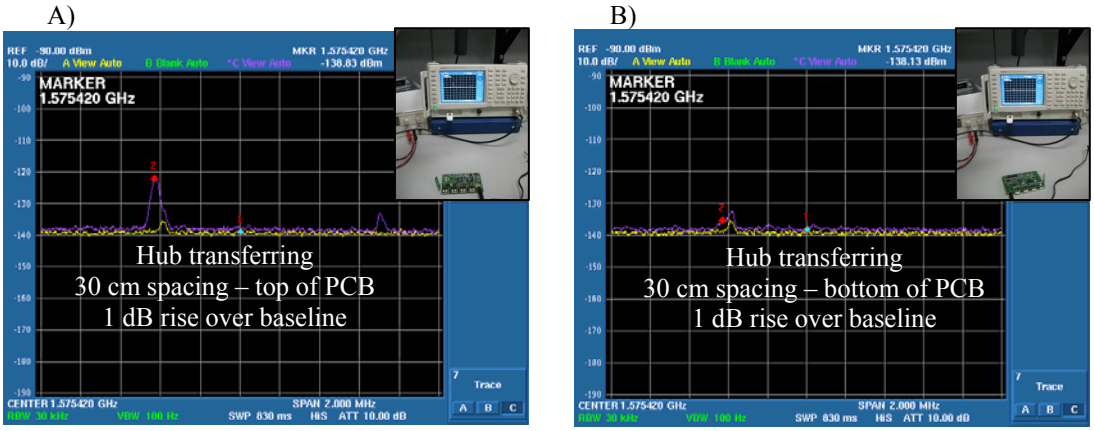

Figure 3-14: Emission levels at GPS L1 measured 30 cm from hub PCB. Span: 2 MHz.

We also measured the emission levels from the hub at a distance of 30 cm. As shown in Figure 3-14, the noise floor rises only about one decibel. In Figure 3-14 A), a spike at about 1,575.0 MHz can be seen. We are unsure about the source of this spike but believe it was radiated from nearby equipment, possibly from the computer. Previous baseline measurements with UWB equipment off recorded the same spike.

3.3.3 Emissions from the Antennas

We measured the emissions produced by the antennas of the UWB dongle and hub. The UWB antenna of the dongle was printed on the main PCB, while the two antennas of the hub were mounted separately and connected to the main circuit board by thin coaxial cables. Close-up photos of the antennas are shown in Figure 3-15.

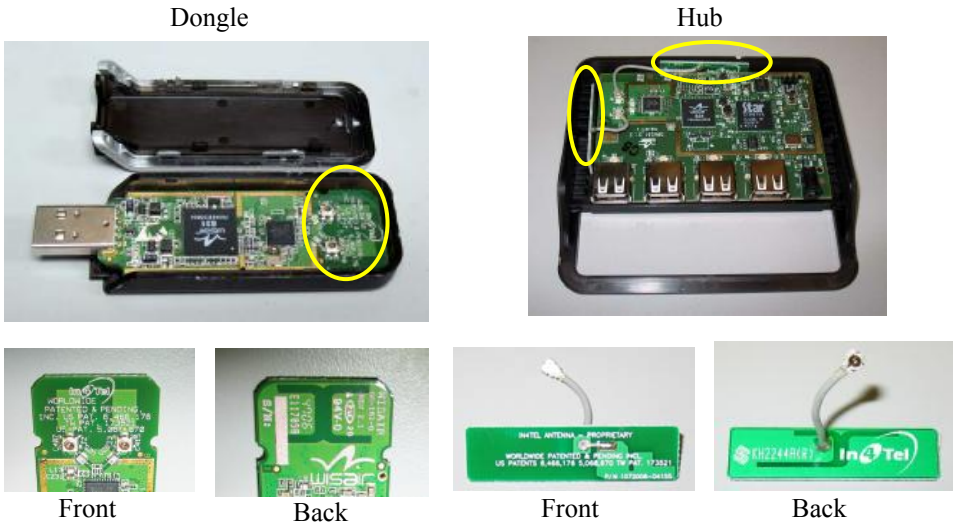

Figure 3-15: UWB antennas in the dongle and hub.

For the UWB dongle, the noise floor rose about 3 dB from the baseline state to the idle state (see Figure 3-16). When the file transfer commenced, the noise floor remained unchanged at about 3 dB above baseline. It is likely that radiation from the chipsets was also measured since the antenna is located on the same PCB.

For the UWB hub, no increase in emission levels was seen from the baseline state to the idle state. When the file transfer commenced, the noise floor rose about 2 dB. Figure 3-16 shows the levels of each state for comparison. We believe that some of the emissions for the dongle idle state likely originated at the chipset, not the antenna, so we consider the idle measurement from the hub to be more accurate.

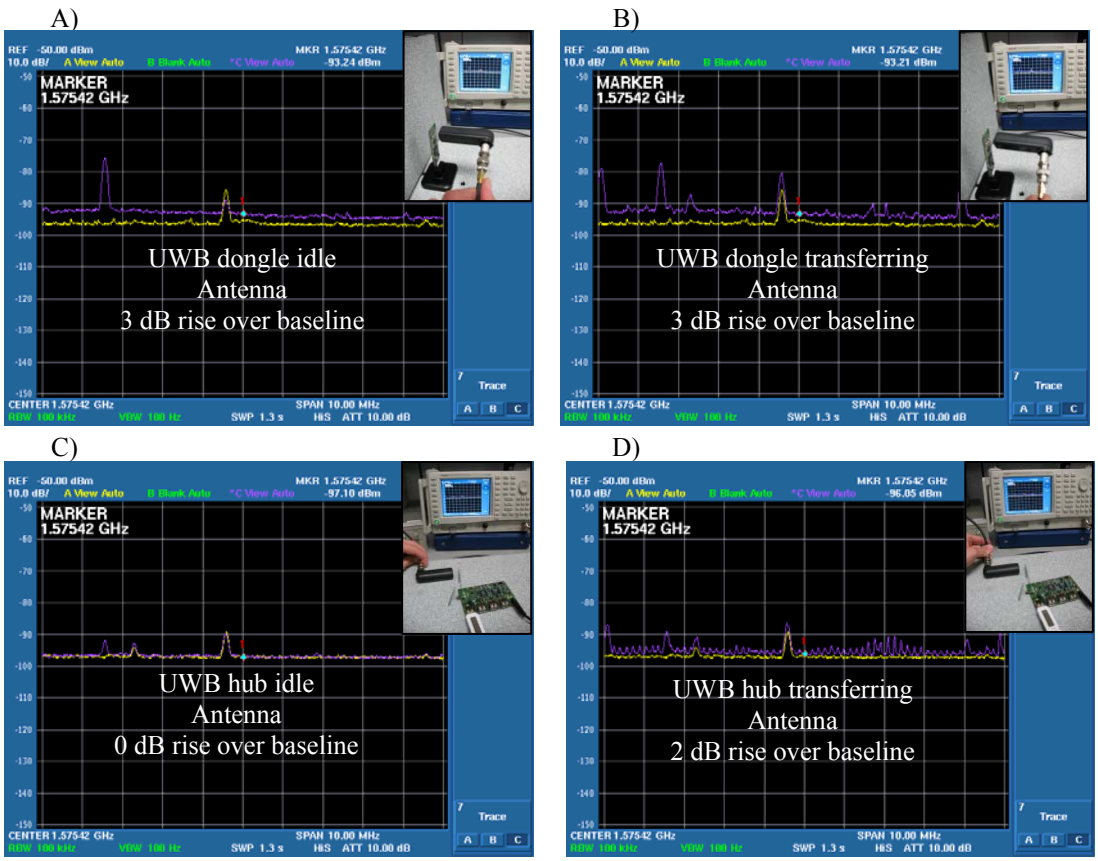

Figure 3-16: Emission levels at GPS L1 measured at the UWB antennas for idle and transferring states. Bottom trace represents baseline state in all graphics, top/superimposed trace represents idle or transferring state. Antenna spacing: 1 cm. Span: 10 MHz.

3.4 Summary of Measured Emissions

From our measurements of the USB cable and the flash drive, we observed that USB data flow produces significant emissions at 1,575 MHz. We also saw that the WiMedia UWB system produces emissions at 1,575 MHz, with the greatest source of emissions being the circuitry around the ARM processor of the hub. The UWB antennas produce some emissions, but not as much as the circuitry. Overall, emissions from the system appear to be well below the FCC guidelines for intentional UWB and unintentional radiation at GPS L1. However, they could still degrade the sensitivity of a nearby GPS receiver by several decibels, depending on the distance between the units.

Figure 3-17 shows the components of the UWB system that we measured, and Table 3-1 lists the amount in decibels that the noise floor rose for the active and transferring states over the baseline state at one centimeter spacing.

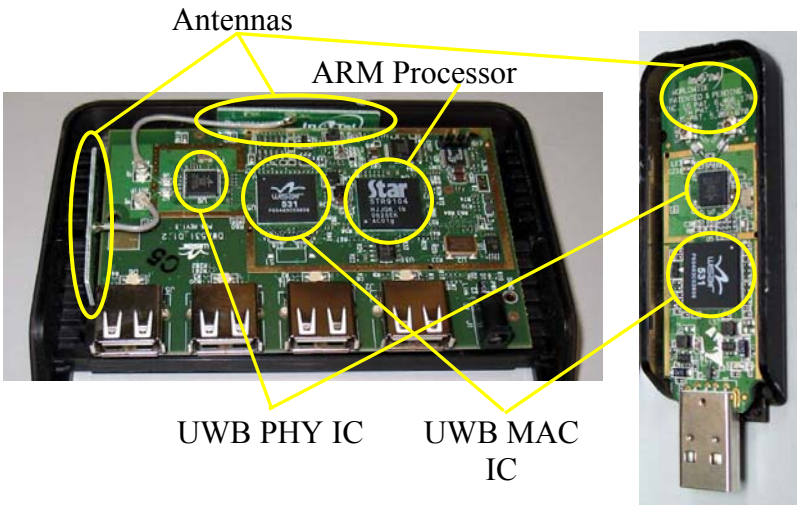

Figure 3-17: Emission measurement areas for hub and dongle.

Table 3-1: Noise floor rise over baseline state. All values in dB at 1,575 MHz.

	USB Cable	Flash Drive	Dongle UWB Chipset	Hub ARM Processor	Dongle Antenna	Hub Antenna
Idle	0	0	5		3	0
Transfer	4	7	7	9	3	2

The worst-case emissions at 1,575 MHz were found when the GPS antenna was placed one centimeter away from the ARM processor of the hub. At this location, the emissions level rose about 9 dB from the baseline state to the transferring state. From a distance of 30 centimeters, the noise floor rose only about one decibel. The emissions measured near the UWB chipset were about the same as the emissions measured near the flash drive and the rest of the hub's circuitry.

Many consumer GPS receivers have similar types of circuitry to the UWB hub (processor, memory, USB chipset), and we believe that a similar UWB chipset could be integrated into a GPS product using shielding over the UWB chipset. Careful layout of the PCB would also be important to minimize radiated interference.

3.5 Measured GPS Performance

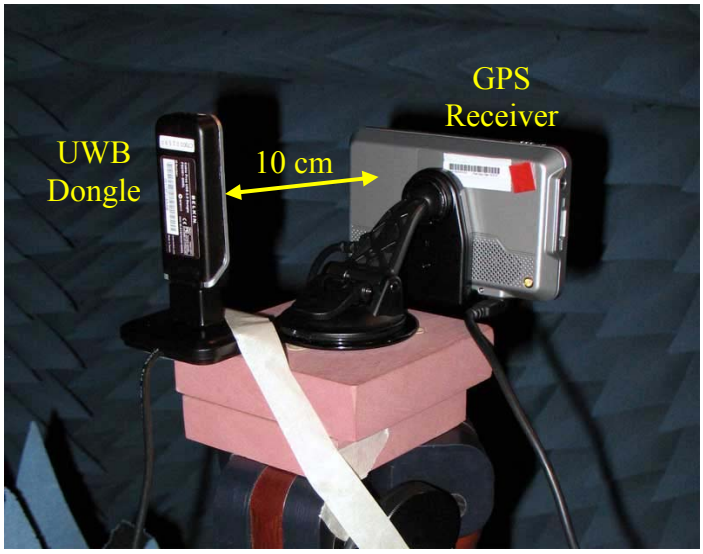

Figure 3-18: GPS and UWB physical proximity test.

To evaluate GPS performance in the presence of the UWB system, we set up the UWB dongle and a consumer GPS receiver at one end of an anechoic chamber as shown in Figure 3-18. The UWB dongle and GPS receiver were separated by 10 cm. The UWB hub was placed about a meter below the dongle and GPS device. We used the Belkin configuration program on the computer to verify that the link quality was poor (30-40%), thus ensuring that UWB output power would be maximal (i.e. not scaled down). A helical GPS reference antenna was mounted about four meters away at the other end of the chamber. The reference antenna, dongle, and GPS unit were aligned linearly, with the

dongle placed between the reference antenna and the GPS antenna of the nüvi. The reference antenna was fed from a GPS signal generator such that the power level of its signal at the nüvi was about -125 dBm. Then, we recorded the carrier-to-noise ratio (CNR), as measured by the nüvi, during the baseline, idle, and transferring states of the UWB system. The CNR was also measured with the dongle removed for the reference (no-shadowing) condition.

Table 3-2: Average change in GPS CNR relative to reference (no-shadowing) condition.

Dongle Baseline	Dongle Idle	Dongle Transferring
-1 dB	-2 dB	-2 dB

From the data in Table 3-2, we see that the physical shadowing of the UWB dongle decreases the GPS sensitivity of the nüvi by 1 dB. Once the UWB system is turned on, sensitivity is degraded by another decibel. There does not appear to be any change in GPS sensitivity from the idle state to the transferring state. This suggests that emissions from antennas are quite low and that most of the interference is radiated from the circuitry or the USB cable. Using the analysis in Section 2.3 with the spacing of 10 centimeters between the UWB emitter and the GPS receiver, we could expect a GPS sensitivity degradation of roughly 20 dB for a UWB emitter that operates at the FCC limit. Our measured degradation of 1 dB suggests that this particular UWB device operates well below the FCC limits or that our analysis is overly conservative when estimating GPS interference.

3.6 Verification of UWB Operation

To observe the RF spectrum of the UWB device, we connected one output of the hub directly to the spectrum analyzer and left the remaining antenna connected. During a file transfer, we observed Band Group 1 activity as shown in Figure 3-19. Band hopping at the OFDM symbol rate of 3.2 MHz can be seen in the plot as gaps in the spectrum. This is due to interaction of the analyzer's sweep with the hopping times. The actual spectrum in MB-OFDM is uniform across the bands. The power levels (roughly -50 dBm/MHz) are lower than the FCC limit because the system is employing power scaling. For situations where the link loss is greater, the system transmits at the maximum, time-averaged limit of -41.3 dBm/MHz. Second harmonic content of the Band Group 1 transmissions can be seen from about 6.5 GHz to 8.0 GHz. The out of band emissions likely extend past 8.0 GHz, but we were unable to view them due to the limit of the spectrum analyzer.

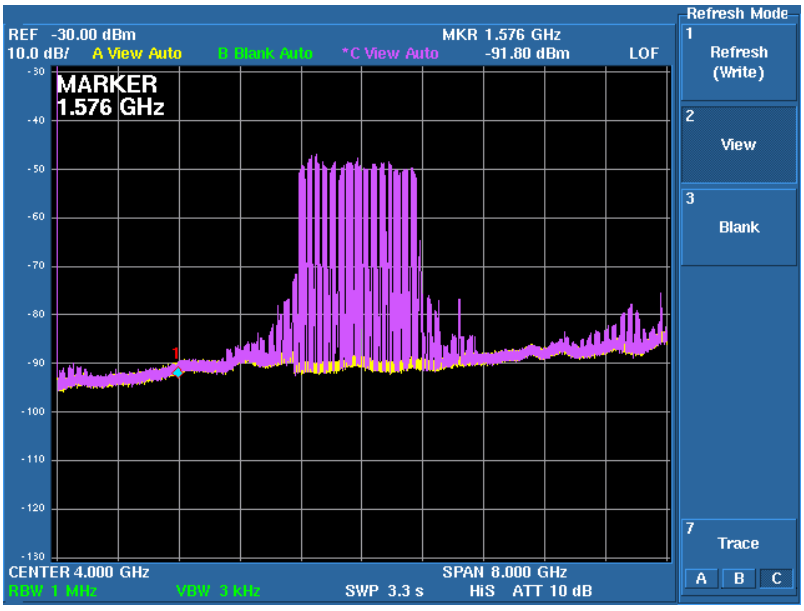

Figure 3-19: Spectral plot at antenna output port from commercial UWB device utilizing bands 1-3.

3.7 Conclusions

Using a low-noise test receiver comprised of a GPS antenna, LNA, and spectrum analyzer, we determined that the Belkin Cable-Free USB system, which utilizes the WiMedia UWB Common Radio Platform, does produce emissions at 1,575 MHz. Most of the emissions are radiated from the digital circuitry, not the UWB antennas. The worst source appears to near the ARM processor in the hub where PCB traces connect the processor to an SRAM chip. The circuitry of the dongle produces emission levels that are similar but slightly lower. Assuming the emissions from any of these areas coupled directly into a close GPS receiver, GPS sensitivity could be degraded by 7 to 9 dB. Therefore, shielding would likely be required to minimize radiated interference in a UWB/GPS product.

Compared to the flash drive, the UWB system appears to produce similar emission levels at GPS L1. Measured emissions from the UWB antennas were relatively insignificant compared to the emissions from the circuitry. Antenna emissions raised the noise floor by 2 dB at a distance of one centimeter only when the system was actively transferring a file.

From the measured emissions, it would appear that the UWB device could have a severe impact on GPS sensitivity. However, we measured very little sensitivity degradation during a test in an anechoic chamber. Another study using pulsed-based UWB signals and a handheld consumer GPS device reported similar results [5]. When our UWB system and GPS receiver were operated in close proximity, the sensitivity of the GPS receiver decreased by only 1 dB. This sensitivity degradation is much lower than

the 20 dB degradation predicted by our analysis, meaning that either the UWB device radiates well below the FCC limit at 1,575 MHz or that our analysis is very conservative.

Either way, the relatively low GPS sensitivity degradation measured in the presence of the UWB system suggests that co-locating GPS and UWB radios in a single device is definitely possible. It would be useful to repeat the test with the UWB dongle and GPS practically touching each other. We believe that a UWB chipset like the Wisair 502/531 could be successfully integrated into a GPS product, but careful component placement and routing, along with shielding, would be necessary to minimize unwanted interference to GPS. More on this subject is discussed in Chapter 7.

Chapter 4

UWB Antennas

Finding an antenna that performs well over a large bandwidth can be challenging. Traditional antenna metrics such as gain and effective aperture are useful for designing narrowband systems, but they can be difficult to define with UWB. These parameters are largely frequency-dependent, and the values obtained at the low end of the UWB band may differ significantly from those at the high end of the band. Instead of relying upon these metrics, taking a time- and/or frequency-domain approach may be more useful, depending upon the type of UWB system being implemented [25], [40].

In this chapter, we present measurement results from three commercially-available UWB antennas. Since this research project is concerned primarily with MB-OFDM, we concentrate on the frequency domain characteristics such as return loss and gain pattern. The most recent version of WiMedia standard defines six band groups. However, many current UWB products work only in Band Group 1, so we have focused our efforts on Band Group 1 operation.

4.1 Desired Antenna Characteristics

Regardless which UWB modulation format is used, a UWB antenna must perform well across a very wide frequency band. One impulse-based proposal submitted to IEEE 802.15.3a required a bandwidth of 3.5 GHz for high-band operation. For I-UWB, critical time-domain characteristics like group delay must be considered in order to minimize pulse distortion [25], [40]. In WiMedia MB-OFDM, the antenna must work across at least 1.5 GHz to cover the first band group and possibly more bandwidth as the other band groups become popular. Fortunately for MB-OFDM, it is typically easier to select an antenna for MC-UWB than it is for I-UWB since the time-domain requirements are more relaxed. [40].

4.1.1 Antenna Characteristics for I-UWB

In I-UWB, proper pulse timing is paramount. An ideal I-UWB antenna acts like a perfect differentiator, transmitting the first derivative of the applied voltage pulse [23], [41], [42]. To ensure that the pulse is accurately transmitted, the antenna must have a linear phase response across the entire frequency band [25]. Relying upon external components for impedance matching introduces non-linear phase distortion, so the antenna should be inherently matched by design. Several types of antennas that usually work well for I-UWB are Vivaldi, ridged transverse electric and magnetic (TEM) horn, tapered slot, and chip-type antennas that have been engineered to 50 ohms [23], [40]. A resonant monopole can be used, provided it is loaded resistively to widen its bandwidth and dampen ringing [23], [43]. Other antennas such as LPDAs and Archimedean spirals have dispersive phase characteristics which preclude their use with I-UWB [25], [40].

Generally, the best antennas for I-UWB have wide, smooth passbands and linear phase characteristics to transmit pulses as accurately as possible [23].

4.1.2 Antenna Characteristics for MC-UWB

In contrast, the time domain characteristics of the antenna are less important in MC-UWB than they are in I-UWB. MC-UWB does not require the same tight phase linearity, and this allows dispersive antennas such as LPDAs and Archimedean spirals to be used [40]. Most of the antennas that are suitable for I-UWB are also suitable for MB-OFDM. The most significant characteristic of the MC-UWB antenna is typically bandwidth. The gain does not need to be flat across the entire band, though, because OFDM requires that the channel (including antenna effects) be flat only for the context of each tone.

4.1.3 Antenna Gain Pattern

The indoor environment is highly dispersive compared to the outdoors, and depending on the type of UWB system being implemented, an antenna with a wide or narrow gain pattern may be preferred for reasons of size or cost. If the multipath energy can be exploited, then an omni-directional antenna can provide slightly better link performance than a directional antenna, especially in NLOS situations [25], [44]. An I-UWB system with a properly-designed RAKE receiver and an MB-OFDM system can both benefit from using an omni-directional antenna. More on the subject of indoor UWB performance is covered in the next chapter.

For a handheld UWB device, an omni-directional pattern is important, because the device could be held in virtually any orientation. Choosing an antenna with

directional gain can be risky because it makes assumptions about the way that the device will be held. Fortunately, most of the antennas that are small enough to be used in a handheld product are roughly omni-directional due to their small electrical size [23].

4.1.4 Physical Size of the Antenna

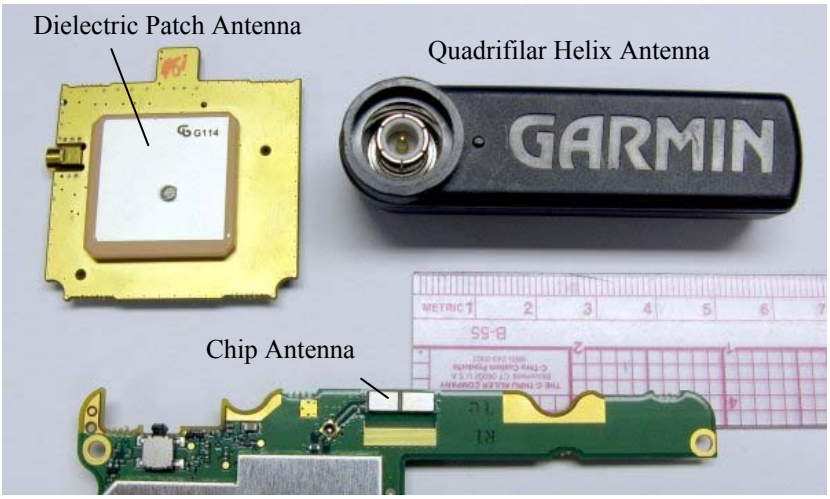

Figure 4-1: Size comparison of GPS dielectric patch, quadrifilar helix, and chip antennas.

Some of the UWB antennas mentioned previously, such as the TEM horn and LPDA, are much too large to fit inside a handheld device. The best solution is likely a chip-type, surface-mount antenna or PCB antenna with 50 ohm tuning [23]. An example of how much smaller a chip-type antenna can be relative to other antenna types is shown by a comparison of some GPS antennas in Figure 4-1. Although the frequency of GPS is lower than those of UWB, a sense of scale can be established. All three antenna types—quadrifilar helix, dielectric patch, and chip—have been used in consumer GPS devices. It should be noted that chip and dielectric patch antennas typically require a substantial amount of surrounding ground plane to perform optimally. The chip antenna uses the

edge of the ground plane to receive or radiate E-fields, and at least one half wavelength (measured in air) of edge space should be reserved for good antenna efficiency [45].

4.1.5 Performance at GPS L1

Ideally, a UWB antenna exhibits good performance in the UWB band and poor performance outside that band. We particularly care about the out-of-band performance at GPS L1 (1,575 MHz), because a UWB antenna with poor performance at GPS L1 will be less likely to radiate signals that jam a nearby GPS receiver.

4.2 Measured Antennas

We obtained samples of three chip-type UWB antennas. Two of the antennas have been publicly released, and they are referenced by their manufacturer's name and model number in Table 4-1. The third antenna has not been released, so it is anonymously referred to as "Antenna #3". An example of how the UWB antennas were supplied to us on evaluation boards can be seen in Figure 4-2. It should be noted that the evaluation boards are constructed using FR-4 material, which is quite lossy at UWB frequencies.

Table 4-1: Evaluated UWB Antennas

Antenna Manufacturer & Model Number	Operating Frequency (GHz)
Johanson 3100AT51A7200	3.1 to 10.6
Pulse W3540	3.1 to 6.0
Antenna #3	3.1 to 5.0

Figure 4-2: UWB chip antenna mounted on an evaluation board.

4.3 Return Loss

The return loss (reciprocal of S11 response) of each antenna was measured with a network analyzer. Return loss *RL* is computed in dB as

$$RL(dB) = -10\log_{10}\left(\frac{P_R}{P_T}\right) \tag{4-1}$$

where P_T is the power transmitted by the source through the feedline and P_R is the power reflected by the antenna back toward the transmitter due to an impedance mismatch of the feedline and the antenna. In a perfectly matched system, all of the transmitted power is delivered to the antenna. P_R goes to zero, which sends *RL* to infinity. This means that the higher the return loss number is, the closer the antenna is matched to the system. A return loss of 10 dB or better is commonly used as a criterion in RF systems. This means that at least 90% of the power is delivered to the load. Alternatively, a lower threshold of 6 dB can be used, where at least 75% of the power is guaranteed to the load.

Return loss also applies to the receiving situation where radiated power that is incident upon the antenna is transferred to the receiver through a feedline. A low return

loss value ensures that little power is wasted due to reflection at the antenna/feedline interface. In this research project, we are interested in seeing low return loss in the UWB band and high values in the GPS band. An antenna with these characteristics will operate efficiently in the UWB band and poorly in the GPS band, thereby maximizing UWB performance and minimizing interference to a nearby GPS receiver.

4.4 Gain Pattern

For each antenna under test, we measured the gain patterns as rotated about its major axes. The measurements were made in an anechoic chamber using the small LPDA and each UWB antenna under test. A signal generator outputting +20.0 dBm at 3.0 GHz was connected to LPDA, and a spectrum analyzer was connected to the UWB antenna. After all the receiving power values were recorded, they were normalized to the maximum value recorded for each antenna to create pattern plots.

4.4.1 Orthonormal Basis and Rotation Plane Definitions

To effectively compare the gain patterns of the UWB antennas, it was necessary to define an orthonormal basis and three rotation planes (Figure 4-3). Each antenna was mounted on a printed circuit board (PCB), and the physical center of the antenna was declared the basis origin. Emanating from the origin, the z axis was defined to be parallel to the antenna feedline, with the $+z$ direction pointing away from the SMA connector on the PCB. The y axis was defined to be normal to the plane of the PCB, with the $+y$ direction pointing upward from the "component" side of the board. Finally, the x axis was defined to be normal to the y and z axes, with the $+x$ direction pointing toward the

right if a person held the board face-up in his or her hand and looked at it from the +*z* direction.

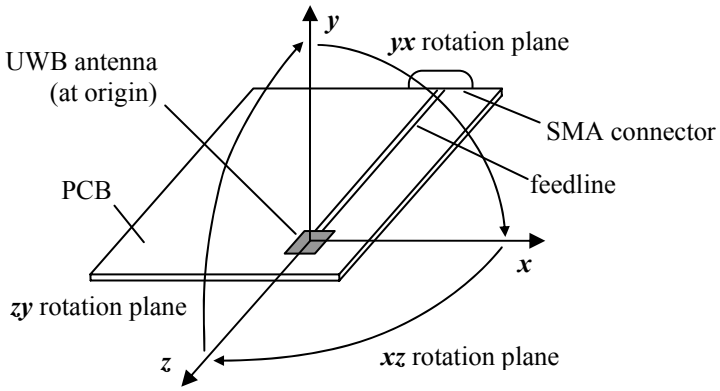

Figure 4-3: Orthonormal basis and rotation planes defined for antenna pattern measurements.

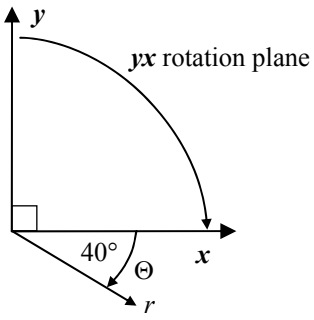

Figure 4-4: Angle definition used in UWB antenna pattern plots.

Three rotation planes were also defined, with a plane being normal to each basis vector and containing the other two vectors. These planes were called ***xz***, ***zy***, and ***yx***. An angle Θ was defined within each plane to be the angle formed by a rotating vector ***r*** with respect to the second basis of the plane's name. The vector rotates unidirectionally from the first basis through the second basis, and Θ always refers to the second basis from this direction of rotation. To simplify references to angles within a plane in this thesis, the convention $\boldsymbol{ab}\angle\Theta$ will be used to imply the angle Θ, as previously defined, within a plane

ab, where ***ab*** represents any of the three planes ***xz***, ***zy***, and ***yx***. Figure 4-4 shows an example of ***yx***∠40° in two dimensions. Figure 4-5, Figure 4-6, Figure 4-7 show the ***xz***, ***zy***, and ***yx*** rotation planes with respect to the chip antenna in greater detail.

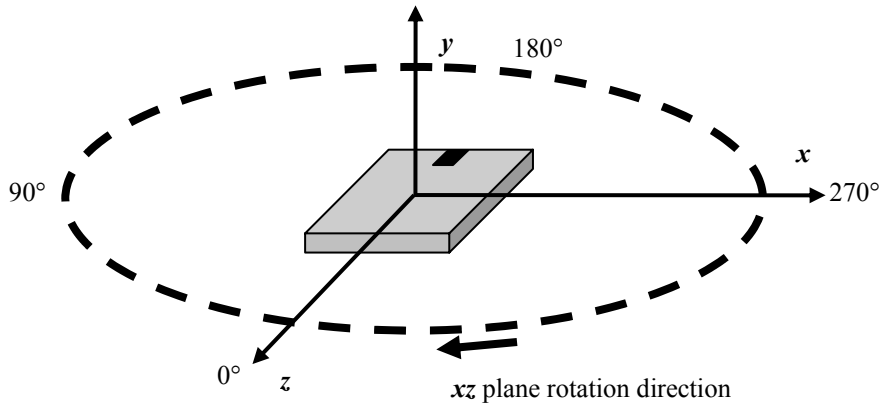

Figure 4-5: *xz* rotation plane.

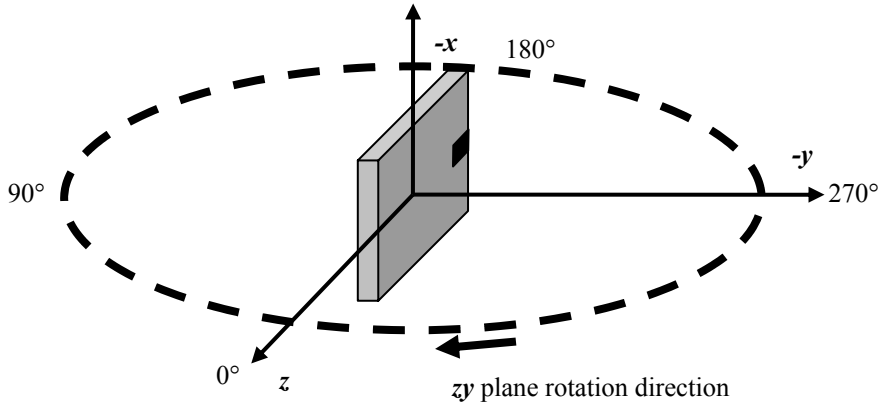

Figure 4-6: *zy* rotation plane.

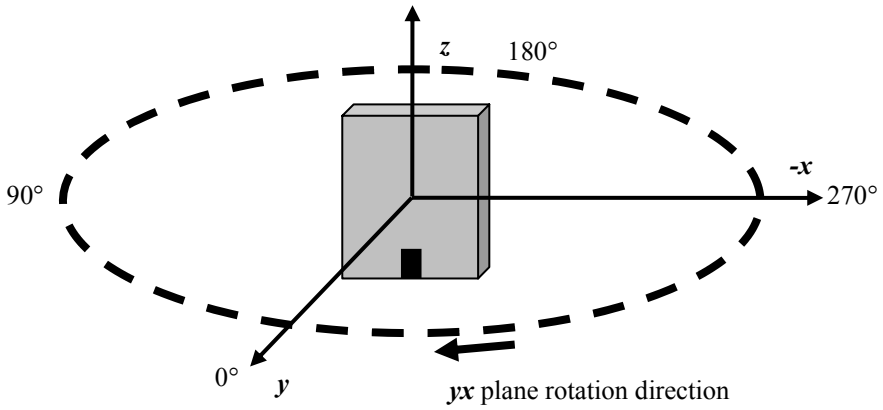

Figure 4-7: *yx* rotation plane.

4.4.2 Gain Pattern Measurement Procedure

To measure the gain patterns of the antennas, we used an anechoic chamber with a rotating platform. The antenna under test was mounted on the rotating platform at one end of the chamber, and the small LPDA was placed at the opposite end of the chamber, roughly four meters away. A signal generator at 3.0 GHz, +20 dBm was connected to the LPDA, and a spectrum analyzer was connected to the antenna under test. Then, the UWB antenna was rotated through each of the three rotational planes by the platform. The strength of the received signal was recorded at each ten degree step. For each scanning cut, measurements were made with the reference LPDA being parallel, then perpendicular, to the rotational plane. Since the UWB antenna was rotated, not the measurement system around it, we reversed the order of the data to present the gain pattern with respect to the UWB antenna. For example, 0° remained 0°, but 10° became 350°, 20° became 340°, and so on, as shown in Figure 4-8.

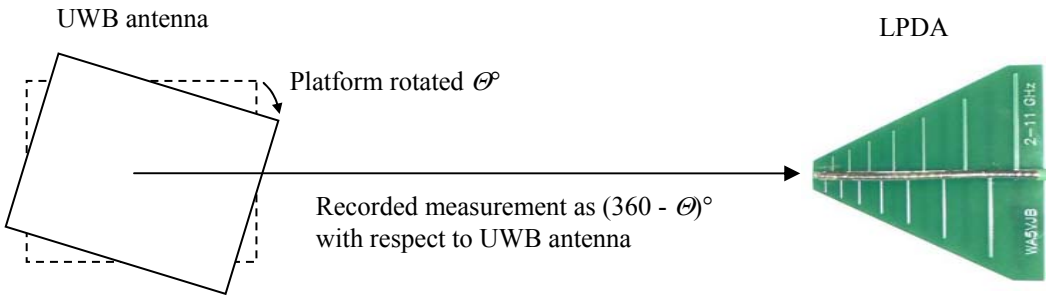

Figure 4-8: Method of recording rotation angle with respect to the UWB antenna.

4.5 Johanson Antenna

Of the three sample UWB antennas we evaluated, the Johanson antenna (Figure 4-9) is the only one that is designed to operate across almost the entire UWB band. The antenna was mounted on an evaluation board which had a ground cutout of approximately 2.5 square centimeters. We measured a return loss better than 10 dB from 3 GHz to 11 GHz, as shown in Figure 4-10. Using another analyzer, we measured a return loss of 2 dB at 1,575 MHz. Figure 4-11, Figure 4-12, and Figure 4-13 show the measured gain patterns for the ***xz***, ***zy***, and ***yx*** rotation planes, respectively.

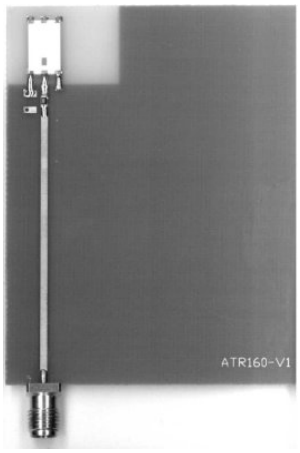

Figure 4-9: Johanson 3100AT51A7200 UWB antenna mounted on an evaluation board.

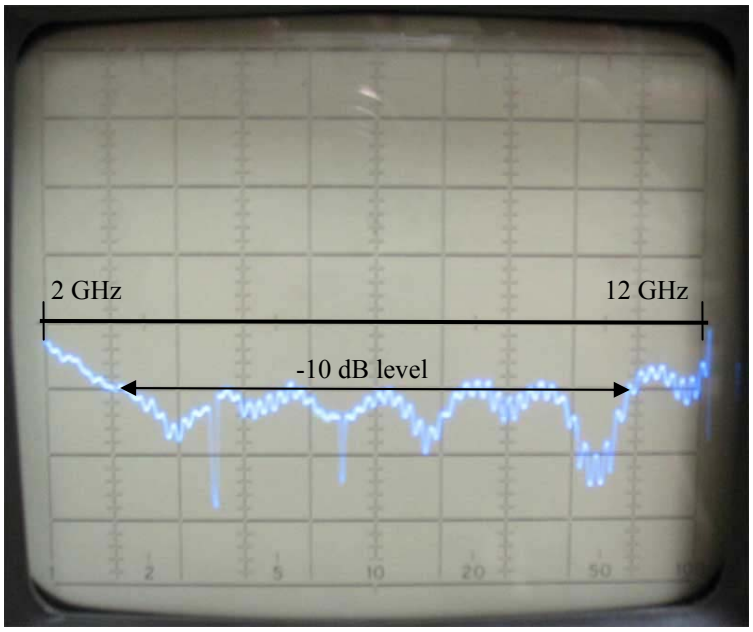

Figure 4-10: Measured S11 plot for Johanson antenna. Start: 2 GHz. Stop: 12 GHz. 1 GHz/division. Center horizontal line is 0 dB. 10 dB/division.

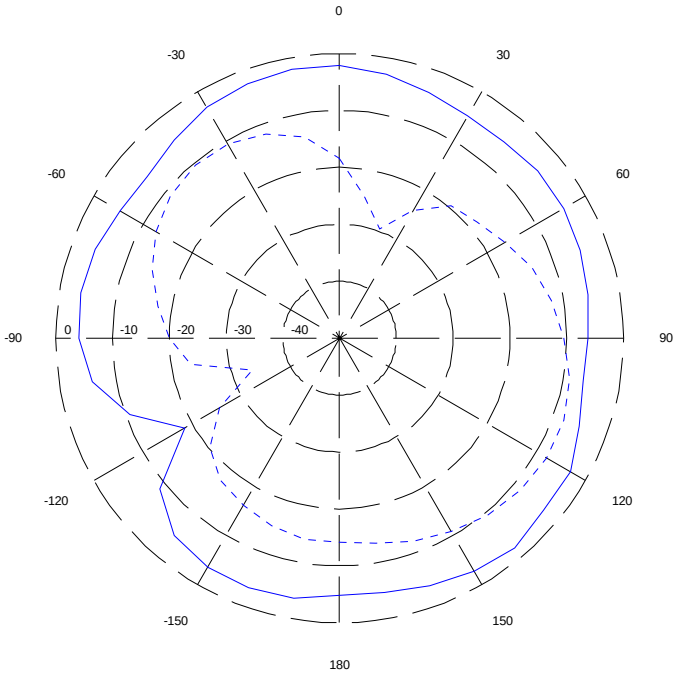

Figure 4-11: Measured gain of Johanson antenna at 3.0 GHz in *xz* rotational plane. Angle is referred to the +*z* axis. Solid line is polarization parallel to *xz* plane. Dashed line is perpendicular polarization.

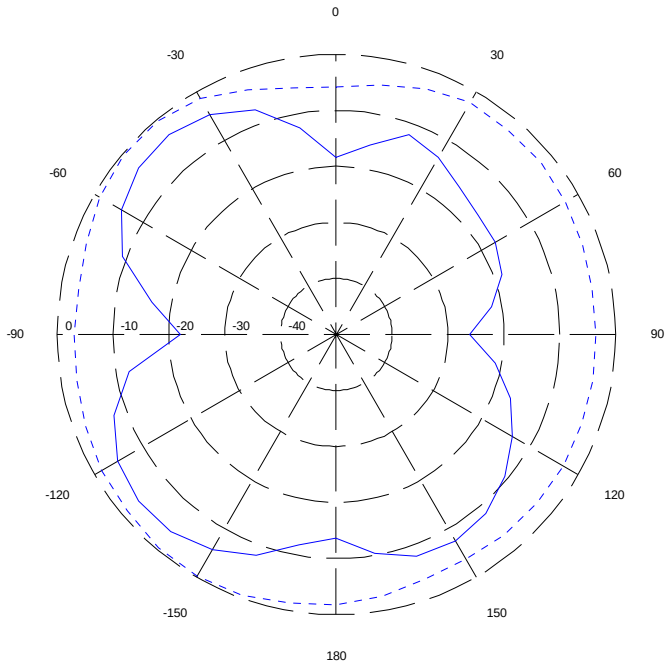

Figure 4-12: Measured gain of Johanson antenna at 3.0 GHz in *zy* plane. Angle is referred to the +*y* axis. Solid line is polarization parallel to *zy* plane. Dashed line is perpendicular polarization.

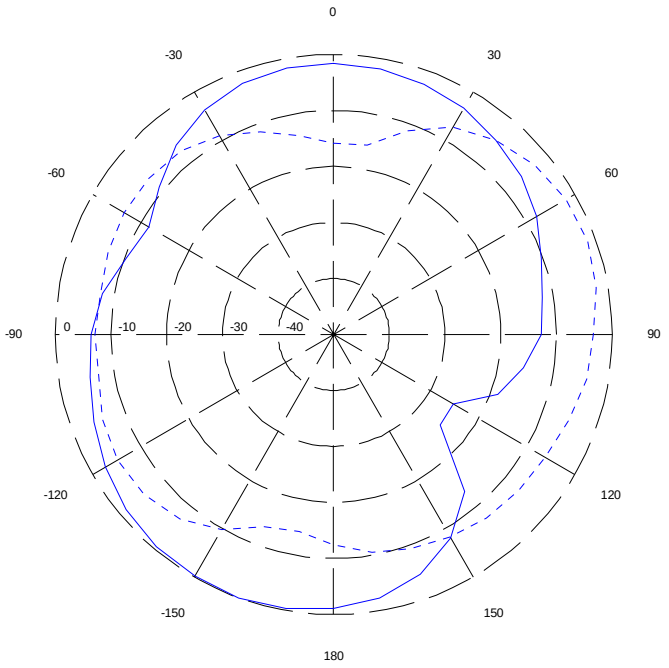

Figure 4-13: Measured gain of Johanson antenna at 3.0 GHz in *yx* plane. Angle is referred to the +*x* axis. Solid line is polarization parallel to *yx* plane. Dashed line is perpendicular polarization.

Our measured gain plots differ from the plots shown in the Johanson datasheet. Likely, this is because we took the measurements at 3.0 GHz, but the plots in the datasheet were made at 5.0 GHz. We intended to take measurements at each 1 GHz step up to 11 GHz, but time did not permit. An important point to note is that our axis and rotation plane definitions differ from those defined in the Johanson datasheet.

4.6 Pulse Antenna

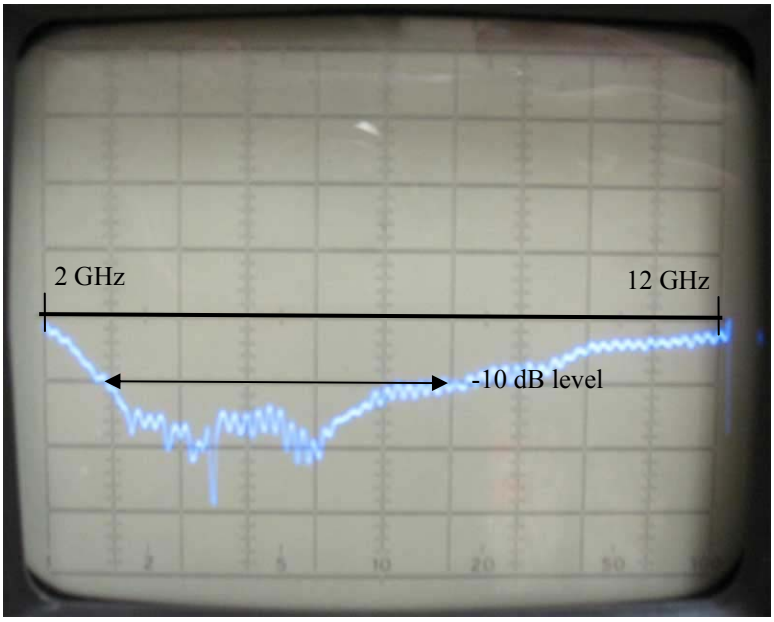

Figure 4-14: Measured S11 plot for Pulse antenna. Start: 2 GHz. Stop: 12 GHz. 1 GHz/division. Center horizontal line is 0 dB. 10 dB/division.

The Pulse W3541K antenna we received was specified to operate from 3.1 to 6.0 GHz. The version that has since been publicly released is rated from 4.5 to 5.9 GHz. Our S11 measurement showed better than -10 dB throughout most of the band from 3 GHz to 8 GHz, as seen in Figure 4-14. At 1,575 MHz, the return loss was about 1 dB. Figure

4-15, Figure 4-16, and Figure 4-17 show the measured gain patterns for the ***xz***, ***zy***, and ***yx*** rotation planes, respectively.

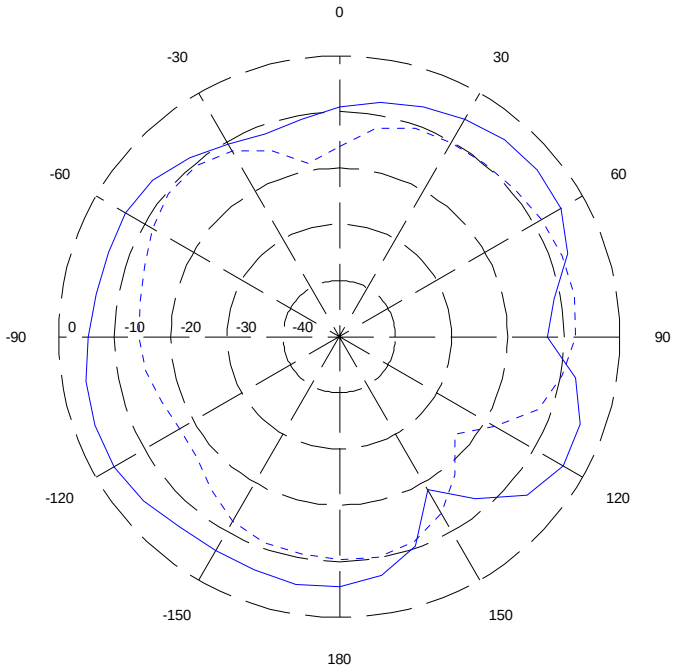

Figure 4-15: Measured relative gain of Pulse antenna at 3.0 GHz in *xz* rotational plane. Angle is referred to the +*z* axis. Solid line is polarization parallel to *xz* plane. Dashed line is perpendicular polarization.

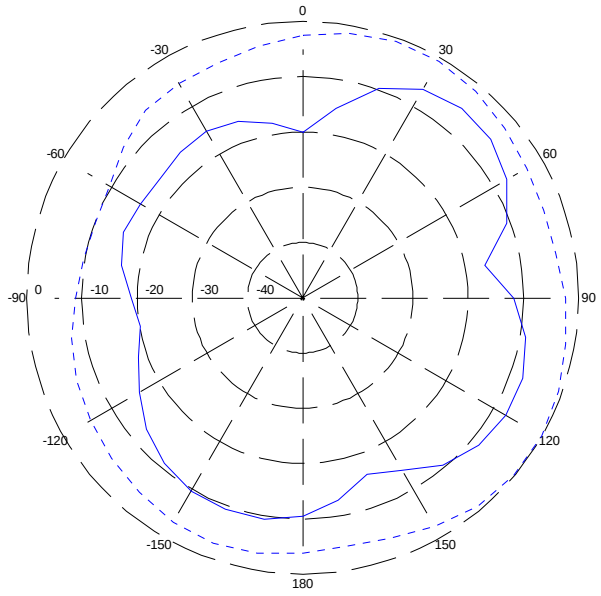

Figure 4-16: Measured relative gain of Pulse antenna at 3.0 GHz in *zy* rotational plane. Angle is referred to the +*y* axis. Solid line is polarization parallel to *zy* plane. Dashed line is perpendicular polarization.

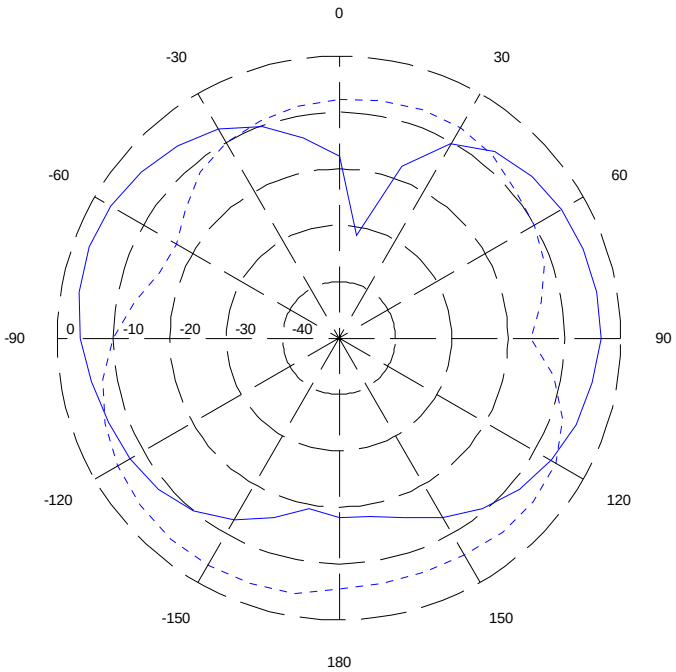

Figure 4-17: Measured relative gain of Pulse antenna at 3.0 GHz in *yx* rotational plane. Angle is referred to the +*x* axis. Solid line is polarization parallel to *yx* plane. Dashed line is perpendicular polarization.

4.7 Antenna #3

The third antenna that we measured was supplied as an engineering sample and was never commercially released. A datasheet for the antenna was not available, but markings on the packaging specified its operation from 3.1 to 5.0 GHz. Our S11 measurement showed that this frequency range only provided a return loss of 5 dB or better. The range for 10 dB or better performance was about 3.3 to 4.0 GHz, as seen in Figure 4-18. The return loss at 1,575 MHz was measured to be about 1 dB. Figure 4-19, Figure 4-20, and Figure 4-21 show the measured gain patterns for the ***xz***, ***zy***, and ***yx*** rotation planes, respectively.

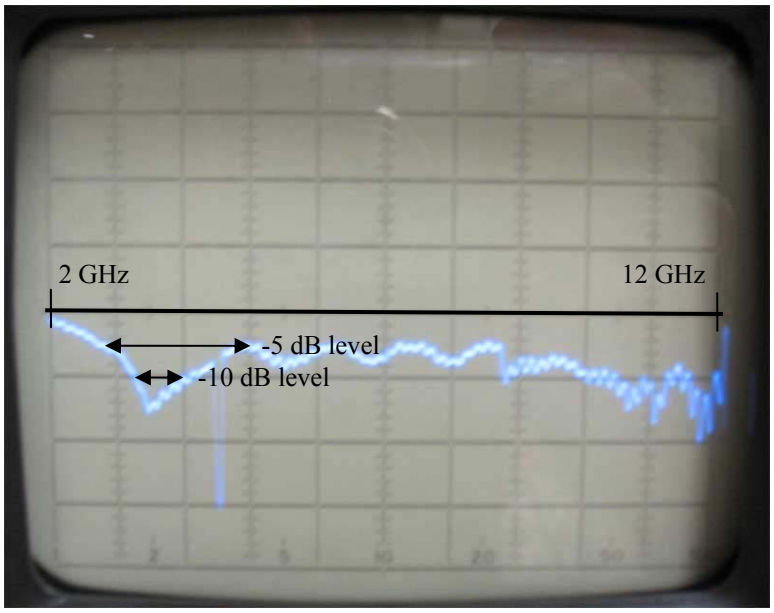

Figure 4-18: Measured S11 plot for Antenna #3. Start: 2 GHz. Stop: 12 GHz. 1 GHz/division. Center horizontal line is 0 dB. 10 dB/division.

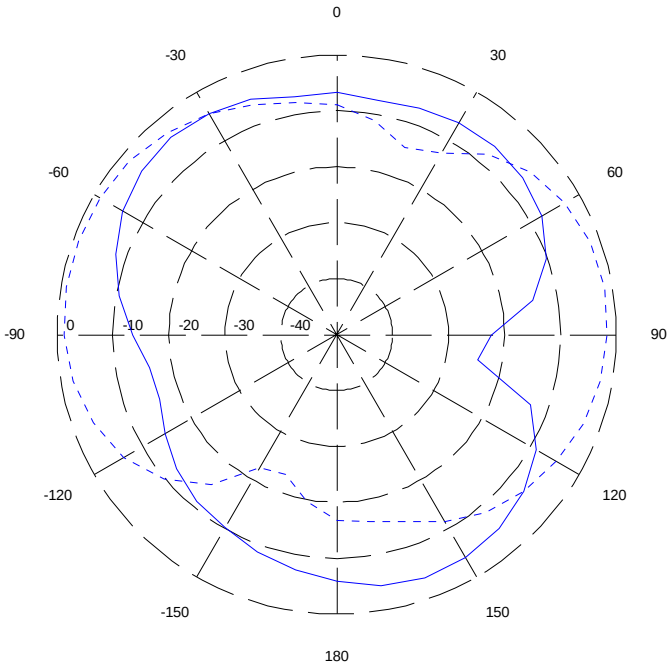

Figure 4-19: Measured relative gain of Antenna #3 at 3.0 GHz in *xz* rotational plane. Angle is referred to the +*z* axis. Solid line is polarization parallel to *xz* plane. Dashed line is perpendicular polarization.

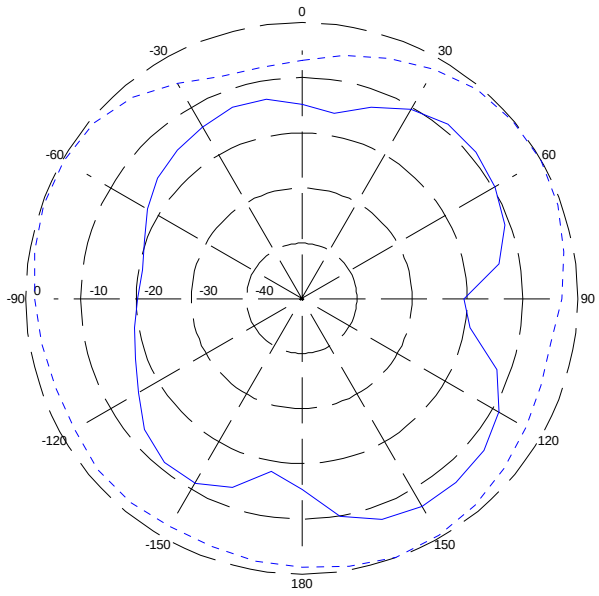

Figure 4-20: Measured relative gain of Antenna #3 at 3.0 GHz in *zy* rotational plane. Angle is referred to the +*y* axis. Solid line is polarization parallel to *zy* plane. Dashed line is perpendicular polarization.

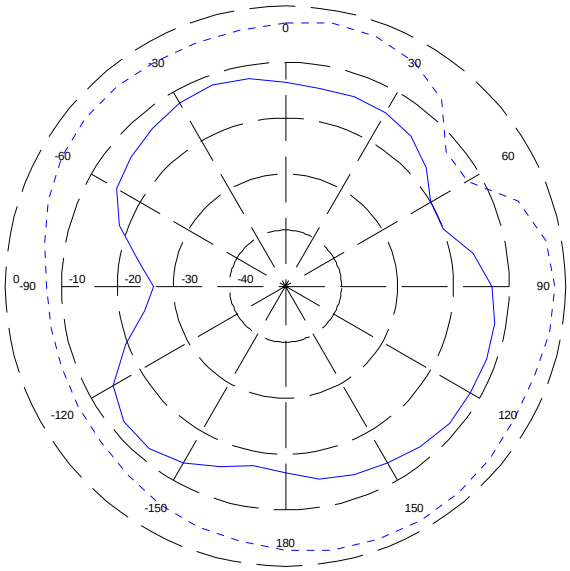

Figure 4-21: Measured relative gain of Antenna #3 at 3.0 GHz in *yx* rotational plane. Angle is referred to the +*x* axis. Solid line is polarization parallel to *yx* plane. Dashed line is perpendicular polarization.

4.8 In4Tel Antenna

In addition to the three UWB antenna samples, we also measured the return loss of one of the In4Tel antennas that was supplied with the Belkin Cable-Free USB Hub. Figure 4-22 shows front and back detail of the antennas and their mounting positions in the hub. Each antenna is constructed from double-sided FR-4 and is fed by a thin coaxial cable. We were unable to measure the gain pattern of each antenna, but we determined experimentally that the pattern is roughly dipole-like, with two nulls extending from the PCB parallel to the long edges. The antennas are mounted perpendicularly in the hub likely to provide diversity gain. We are unsure how the Wisair 502/531 UWB chipset actually performs optimized diversity combining.

Belkin Hub

Front Back

Figure 4-22: In4Tel antennas supplied with the UWB Hub.

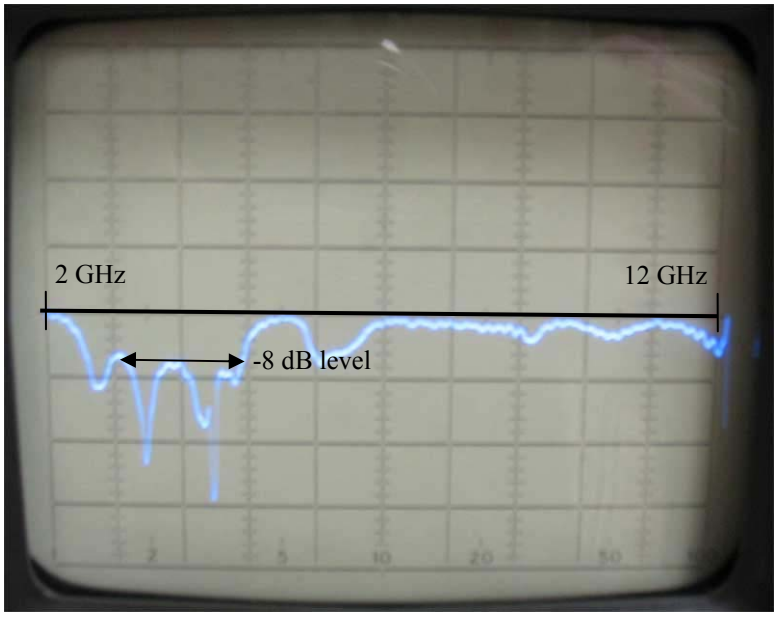

Figure 4-23: Measured S11 plot for In4Tel antenna. Start: 2 GHz. Stop: 12 GHz. 1 GHz/division. Center horizontal line is 0 dB. 10 dB/division.

It is easily seen from the S11 plot in Figure 4-23 that the In4Tel antenna is designed for operation only in Band Group 1. From 3.1 to 5.0 GHz, the return loss is 8 dB or better. At 1,575 MHz, the return loss is 1 dB.

4.9 Polarization Sensitivity

We wanted to assess how sensitive the antennas are to signal polarization, so we compared the parallel and perpendicular pattern data at the major axes (±***x***, ± ***y***, and ±***z***) for each antenna. Polarization sensitivity is not just a property of the antenna; it is also related to how dispersive the channel is. We conducted measurements in an anechoic chamber and a laboratory for comparison.

Table 4-2: Polarization sensitivity in an anechoic chamber at 3.0 GHz.

Direction	Johanson (dB)	Pulse (dB)	Antenna #3 (dB)
+***z***	18	8	8
-***z***	13	7	15
+***y***	4	9	0
-***y***	2	9	10
+***x***	2	9	2
-***x***	5	3	1
Average	**12**	**8**	**9**

During rotations through the three planes, actually two data points were taken at each axis and polarization. We averaged these two signal power values using a linear average (not a dB average) and compared this averaged power value to the averaged power value from the other polarization at that axis. Then the absolute value of the result was converted back to the dB domain to represent the "polarization sensitivity" at that axis. A low value indicates that the antenna is not very sensitive to signal polarization in

that direction, and a high value suggests the opposite. Table 4-2 shows the polarization sensitivity of each antenna measured at 3.0 GHz in the anechoic chamber.

Of the three antennas, the Pulse antenna shows the most consistent polarization sensitivity as well as the lowest average polarization sensitivity in the few directions that we evaluated. The other two antennas show little sensitivity in some directions and great sensitivity in others. To absolutely define the polarization sensitivity of the antennas, measurements would need to be averaged over the entire 4π steradian space around the antennas.

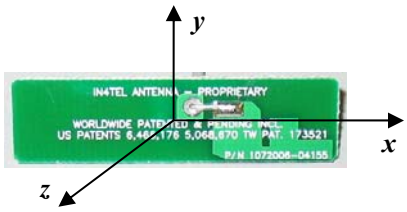

Figure 4-24: Axes defined for In4Tel antenna measurements.

We repeated the same measurement in the laboratory at a separation distance of 24 cm, making no attempt to prevent signal reflections. The In4Tel antenna was also measured for comparison using definitions of the major axes as shown in Figure 4-24. The sensitivity results in Table 4-3 are strikingly different than those obtained in the anechoic chamber. The Pulse antenna had the lowest polarization sensitivity in the chamber but the highest sensitivity in the lab. The sensitivity of the Johanson antenna was roughly the same, though. Surprisingly, the In4Tel antenna had the lowest polarization sensitivity of the four antennas measured in the lab, although it had the lowest average directional sensitivity by about 1 dB.

Table 4-3: Polarization sensitivity in the lab at 3.0 GHz.

Direction	Johanson (dB)	Pulse (dB)	Antenna #3 (dB)	In4Tel (dB)
+z	9	18	18	8
-z	17	13	9	8
+y	8	5	1	7
-y	3	5	4	8
+x	17	26	18	3
-x	15	15	8	4
Average	**14**	**20**	**14**	**7**

We expected the polarization sensitivity values in the lab to be lower than in the anechoic chamber, since the chamber is essentially free of multipath propagation. The indoor environment is highly dispersive, and it should relax the need for co-polarized antennas. Since the contrary was measured, we suspect the values from lab and recommend that additional data be taken across larger separation distances. Care should be taken to minimize cable radiation, possibly by using a ferrite choke around the cable near the antenna.

In an alternative measurement, we used a network analyzer and two antennas at a spacing of three meters to verify that the indoor environment randomizes the polarity of UWB signals. The Johanson antenna, which was shown in the chamber to have relatively strong polarization sensitivity in the +z direction, was mounted on a wooden dowel rod next to a lab bench. The small LPDA was held three meters away as shown in Figure 4-25. The network analyzer was placed in S21 mode, and the response was calibrated with the antennas in a co-polarized orientation. At such a great distance, the response quickly evolved from a straight line at 0 dB to the plot a) shown in Figure 4-26. Then the log-periodic antenna was rotated 90° to a cross-polarized orientation, yielding the plot b) of Figure 4-26. Both plots look similarly disheveled, with certain frequency components

being high in one orientation and low in the other. The wideband magnitude of the S21 response does not appear to change overall, though, suggesting that multipath propagation indeed relaxes the need for co-polarized antennas at typical separation distances of the UWB transmitter and receiver.

Figure 4-25: Evaluating wideband S21 response in a laboratory environment using two antennas at a distance of 3 m.

a) b)

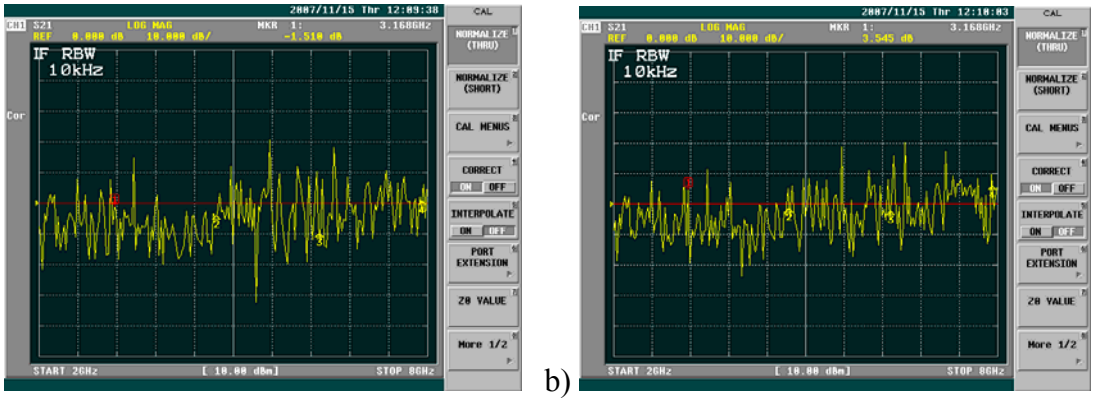

Figure 4-26: S21 response of a) co-polarized and b) cross-polarized Johanson and log-periodic antennas at a distance of three meters. Start: 2 GHz. Stop: 8 GHz.

4.10 Summary

We evaluated three chip-type UWB antennas using return loss and gain pattern measurements. For a GPS product with an integrated UWB radio, a UWB antenna with low return loss in the UWB band is desired to optimize UWB operation, and a high return loss in the GPS band is desired to minimize radiated interference to GPS. In WiMedia Band Group 1 (3.1 GHz to 4.8 GHz), we found that the Johanson and Pulse antennas had the best performance with return loss values of 10 dB or better. Of the two, the Pulse antenna exhibited superior return loss with values significantly better than 10 dB throughout the band. The worst case return loss values of all the antennas in Band Group 1 are compared in Table 4-4.

Table 4-4: Worst return loss measured in Band Group 1 (3.1 to 4.8 GHz).

Johanson	Pulse	Antenna #3	In4Tel
10 dB	10 dB	5 dB	8 dB

The Johanson antenna had the widest 10 dB return loss bandwidth. It extends from 3 GHz up to 11 GHz, making it suitable for use in any of the WiMedia band groups. Based on our return loss measurements, we have suggested the best band groups for each antenna in Table 4-5.

Table 4-5: Best WiMedia band groups to use with each antenna.

Johanson	Pulse	Antenna #3	In4Tel
1-6	1-3	1	1

In the GPS band, all of the antennas had fairly comparable return loss values of 1 to 2 dB. Table 4-6 summarizes the results.

Table 4-6: Return loss measured at 1,575 MHz.

Johanson	Pulse	Antenna #3	In4Tel
2 dB	1 dB	1 dB	1 dB

Comparing the gain patterns of the antennas is difficult since we only measured the patterns in three rotational planes. If gain data were available over the entire 4π steradian space around the antennas, a better comparison could be made. Regarding polarization sensitivity, the results in Table 4-2 and Table 4-3 do not conclusively prove that any single antenna is less sensitive than the others to polarization in the directions we measured, although the In4Tel antenna included with the UWB hub appears to be the least sensitive of the group to polarization. This could mean that it is the most directional antenna of the group.

We recommend that additional data be taken to determine the sensitivity of the antennas to signal polarization in typical indoor channels. When multipath is present, we expect the polarization sensitivity to be lower than when RF absorbent material is used. Our data indicate the contrary, which raises suspicion about the test setup. In future measurements, more care should be taken to limit cable radiation by using RF chokes. When the test is conducted properly, the dispersive nature of the indoor environment should render the polarization sensitivity inconsequential at distances greater than one or two meters, the distances over which UWB systems typically operate.

Based on the data presented in this chapter, predicting which UWB antenna would work best for a GPS/UWB product is difficult. In terms of minimizing radiation at GPS L1, the antennas perform roughly the same. They are all quite inefficient at 1,575 MHz, suggesting that radiated interference to GPS will be low. It is hard to choose a

winner in the UWB band, because the effects of the return loss and gain pattern on UWB performance are not yet considered or recognized. To provide clarity to this evaluation, a measurement of radiated antenna efficiency is needed.

In Chapter 6, we present real throughput data from operating the UWB system with each of the antennas. In our tests, we verified that the laboratory environment tends to disperse UWB signals and noted that antenna polarization and orientation did not appear to have significant effects on throughput data rate. More research is needed to determine if return loss, gain pattern, polarization sensitivity, or radiation efficiency are good predictors of overall UWB performance. Until more is known about this subject, we believe that the best way to evaluate UWB antennas is to measure their return loss and then compare their performance in an actual UWB system using throughput data rate as a metric.

In the next chapter, we explore the basics of indoor UWB channel modeling in an effort to understand how UWB overcomes some of the difficulties that plague narrowband systems.

Chapter 5

UWB Channel Modeling

The indoor environment poses a challenge to many types of wireless communication systems. The typical home or office contains numerous objects ranging in size and composition that can reflect, diffuse, and diffract electromagnetic signals. Sometimes signals reinforce themselves positively to increase received signal power at the receiver; other times the reinforcement is negative, attenuating the received signal. Of these complex signal-environment interactions, the deep fades at the receiver are more problematic, because they severely limit the capacity of the system. Narrowband systems with a single receiving antenna are particularly vulnerable to indoor fading, since they have little diversity. Spread-spectrum systems have some resistance to fading, but not nearly as much as UWB systems have [26], [30], [33], [35], [36].

For UWB, the channel is so wide that several deep notches in the spectrum do not adversely affect overall performance [23]. This resistance to small-scale fading enables UWB to provide high data rates at low transmit power in the indoor setting, where the

link is typically short-range (less than 10 meters) and the physical environment is highly cluttered [32].

5.1 Indoor UWB Channel Modeling

A substantial amount of research has been conducted to characterize the UWB indoor channel using empirical and analytical methods [25], [29], [33], [35], [46], [47], [48], [49]. In fact, there are too many notable papers to list them all here. To understand UWB signal propagation, both empirical and analytical models can be useful. It is important, though, to recognize the inherent strengths and weaknesses of each.

Experimental results can be obtained while making few assumptions about the channel; however, collecting enough data to create an accurate model typically requires significant time and effort in addition to expensive, high-frequency measurement equipment. A time-domain measurement approach requires a very fast pulse, which translates into a wide frequency band over which the propagation characteristics can be measured. To produce the impulse response of the channel, the shape of the non-ideal pulse must be de-convolved from the data. Alternatively, the impulse response of the channel can be obtained from frequency domain measurements via the inverse Fourier transform [48]. It should be noted that, in working with empirical data, it is virtually impossible to separate the effect of the antenna from the effect of the channel, because the broadness of the antenna's gain pattern determines how much multipath energy can be collected. For many UWB systems, the antenna pattern is roughly omni-directional, so the effect of the antenna can be neglected.

Unlike empirical results, analytical data can be obtained via simulation on a computer; expensive lab equipment is not needed. A popular type of simulation is ray-

tracing. This approach attempts to model a specific environment and account for each interaction the signal has with it, whether it be reflection or absorption. A drawback to this approach is that one must assume a very specific environment and channel. The calculations are computationally very intense, even for simple environments. This method can yield results that fit well for one environment but poorly for another. For this reason, the IEEE 802.15.3a working group decided to take an empirical, statistical approach when it created its model of the UWB channel [48].

5.2 Large-Scale Path Loss

It is widely agreed that the large scale path loss for a short LOS UWB link can be estimated easily by modifying the simple free-space model to accommodate a different path loss exponent [32], [46], [50]. The classic Friis transmission formula can be arranged to estimate the path loss of a UWB LOS link. It is given as

$$PL(f_g, d)[dB] = 10n \log_{10}\left(\frac{4\pi f_C d}{c}\right) \text{ for } d >> \frac{c}{f_g} \tag{5-1}$$

where n is the path loss exponent, f_C is the geometric center frequency of the band, d is the distance between the transmitter and receiver, and c is the speed of light. For this estimate to be valid, the separation distance should be much greater than the wavelength at the frequency of interest. This is the model that the IEEE 802.15.3a task group preferred [30]. A frequency-independent version of the free space model, called the log-distance model, is also commonly used to estimate UWB path loss [51]. It is given as

$$PL(d)[dB] = \overline{PL}(d) + X_\sigma = \overline{PL}(d_0) + 10n \log_{10}\left(\frac{d}{d_0}\right) + X_\sigma \tag{5-2}$$

where PL is the large-scale path loss over separation distance d, $\overline{PL}(d_0)$ is the path loss at a reference distance d_0, n is the path loss exponent, and X_σ is a random variable (in dB) with standard deviation σ (also in dB) to represent fading [52]. This fading variable can also be added to equation (5-1) to complete the path loss model. Both models show that the average amount of link attenuation increases logarithmically with the distance. How quickly the attenuation grows depends upon the path loss exponent n. In a free space environment, the path loss exponent is equal to two. In an environment where the signal can blocked or attenuated by clutter, the path loss exponent is usually greater than two. Interestingly, many researchers have measured path loss exponents that are less than two for indoor UWB LOS channels.

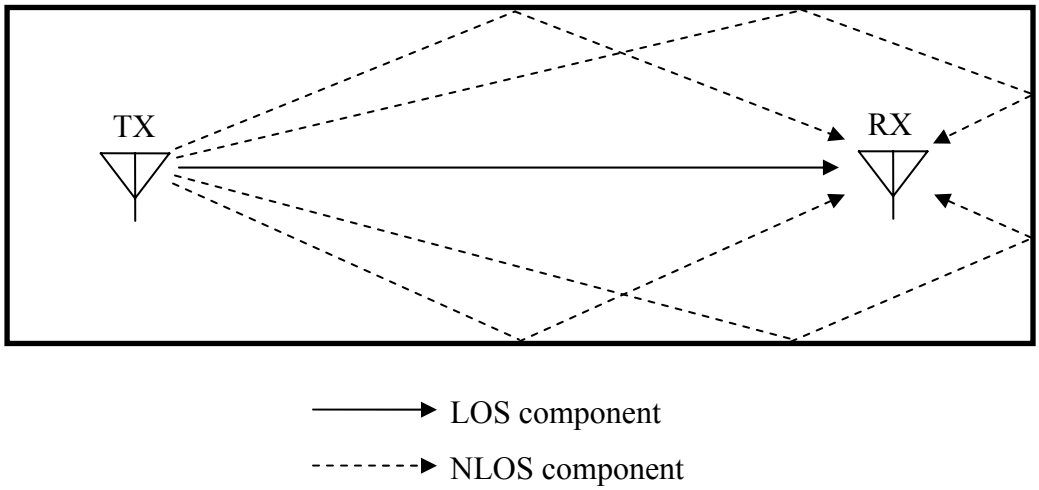

Figure 5-1: Scenario in which environmental interactions can contribute to a path loss exponent that is less than two.

Figure 5-1 illustrates a scenario in which NLOS components contribute to a path loss exponent that is less than that of free space. A free space LOS environment would lack walls and, subsequently, the NLOS components. An NLOS environment, by

definition, would contain clutter that blocks the main LOS component so that only NLOS components could be received.

Along with the environment, the directivity of the antennas also affects the path loss. It has been observed experimentally that the path loss is slightly lower for indoor UWB links using omni-directional antennas than it is for those using directional antennas [25], [44]. An omni-directional antenna has less forward gain than a directional antenna, but it improves the average received signal power by capturing (as a receiver) or creating (as a transmitter) more multipath components. Assuming the receiving antenna in Figure 5-1 is omni-directional, it can capture the signal reflections off the wall at the far right. Otherwise, it receives only the components arriving from the front. Therefore, using an omni-directional antenna can yield slightly lower path loss than using a directional antenna for indoor UWB.

Model parameters have been obtained for both types of antennas. As stated previously, completely removing the antenna dependency from the empirical channel model is difficult, but the path loss should be similar for antennas with similar directivity [40]. Model parameters have been obtained for both directional and omni-directional antennas [44]. In some studies, the differences between omni- and directional antennas have been small enough that they have been lumped together.

Researchers at Virginia Tech have published papers [25], [51] indicating that the path loss exponent in the UWB channel remains roughly constant across frequency for bicone (omni-directional) and TEM horn (directional) antennas. A list of published path loss exponents and fading standard deviation values is given in Table 5-1. From the

campaigns listed, the average path loss component in the LOS case is about 1.6. The average path loss exponent for NLOS is roughly 2.9.

Table 5-1: Measured path loss exponents and fading standard deviation values in published measurement studies. Adapted from [40].

Researchers	Condition	*n*	σ (dB)
AT&T [47]	LOS NLOS	1.7 3.5	1.6 2.7
Cassioli/Molisch/Win [40]	d < 11 meters	2.04	4.3
CEA-LETI [40]	Lab LOS Flat LOS Lab/office NLOS Flat NLOS	1.6 1.7 3.7 5.1	4 4 4 4
France Telecom [40]	LOS NLOS	1.5 2.5	
IKT, ETH Zurich [40]	On body Around torso	2.7-3.3 4.1	
Intel [40]	LOS NLOS	1.7 4.1	1.5 3.6
New Jersey Institute of Technology [44]	Omni/Omni Omni/Dir Dir/Dir	1.55 1.65 1.72	1.98 1.19 0.77
Oppermann et al. [23]	LOS NLOS	1.1, 1.4, 1.8 3.2, 3.3, 3.9	
Time Domain Corp. [33]	LOS/NLOS	2.1	3.6
U.C.A.N. [40]	LOS Soft NLOS Hard NLOS	1.4 3.2 4.1	0.35 1.21 1.87
Virginia Tech [25]	Office LOS Office NLOS	1.3-1.4 2.3-2.4	2.5-3 2.6-5.6
Whyless [40]	LOS NLOS	1.58 1.98	

The IEEE 802.15.4a task group, which focused on low data rate WPANs, published a report on channel modeling that includes path loss estimates for frequency ranges in the UWB spectrum [53]. Table 5-2 contains the LOS and NLOS path loss exponents for five environments: indoor residential, indoor office, outdoor (general), outdoor (open), and industrial. The industrial environment provides the lowest path loss exponents presumably due to massive multipath from large, metallic equipment that

reflects RF signals well. In contrast, the home environment contains materials such as carpet and upholstery which tend to absorb RF signals, so the path loss exponent is higher. The office environment is somewhere in between, containing metal filing cabinets and shelves in addition to carpet and some upholstery.

Table 5-2: UWB path loss exponent values utilized by IEEE 802.15.4a. [53].

Environment	LOS *n*	LOS Path Loss at 1m (dB)	NLOS *n*	NLOS Path Loss at 1m (dB)	Comment
Indoor residential	1.79	43.9	4.58	48.7	7-20m, up to 10GHz
Indoor office	1.63	35.4	3.07	57.9	3-28m, 2-8GHz
Outdoor (general)	1.76	45.6	2.5	73.0	5-17m, 3-6GHz, NLOS educated guess
Outdoor (open)	1.58	48.96	---	---	Snow-covered area
Industrial	1.2	56.7	2.15	56.7	2-8m

We estimated (experimentally) that the path loss is roughly 40 dB at 3.0 GHz and at one meter in our laboratory environment. To make the measurements, we mounted each of the three UWB antennas to a wooden block and held the small LPDA at a distance of 24 cm from the UWB antenna. The test setup is shown in Figure 5-2. (At the time, we were not intending to estimate the path loss; we were measuring the gain patterns of the antennas in the lab environment. If we had intended to measure the path loss, then we would have used a reference distance of one meter.)

A network analyzer was used to record S21 values at 3.0 GHz with the LPDA oriented at each of the major axes and polarizations of the UWB antenna under test. Then the twelve S21 values for each antenna were averaged in the linear domain (not the dB domain). We assumed a conservative gain of 2 dBi for the LPDA and subtracted it from the averaged S21 values. Assuming that the UWB antennas have omni-directional patterns, the overall path loss at 24 cm was about 31 dB for each of the antennas.

Therefore, the average path loss of all three antennas is also about 31 dB. Working backwards with (5-2), we can estimate the path loss at one meter as 38 dB for n = 1.2 and 43 dB for n = 2.0, which meshes well with the indoor values given in Table 5-2. As we mentioned in the antenna polarization sensitivity measurements in Chapter 4, radiation from the cables might have interfered in this measurement. Applying an RF choke to the cable could have limited cable radiation and improved the accuracy of the measurement.

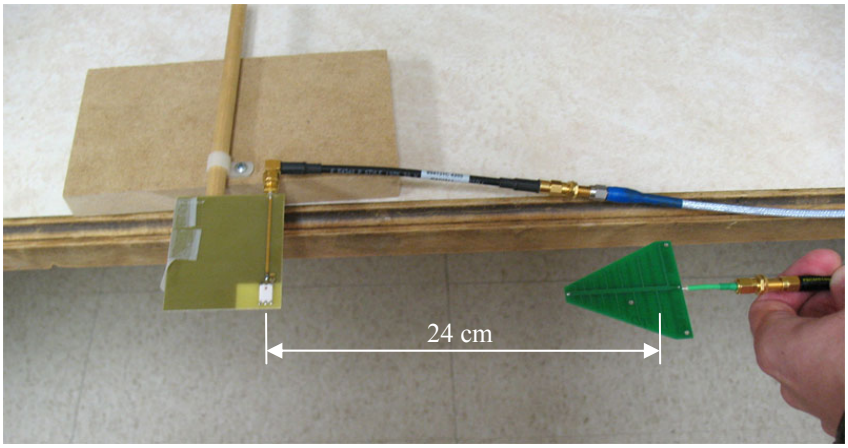

Figure 5-2: Evaluating path loss at 3.0 GHz in a laboratory environment.

Although many of the published studies Table 5-1 report LOS path loss exponents below 1.5, assuming a value of 1.8 to 2.0 is probably a conservative guess for almost any type of environment, including a vehicle. A good estimate for the NLOS path loss exponent is roughly 3.2. For path loss at a reference distance of one meter, 40 dB and 60 dB are suitable estimates for LOS and NLOS cases, respectively. IEEE 802.15.3a elected to lump LOS and NLOS together, using n = 2.0 for both. This is slightly conservative for estimating path loss in LOS links but quite unrealistic for NLOS links. Ghassemzadeh showed experimentally (Figure 5-3) that the path loss exponents in LOS and NLOS links are distinctly different for TX/RX separation distances up to ten meters [47].

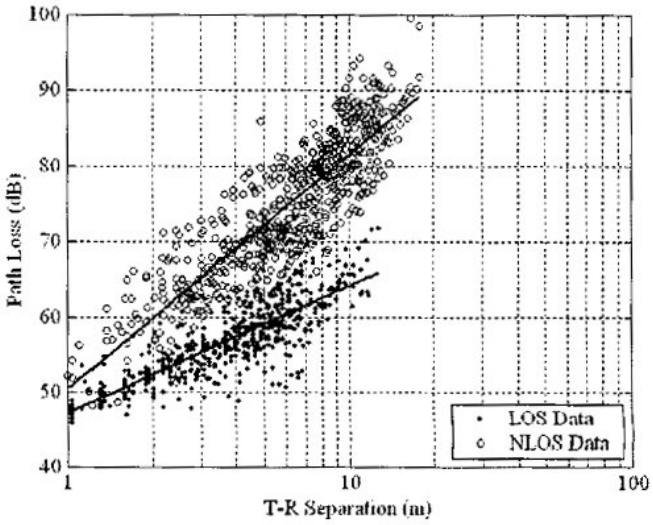

Figure 5-3: Scatter plot of UWB path loss versus TX/RX separation distance [47].

The main purpose in discussing large scale path loss is to show that simple models can be used to easily estimate UWB link attenuation for both LOS and NLOS situations. In the indoor UWB environment, the path loss is often less than it is in free space, thanks to multipath, and an omni-directional antenna is desirable to help capture multipath energy. A broad gain pattern is also important for a handheld UWB device, because the device could be held in potentially any orientation by the user.

5.3 Small-Scale Fading

While large scale fading describes the average link attenuation at a given distance, the local variations are called small-scale fading. In the model given in equation (5-3), the variable X_σ represents the fading. The value of X_σ is essentially the net interaction of all the local multipath components arriving at the receiver. In LOS links, the main LOS component tends to dominate the multipath components. For NLOS links, some degree of fading can be observed if multipath components interfere at the receiver. If they interfere

constructively, then the path loss decreases and the received signal power rises. Conversely, if their interference is destructive, then a deep signal fade can occur at the receiver.

True free space contains no clutter to disperse signals, unlike the indoor environment. Intuitively, no multipath exists in free space. As the amount of clutter increases, multipath and fading also increase. The indoor environment is highly cluttered at UWB frequencies, and it typically causes severe fading for narrowband systems. Fortunately, fading is frequency-selective, and this fact gives UWB a distinct advantage over narrowband [33], [35].

At a particular location and frequency, the amount of fading depends upon the amplitude and phase relationships of the received multipath components. If the path lengths of two interfering components differ by exactly a multiple of a wavelength, then the signals arrive at the receiver in-phase (0° difference), and their interference is constructive. If they arrive out-of-phase (180° difference) with the same amplitudes, then they cancel each other. Along the same paths, multipath components at another frequency will likely arrive with a different phase relationship, due to differing wavelengths.

Generally, fading is similar for frequencies in the coherence bandwidth of the channel [52], but it varies across a large frequency band. A UWB system exploits this principle by spreading signal energy across the band, acknowledging that the band will have strong and weak parts. As long as the strong parts of the band are able to relay enough signal energy, the system can still provide sufficient QoS. A narrowband system does not have this type of diversity, so it must suffer the effects of frequency-selective fading.

The Rayleigh fading model is used extensively to describe the fading that is experienced in narrowband systems, but it is actually not a good fit for UWB [30], [36], [51]. This is due to the UWB's short path length resolution distance, which happens to be on the order of several centimeters. When considering the few multipath components that arrive in each small resolvable delay "bin," it can be seen that the Central Limit Theorem no longer applies. Therefore, the distribution cannot be Rayleigh [57]. Several other probability distributions have been proposed, including the Weibull, Nakagami, and Log-Normal [23]. While we can quickly see that Rayleigh does not fit the UWB fading variable X_σ, actually deriving an analytical distribution is not easy. Multipath components can arrive at the receiver randomly from any angle, and their frequency, magnitude and phase can vary drastically. As a result, many UWB experts rely upon empirical results instead.

Quite a few measurement campaigns have shown that a log-normal distribution (normal in dB) fits X_σ fairly well [30], [47], [54]. Some have shown that a Nakagami distribution with the appropriate parameters has a good fit [30], [57]. An advantage of working with log-normal distributions is that their addition produces subsequent log-normal distributions. Figure 5-4 shows an example of log-normal fading observed in a typical home. Table 5-1 contains fading standard deviation values from a number of published studies which assume a log-normal distribution. The standard deviation for UWB fading is significantly smaller than that for narrowband fading, meaning that UWB is more robust against deep fades.

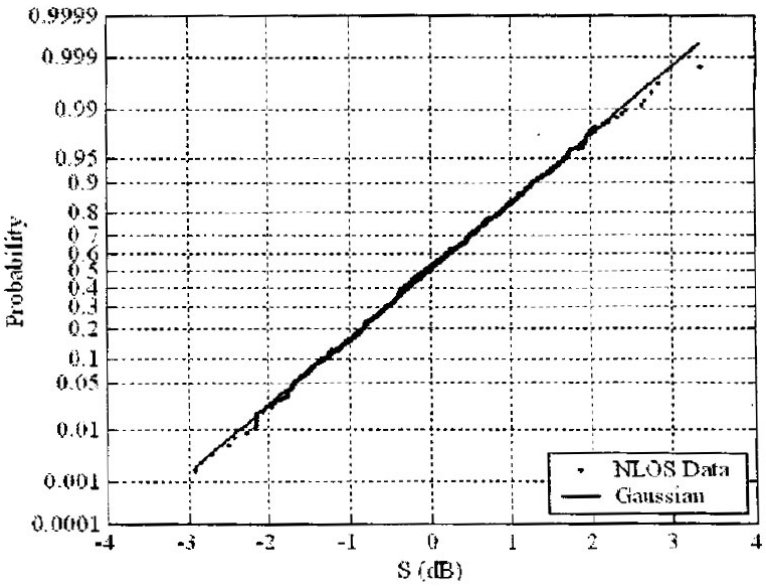

Figure 5-4: CDF of UWB fading in a typical home [47].

Win and Scholtz [35] verified that UWB resists fading by sounding an office environment using sub-nanosecond pulses. A pulse transmitter was set up in a laboratory that was surrounded by offices and hallways, and the received signal was measured at locations in the same lab and nearby offices. In each room, signal measurements were made at 49 locations within a grid area of three feet by three feet. The data showed that the strength of the received signal varied less than 5 dB within each grid area. This result is consistent with other studies [40], [49].

Two other factors affecting small-scale fading are the speed at which the receiver moves and the speed at which objects move around it. The relative motion of the radios and/or surrounding clutter can create Doppler frequency shifts in the signal which cause fading. Doppler shift is directly related to the coherence time of the channel and should be considered when designing mobile receivers such as cell phones or aircraft radios which can move at high speed. For indoor UWB, velocities are low enough that Doppler

shift is essentially zero. Therefore, the channel can be considered slow-fading or quasi-static. This was the conclusion of Saleh and Valenzuela in their indoor 1.5 GHz sounding study, in addition to others specifically studying the UWB channel [40], [55].

In summary, UWB offers superior resistance to fading thanks to frequency diversity. Indoor measurements have shown that UWB fading is normally distributed (in dB) and that most fading values lie within 3 dB of the mean. This allows the fading margin of a UWB system to be much lower than that of a narrowband system.

5.4 Time Dispersion

The amount of clutter and the distances between objects in a channel affect the magnitude and delay of received multipath components. As channel clutter increases, the time period grows over which delayed copies of the original signal are received. The channel's power decay (or delay) profile (PDP), which is related to the impulse response, must be considered when designing any wireless system. Two averaged PDPs for LOS and NLOS links in an office environment are shown in Figure 5-5.

The PDP can be obtained experimentally by sounding the channel with short pulses in time. It can also be estimated using frequency domain measurements, but the time domain approach is more popular. Multiple PDPs are often averaged to describe a particular channel. From the averaged PDP, three parameters are commonly derived that characterize the channel's time dispersion. They are defined with respect to the first detectable signal arriving at the receiver and are called mean excess delay, RMS delay spread, and maximum excess delay with respect to a threshold value.

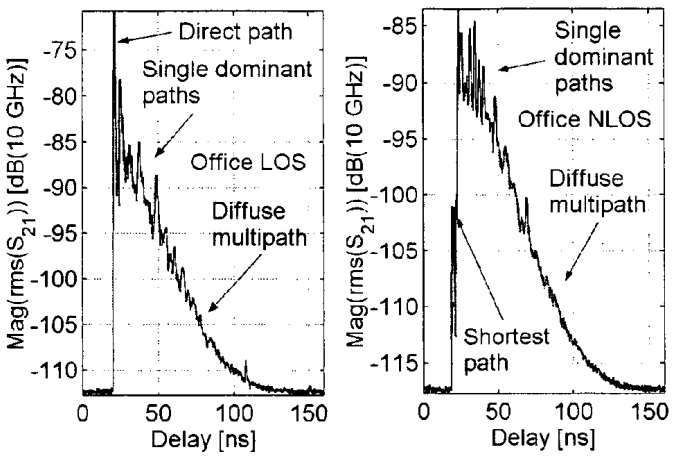

Figure 5-5: Averaged PDPs for LOS and NLOS links in an office environment [56].

The mean excess delay, commonly noted as τ_m, is calculated as the first central moment, or mean, of the PDP. Mean excess delay can then be used to calculate the RMS delay spread, τ_{RMS}, which is the square root of the second central moment of the PDP—simply the standard deviation of the multipath delays with weighting given to their energies. RMS delay spread is commonly mentioned among the temporal characteristics of a channel. Maximum excess delay with respect to a threshold value is the amount of time over which the magnitude of received delayed components is greater than the given value with respect to the dominant LOS or NLOS path [52].

It should be noted here that the IEEE 802.15.3a task group made great efforts to develop a multipath channel model that would be useful to evaluate the many UWB PHY proposals it received. After comparing various channel models to the results of several UWB sounding campaigns, the task group selected a modified version of the Saleh-Valenzuela model [55]. The model was originally developed from sounding measurements taken in an office building using 1.5 GHz pulses, and it is typically applied to systems which would be considered narrowband with respect to UWB. TG3a found

that by adjusting some of the model's distributions and parameters, it could be made to fit UWB experimental results nicely [57].

A key observation from UWB channel soundings is that multipath components tend to arrive in clusters [57]. This is due to the fine temporal resolution that is provided by the high frequency signals of UWB. A flat surface in the channel that is significantly larger than a UWB wavelength can splay many resolvable multipath rays which later arrive at the antenna as a cluster in time [30]. Multiple surfaces can create multiple clusters. Within each cluster, the individual rays typically decay at a certain exponential rate while the maximum amplitudes of the clusters tend to decay at a different exponential rate. This phenomenon is shown in Figure 5-6 as it was presented in Saleh and Valenzuela's landmark paper [55].

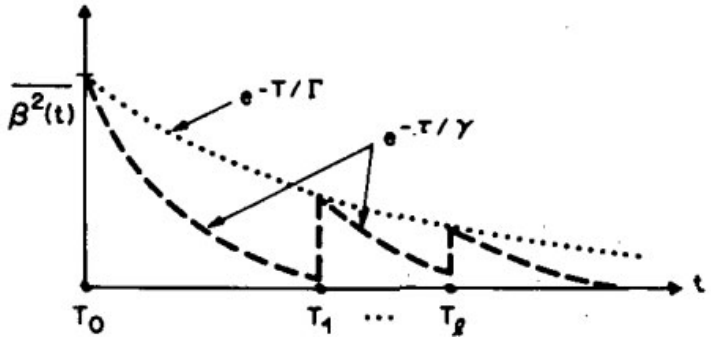

Figure 5-6: Exponentially-decaying ray and cluster average powers [55].

In addition to adjusting the decay and arrival rate parameters to fit the Saleh-Valenzuela model to the observed UWB channel data, TG3a modified the amplitude statistics to follow a log-normal distribution rather than a Rayleigh distribution. Rayleigh works well for narrowband systems but not UWB [30], [36]. TG3a created four channel models (CMs), three of which were modeled to fit actual data, the fourth representing a

theoretical scenario of extreme multipath. Some temporal characteristics of the CMs are given in Table 5-3 for the scenarios as follows [57]:

- CM1: based on LOS, 0-4 meter measurements.
- CM2: based on NLOS, 0-4 meter measurements.
- CM3: based on NLOS, 4-10 meter measurements.
- CM4: synthesized as an extreme multipath channel.

Table 5-3: Temporal characteristics of IEEE 802.15.3a channel model [57].

Channel Model	Model τ_m (ns)	Model τ_{RMS} (ns)
CM1	5.0	5
CM2	9.9	8
CM3	15.9	15
CM4	30.1	25

Many researchers have verified that the RMS delay spread of the indoor UWB channel is on the order of that which is assumed by the 802.15.3a model [25], [30], [47], [51], [54]. The RMS delay spread is an important figure, because it can be used to estimate the coherence bandwidth B_c of the channel—the bandwidth over which two sinusoids of differing frequencies can be expected to have similar amplitude and phase. We previously mentioned that the wireless channel is considered flat for the context of each 4.125 MHz WiMedia tone. We can confirm this assumption using τ_{RMS}. With an approximation in [52], we estimate the maximum allowable RMS delay spread $\tau_{RMS(MAX)}$ as

$$\tau_{RMS(MAX)} \approx \frac{1}{5B_c}. \tag{5-3}$$

Let us assume that the coherence bandwidth of the channel is 4.125 MHz, the minimum bandwidth over which no complex equalization is required. This yields a maximum RMS delay spread of 48 ns. Virtually all of the soundings have shown τ_{RMS} to be less than this value, reinforcing the notion that the channel really is flat for the context of each OFDM tone. In the time domain, a WiMedia data frame includes 70.28 ns as a ZPS [4]. It has been shown that a ZPS can provide as much multipath robustness as a cyclic prefix [30]. During the waiting period, multipath components diminish to low levels before the next symbol is transmitted; ISI is minimized.

As clutter and/or the separation distance increase, so does the RMS delay spread. Yano [33] and McKinstry [50] demonstrated this relationship (see Figure 5-7). As long as τ_{RMS} provides the necessary coherence bandwidth, the UWB system remains virtually immune to the negative effects of multipath propagation.

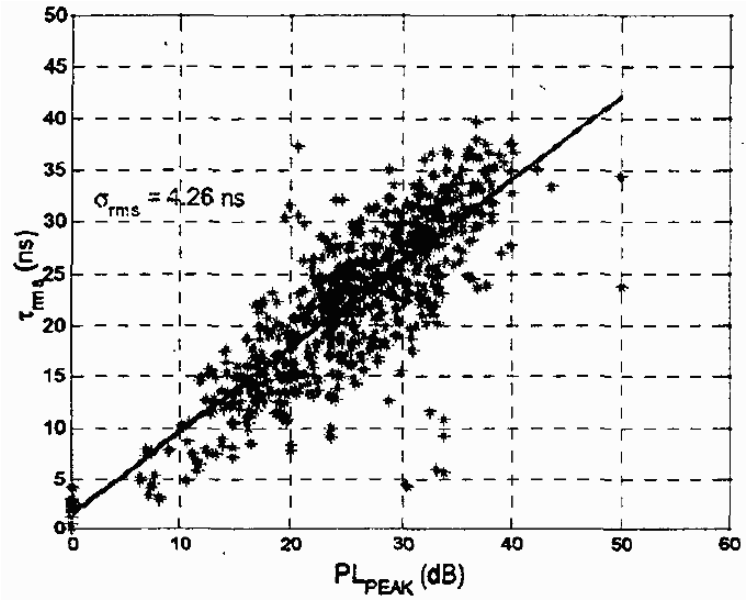

Figure 5-7: RMS delay spread and peak path loss are highly correlated [33].

5.5 MB-OFDM Link Budget

In Table 2-5, we listed the minimum receiver sensitivity levels for the various WiMedia data rate profiles in an AWGN channel. These levels are given for a PER of less than 8%, a 6.6 dB noise figure, 2.5 dB implementation losses, and 3 dB margin [4]. Several other key parameters are needed to complete a link budget, specifically the path loss, minimum SNR, and transmit power level. A good example of an MB-OFDM link budget can be found in [30]. We need to adjust some of the values in the example, because the paper was written before the WiMedia standard was published.

5.5.1 Path Loss

As discussed previously, equation (5-1) can be used to estimate the path loss. For simplicity, we will assume an AWGN channel where no multipath exists. Therefore, n = 2.0 [30], [57]. This is a conservative estimate for indoor LOS links, where path loss exponents below 1.5 have been reported (Table 5-1). An NLOS link would have a higher path loss exponent—likely in the 3.x range. The geometric center frequency f_C is calculated as

$$f_C = \sqrt{f_L f_H} \tag{5-4}$$

where f_L is the lowest frequency of the lowest band of the group and f_H is the highest frequency of the highest band of the group. For Band Group 1 operation, f_L is 3,168 MHz, f_H is 4,752 MHz, and the resulting f_C is 3,880 MHz. The only other quantity needed to estimate the path loss is the distance d between the transmitting and receiving antennas.

5.5.2 Signal to Noise Ratio

The minimum SNR to achieve a given error rate depends on the type of noise and interference in the channel, along with the data rate and symbol mapping used. For an AWGN channel, the minimum SNR to achieve a PER of less than 8% can be calculated from the minimum receiver sensitivity values given in ECMA-368. *SNR* in dB can be calculated for each data rate profile using the following relationship:

$$SNR = SL + I - N_0 . \tag{5-5}$$

SL is the sensitivity level in dBm, *I* is the implementation loss in dB, and N_0 is the overall average noise power per bit in dBm. *I* is assumed to be 2.5 dB in ECMA-368, and N_0 can be calculated as

$$N_0 = N + NF , \tag{5-6}$$

where *N* is the average noise power per bit in dBm and *NF* is the receiver noise figure, in dB, referred to the antenna. ECMA-368 assumes *NF* = 6.6 dB. *N* can be found using

$$N = -174 + 10\log(R_B), \tag{5-7}$$

where -174 (dBm) is the noise power per 1 Hz bandwidth and R_B is the payload data rate of the selected profile (53.3 Mbps, 80 Mbps, 106.7 Mbps, etc.). Solving equations (5-5), (5-6), and (5-7) yields the minimum SNR values of Table 5-4.

Table 5-4: Minimum SNR values to achive PER < 8%.

Mbps	**53.3**	**80**	**106.7**	**160**	**200**	**320**	**400**	**480**
SNR	6.8	7.0	6.8	7.0	7.4	7.0	7.4	7.7

5.5.3 Transmit Power Level

In the UWB operating band, the FCC limit for EIRP is -41.3 dBm per 1 MHz [20]. Due to the hopping pattern of the WiMedia TFCs, only one band can be active at any time. No signal is transmitted during the ZPS between OFDM output symbols. The FCC rules specify the average power per MHz, so a pulsed transmission can have a higher instantaneous power level.

The duty cycle of the transmission changes, depending which TFC is selected. In Band Group 1, TFCs 1-4 utilize all three bands of the group, TFCs 5-7 use only one band (FFI), and TFCs 8-10 use two bands. If N_B is the number of bands used per TFC, t_{OFDM} is the duration of the OFDM symbol (242.42 ns), and t_{ZPS} is the duration of the ZPS (70.08 ns), then D can be calculated as

$$D = \frac{1}{N_B\left(1 + \frac{t_{ZPS}}{t_{OFDM}}\right)}. \tag{5-9}$$

This equation holds for closely-packed data frames. As the space between frames increases, the duty cycle decreases along with the average transmit power. The maximum transmitted power P_T satisfying the FCC limit can be calculated over one band as

$$P_T = -41.3 + 10\log\left(\frac{N_T BW_T}{D}\right). \tag{5-10}$$

Here, N_T is the number of active tones (or carriers) per band, which is 122. Recall that the remaining six tones are null carriers which have no energy. BW_T is the bandwidth of each tone in MHz (4.125). D is the duty cycle of the transmitted OFDM symbol in each band as found in (5-9).

Table 5-5: Peak transmit power per band for Band Group 1 TFCs.

TFCs	Peak TX Power per Band (dBm)
1-4	-8.4
5-7	-10.2
8-10	-13.2

Taking into account the width of each band and the duty cycle, the maximum, permissible, instantaneous power levels for the TFCs in Band Group 1 are given in Table 5-5. It is readily apparent that multi-band TFCs yield higher performance than single-band TFCs, since more bandwidth is utilized. Interestingly, the implementation of MB-OFDM outlined in [30] proposed similar durations for the OFDM symbol and the entire data frame, but it used a 60.61 ns cyclic prefix (CP) and 9.47 ns guard interval instead of the ZPS. A negative effect of using the CP is an increased duty cycle, which lowers the permissible transmit power by about 1 dB. Perhaps this fact, along with the fact that a ZPS can perform as well as a CP, was the impetus for WiMedia choosing to use the ZPS over the CP.

5.5.4 Complete Link Budget

Only a few additional parameters are needed to create a complete link budget. Let us assume that the transmitting and receiving antennas are omni-directional. Also, we will assume that the minimum link margin is 3 dB to combat fading, per the WiMedia specification [4]. Using the path loss, SNR, and transmit power values calculated in the three previous sections, the complete theoretical link budget for an AWGN channel is

shown in Table 5-6. The separation distance values have been adjusted to provide a margin of at least 3 dB at the receiver.

One can see that the highest data rates should be achievable only for distances less than three to four meters. Using the lowest data rate profile, the maximum LOS distance is about ten meters. We have chosen the maximum transmit power of -13.2 dBm (for single-band TFCs 8-10) conservatively, assuming that the WiMedia chip does not scale the output power according to which TFC is selected. If this type of power scaling is implemented, then the theoretical range increases to 18 m for the 53.3 Mbps profile and 5.5 m for the 480 Mbps profile when TFCs 1-4 are used.

Table 5-6: Theoretical LOS link budget for an AWGN channel.

Data rate profile	R_B	**Mbps**	**53.3**	**80.0**	**106.7**	**160.0**	**200.0**	**320.0**	**400.0**	**480.0**
TX power (duty-cycle adjusted)	P_T	**dBm**	-13.2	-13.2	-13.2	-13.2	-13.2	-13.2	-13.2	-13.2
TX antenna gain	G_T	**dBi**	0.0	0.0	0.0	0.0	0.0	0.0	0.0	0.0
Geometric center freq. of band	f_C	**MHz**	3880	3880	3880	3880	3880	3880	3880	3880
TX/RX separation distance	d	**m**	**10.0**	**8.0**	**7.0**	**5.5**	**5.0**	**4.0**	**3.5**	**3.0**
Path loss exponent	n	-	2.0	2.0	2.0	2.0	2.0	2.0	2.0	2.0
Path loss at d meters	PL	**dB**	64.2	62.3	61.1	59.0	58.2	56.3	55.1	53.8
RX antenna gain	G_R	**dBi**	0.0	0.0	0.0	0.0	0.0	0.0	0.0	0.0
RX power	$P_R=P_T+G_T+G_R-PL$	**dB**	-77.4	-75.5	-74.3	-72.2	-71.4	-69.5	-68.3	-67.0
Avg. noise power per bit	$N=-174+10*\log(R_B)$	**dBm**	-96.7	-95.0	-93.7	-92.0	-91.0	-88.9	-88.0	-87.2
RX noise figure referred to ant.	NF	**dB**	6.6	6.6	6.6	6.6	6.6	6.6	6.6	6.6
Overall avg. noise power per bit	$N_0=N+NF$	**dBm**	-90.1	-88.4	-87.1	-85.4	-84.4	-82.3	-81.4	-80.6
E_b/N_0 for PER < 8%	SNR	**dB**	6.8	7.0	6.8	7.0	7.4	7.0	7.4	7.7
Implementation loss	I	**dB**	2.5	2.5	2.5	2.5	2.5	2.5	2.5	2.5
Link Margin (want > 3 dB)	$M=PR-N_0-SNR-I$	**dB**	**3.4**	**3.4**	**3.5**	**3.6**	**3.1**	**3.4**	**3.2**	**3.4**
Minimum RX sensitivity	$SL=N_0+SNR+I$	**dBm**	-80.8	-78.9	-77.8	-75.9	-74.5	-72.8	-71.5	-70.4

Operating in a real channel with dense multipath allows shorter maximum distances than the AWGN case, because multipath interference adds to the noise to degrade the SNR and overall margin [29]. However, the path loss exponent in such an environment is likely less than 2.0, which could result in less path loss. Assuming the

RMS delay spread is not too large, MB-OFDM can actually exploit multipath to provide slightly increased range [30].

5.6 Conclusions

The deliberate design of the WiMedia PHY and the inherent characteristics of wideband transmission allow UWB to thrive at low power levels indoors where many other wireless systems can only boost the transmit power to overcome fading. While UWB systems differ substantially in concept and architecture from traditional narrowband systems, relatively easy ways exist to estimate the path loss and fading. For UWB, the log-distance path loss model can be used for both LOS and NLOS links. A log-normal distribution has been shown to represent the small-scale fading very well.

In Table 5-7, we suggest some basic parameters for estimating the effect of the UWB channel. These parameters are recommended mostly from surveying the UWB literature and partially from our own measurements. While they are not exact averages of what has been reported, they are rounded to be good "working numbers" that provide ballpark estimates. Alternatively, the path loss estimate of equation (5-1) can be used if frequency dependency is required.

Table 5-7: Recommended UWB channel parameters.

Link Type	Path Loss at 1 m (dB)	Path Loss Exponent	Fading Std. Dev (dB)	RMS Delay Spread (ns)
LOS	40	1.8	3	5
NLOS	60	3.2	3	10

When undertaking a GPS and UWB radio integration project, estimating the UWB path loss is likely to be relevant, since chipsets are specified with varying

sensitivities. With the example link budget of Table 5-6, the path loss and receiver sensitivity can be used to predict the maximum separation distance over which a UWB link could be supported for each of the WiMedia data rate profiles. We have presented the temporal characteristics of the UWB channel in this chapter, although we do not expect that they would need to be given heavy consideration when designing a product using a WiMedia-certified UWB chipset; most of these aspects have already been addressed in the design of the WiMedia PHY.

Chapter 6

Performance of the Evaluated UWB Device

In the previous chapter, we covered the basics of modeling the indoor UWB channel and we provided an example link budget. In this chapter, we present measured throughput and distance performance figures from the Belkin UWB system, operated in a laboratory environment using the three UWB antennas from Chapter 4. We showed previously that the UWB antennas have roughly omni-directional patterns and some degree of polarization sensitivity. We concluded that the laboratory environment is dispersive enough to relax the need for maintaining antenna polarity alignment without actually testing this assumption with the UWB system. For the remainder of this chapter, we focus on the performance of the Belkin UWB system using the antennas in various orientations.

6.1 Reported Signal Strength

The only measure of UWB signal strength available to us was a signal strength indicator in the Belkin configuration software. The indicator was a percentage that ranged from 0% to 100% in 10% increments—not useful for making any real link calculations. Since we were unsure how this signal strength number was calculated, we used a variable attenuator to map the relationship between the reported signal strength and the amount of link attenuation. The Belkin system was configured to automatically adjust the data rate based on the channel conditions.

To perform the measurement, the UWB dongle and one of the antennas from the hub were set up facing each other at a fixed distance of 10 cm. The antennas faced each other in a co-polarized fashion in the direction of their strongest (estimated 2 dBi) gains. The other hub antenna was removed to prevent multiplexing gain. The separation distance was roughly equal to one wavelength at the lowest UWB frequency of 3.1 GHz. Such a close distance was chosen in an effort to minimize the effects of multipath. (We observed earlier that the signal strength indicator typically varies ±10% at distances of several meters, but it was very stable at close distances.)

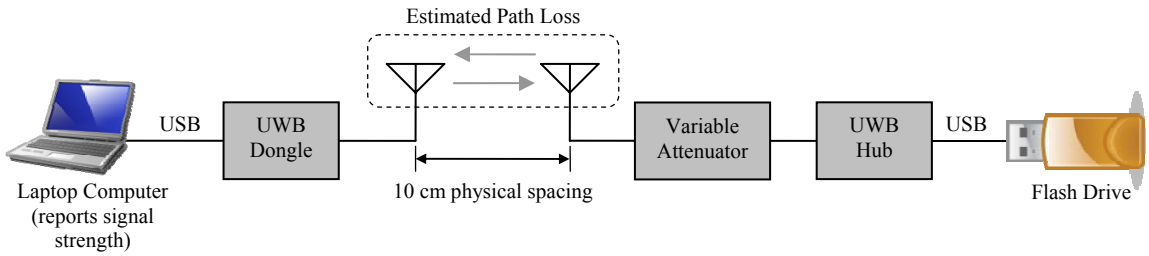

Figure 6-1: Setup used to measure signal strength, relative link attenuation, and payload data rate.

A variable attenuator was inserted between the hub antenna and the hub itself to create additional "path loss". Initially, the attenuator was set to 0 dB. The reported signal strength was 100% at this point. As the attenuation was increased, the signal began to occasionally dip down to 90%. Once the signal strength was judged to spend equal time at 100% and 90%, the amount of additional attenuation was noted and assigned to the "95%" signal strength point. We continued to increase the amount of attenuation until we had noted each of the "x5" (85%, 75%, etc.) percentage signal strength points. Table 6-1 lists the attenuation values and the signal strength numbers that were observed.

Table 6-1: Relationship between reported signal strength and additional path loss.

Signal Strength (%)	Variable Attenuator (dB)
95	27
85	29
75	32
65	34
55	37
45	39
35	41
25	46
15	48
5	62

Figure 6-2 shows that a strong linear relationship exists among the values between 15% and 95% signal strength. In this middle range, the amount of attenuation per 10% signal strength point is roughly 2.6 dB. Measurement studies of the indoor UWB channel (Chapter 5) reveal that the standard deviation of fading is typically about 3 dB. This explains why we noticed that the signal strength indicator typically varies ±10% for separation distances greater than a few meters.

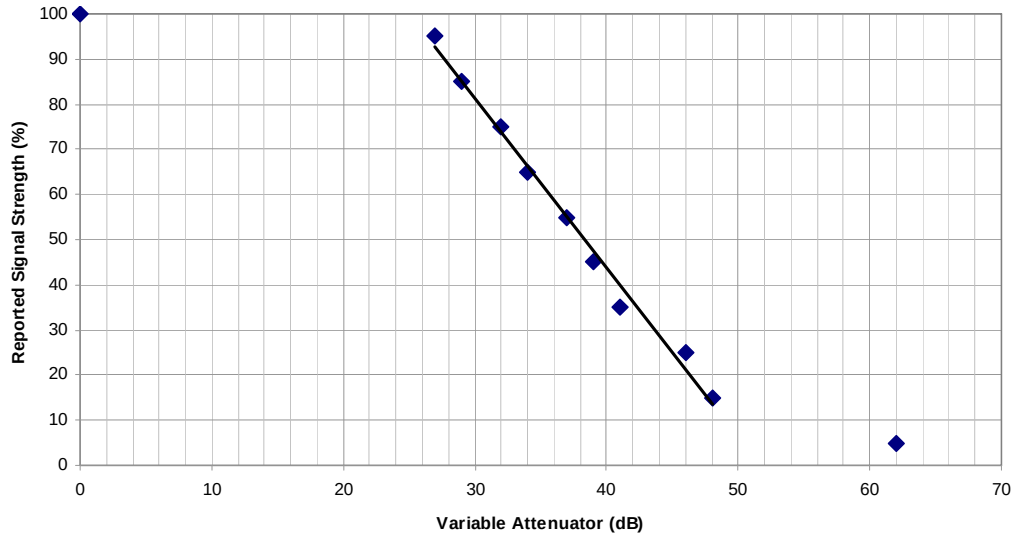

Figure 6-2: The reported signal strength decreases roughly 10% per 2.6 dB of added path loss.

6.2 Reference Path Loss

To estimate the reference path loss across the antenna separation distance of 10 cm, we must make some assumptions about the path loss exponent and the gain of the antennas. Since the antennas were much closer to each other than they were to other objects, we will assume n = 2.0. We estimated the dongle's antenna and the hub's antennas to have gains of 2 dBi each. The path loss PL_d was estimated to be 20 dB by subtracting the antenna gains from the result of equation (5-1):

$$PL_d = 10n\log\left(\frac{4\pi d f_C}{c}\right) - G_R - G_T, \qquad (6\text{-}1)$$

where d is the separation distance (0.1 m), f_C is the geometric center frequency of Band Group 1 (3,880 MHz), c is the speed of light (3.0E8 m/s), G_R is the gain of the receiving antenna (2.0 dB), and G_T is the gain of the transmitting antenna (2.0 dB).

6.3 Estimated Maximum Distance

During the first measurement, the UWB system was configured to automatically adjust the data rate. The next step was to determine the greatest amount of path attenuation that could allow the system to function at each data rate. The system was forced to remain at one data rate at a time, and the attenuation was increased until the system could no longer maintain the connection. Since the effects of multipath were minimal, we assume that the link margin was essentially zero. This is less margin than could be utilized over separation distances of several meters, given the amount of fading that is typically experienced [26], [47], [49].

Table 6-2: Maximum path loss per data rate profile.

Data Rate Profile (Mbps)	Path Loss (dB)
480	54
400	55
320	57
200	58
160	60
106.7	62
80	63
53.3	65

We added the reference path loss estimate of 20 dB to the maximum amount of additional attenuation for each data rate profile to estimate the total path loss. Then we used the link budget in Table 5-6 to compute the link margins. They were about 1 dB or lower, as we predicted. Acknowledging that the margins would need to be at least 3 dB to operate at typical antenna separation distances, we decreased the path loss values to obtain 3 dB margins, and then we decreased the path loss by another 4 dB to account for the gain of the Belkin antennas. This was done to remove directionality from the

calculations. The estimated greatest amounts of path loss are given in Table 6-2. Then, we calculated the maximum link distances over which the various data rate profiles could be supported in an AWGN channel (shown in Table 6-3). Interestingly, these results compare very closely to those of the theoretical link budget given in Table 5-6.

Table 6-3: Estimated maximum LOS distance for the Belkin device in an AWGN channel.

Data Rate Profile (Mbps)	Estimated Maximum Distance (m)
480	3
400	4
320	4
200	5
160	6
106.7	7
80	8
53.3	10

6.4 Measured Maximum Distance

We actually measured the maximum distance for each data rate profile by setting the hub on the edge of a lab bench and the laptop and dongle on a mobile cart. The antennas of the hub and dongle were pointed at each other and were located roughly at the same height. For each data rate profile, the dongle was moved away from the hub until the link could no longer be maintained. The values in Table 6-4 reveal that the actual distance performance of the Belkin system is not as good as the estimates in Table 6-3 would suggest. Figure 6-3 compares the estimated and measured maximum link distances in a graphical format.

Table 6-4: Measured maximum link distance for the Belkin device.

Data Rate Profile (Mbps)	Measured Maximum Distance (m)
480	1.4
400	1.8
320	2.6
200	3.2
160	3.6
106.7	4.0
80	4.2
53.3	5.0

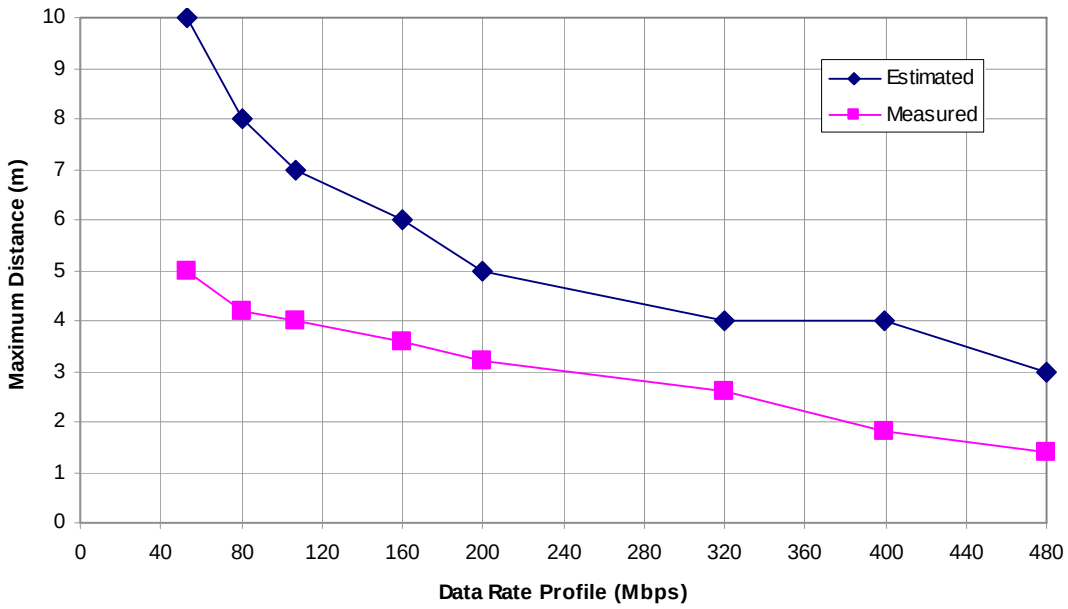

Figure 6-3: Comparison of estimated and measured maximum UWB link distances.

If the maximum path loss values of Table 6-2 are plugged into the link budget along with the measured distances, then the path loss exponent can be estimated to be about 2.2 with each profile. This could suggest that the link is not truly LOS at large distances and the path loss exponent is much greater than 1.2 or 1.3, as reported by some of the studies in Table 5-1, even when nothing obstructs the path between the transmitter

and receiver. However, it has been confirmed that the link can be considered LOS with a path loss exponent well below 2.0 even at ten meters [47].

Alternatively, the deviation of the fading indoors could be greater than 3 dB, which would necessitate a larger link margin to maintain the minimum SNR at the receiver. This, in turn, translates to less allowable path loss and distance. If brief signal dropouts were occurring, they were not visible to us in the reported signal strength of the system. Without direct access to the received signal power values in the UWB device, this theory is difficult to prove.

Another possible explanation is that the implementation loss of the UWB product is greater than the assumed value of 2.5 dB [4]. Again, without access to the actual link parameters measured by the Belkin device, it is tough for us to speculate. It would be interesting to repeat this experiment in a hallway—an environment typically assumed to have a lower path loss exponent—to see if the maximum measured distances increase.

6.5 Measured Payload Data Rates

Having found the distance performance of the Belkin system to be lower than expected, we turned our attention to one of WiMedia UWB's strongest claims: the high data rates. We measured the system's highest transfer rate with a small distance separating the hub and dongle. To do this, we copied our large test file (109E6 bytes) from the flash drive to the computer several times, and then we averaged the transfer times to compute the actual throughput data rate. Table 6-5 shows that the link efficiency of this particular UWB device is quite low, especially at high data rate settings (480, 400, and 320 Mbps) where the measured payload rate is only about 20 Mbps.

Table 6-5: Measured throughput of each data rate profile.

Data Rate Profile (Mbps)	Avg. Time to Transfer 109 MB File (s)	Payload Data Rate (Mbps)	Link Utilization (%)
480	43	20	4
400	44	20	5
320	44	20	6
200	47	19	9
160	49	18	11
106.7	57	15	14
80	72	12	15
53.3	72	12	23

We are unsure why the measured payload rate is so low compared to our expectations. For a system implementing legacy USB over UWB, the theoretical limit is about 80 Mbps [2]. The Belkin system was the first commercial UWB product available in the US; perhaps the Wisair 502/531 chipset was not optimized at the time this product was released. Although a payload rate of 20 Mbps is a significant improvement compared to that which is offered by current WPANs, even larger bandwidth utilization is necessary to deliver streaming high-definition video content.

We learned from a recent report [38] that at least one newer WiMedia chipset is capable of delivering high-definition video. In the report, the authors measured data rates exceeding 100 Mbps for distances of ten meters and beyond, depending on channel conditions, using a Tzero ZeroWire system. It should be noted that the Tzero system was specifically designed to deliver streaming media content, while the Belkin system was not.

6.6 Effect of UWB Antennas

In Chapter 4, we provided results from evaluating three commercially-available UWB antennas. We found that the antennas had differing gain patterns and return loss

values. In an effort to determine how these factors affect UWB performance, we used each antenna in the Belkin UWB system. We removed the In4Tel antennas in the UWB hub and replaced them with one of the antennas under test. The test was conducted using two lab benches in an open laboratory with little attempt to prevent signal reflections. The computer and UWB dongle were placed on one bench, and the UWB hub and antenna under test were placed 1.5 meters away, LOS, on the other bench. Figure 6-4 illustrates the configuration.

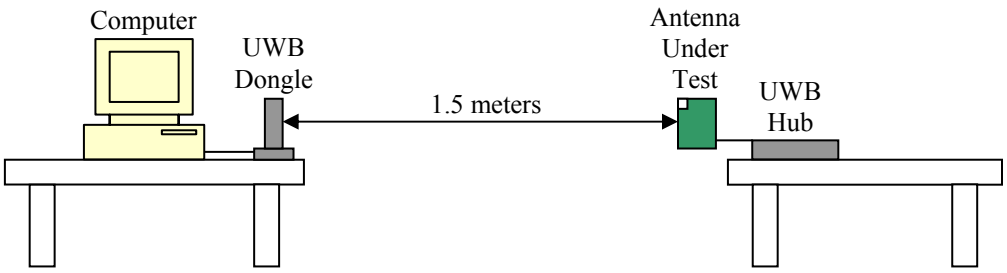

Figure 6-4: Lab setup used to compare performance of UWB antennas.

To perform the measurements, the 109 MB test file was transferred from the flash drive to the computer in the ±***x***, ±***y***, and ±***z*** directions and both polarizations with respect to antenna under test. (Details about the directional definitions are provided in section 4.4.1.) The In4Tel antenna was measured as a reference. For the duration of the tests, the dongle remained stationary, facing the hub antenna.

Once the transfer times had been recorded for each antenna, direction, and polarization, the throughput data rates were computed. Table 6-6 shows that the highest average data rate was achieved using the In4Tel antenna, followed by Pulse and Johanson, then Antenna #3. The In4Tel antenna clearly outperforms the other three antennas. It is difficult to rank the remaining antennas, though, because the data rate performance is very similar. Some degree of polarization sensitivity is observed. More

testing is needed in this area to conclusively determine the best antenna of the sample group.

Table 6-6: Measured throughput rates using each UWB antenna.

	Johanson		Pulse		Antenna #3		In4Tel	
Direction	**Time (s)**	**Mbps**	**Time (s)**	**Mbps**	**Time (s)**	**Mbps**	**Time (s)**	**Mbps**
+***z***//***xz***	42	20.7	60	14.5	71	12.3	60	14.5
+***z***//***zy***	61	14.3	56	15.6	75	11.6	51	17.1
-***z***//***xz***	63	13.8	69	12.6	51	17.1	66	13.2
-***z***//***zy***	59	14.8	78	11.2	85	10.2	69	12.6
+***y***//***zy***	61	14.3	69	12.6	56	15.6	63	13.8
+***y***//***yx***	73	11.9	54	16.1	69	12.6	43	20.3
-***y***//***zy***	56	15.6	55	15.9	70	12.4	48	18.1
-***y***//***yx***	58	15.0	56	15.6	60	14.5	48	18.1
+***x***//***yx***	66	13.2	57	15.3	58	15.0	51	17.1
+***x***//***xz***	56	15.6	79	11.0	58	15.0	72	12.1
-***x***//***yx***	61	14.3	50	17.4	50	17.4	48	18.1
-***x***//***xz***	72	12.1	50	17.4	68	12.8	52	16.8
Average	61	**14.6**	61	**14.6**	64	**13.9**	56	**16.0**
Std. Dev.	8	**2.3**	10	**2.2**	10	**2.2**	10	**2.6**

We are unable to conclude why the In4Tel worked so much better than the other antennas despite its relatively weak return loss. Our best guess is that the radiation efficiency of the In4Tel antenna is actually higher than the others; therefore it performs better. The evaluation boards of the other antennas are made of FR-4 material which is not well-suited for microstrip lines at UWB frequencies. The In4Tel antenna is also made from FR-4, but it does not have a long microstrip feedline. A measurement of antenna radiation efficiency would be needed to verify this theory.

Knowing how dispersive the channel is, we would expect the omni-directional antennas to perform better than the In4Tel antenna, which is slightly directional. Perhaps the directionality of the In4Tel antenna is revealed in the standard deviation of the throughput rates. The three chip antennas have similar standard deviations of about 2.2-

2.3 Mbps, but the In4Tel antenna has a standard deviation of 2.6 Mbps. More testing is needed to confirm whether a true relationship exists.

6.7 Conclusions

Measurements of the Belkin Cable-Free USB system show that the throughput data rates—and distances over which they can be achieved—are lower than expected. We measured a maximum range of five meters and a maximum throughput of 20 Mbps. One partial reason for the low data rates is the limit of implementing the wired USB protocol over UWB. We recommend that newer UWB products be examined, such as the system described in [38] that delivers high-definition video well in excess of 100 Mbps.

We are unable to confidently determine from our limited data which of the three sample antennas offers the best UWB performance. They each had similar average data rates in lab testing. It was clear that just one of the antennas supplied with Belkin product outperforms the sampled antennas. We recommend measuring the payload throughput in a variety of environments and at various distances to determine "real world" performance. To provide more conclusive results about the antennas by themselves, we recommend measuring their radiation efficiency.

Chapter 7

Co-Location Strategies for UWB and GPS Radios

From testing in the anechoic chamber, we learned that the radiated interference from the UWB antenna of a particular device to a GPS receiver is much less than the worst-case theory suggests. The test was conducted with only one particular UWB product and one particular GPS unit, so it does not necessarily represent either technology as a whole. If tests with other products yield similar results and radiated jamming is not considered a significant issue, then the real challenge to integrating UWB and GPS radios is avoiding conducted jamming. In this chapter, we highlight several key areas that should be considered in order to successfully co-locate UWB and GPS radios in a handheld device.

7.1 Minimizing GPS Jammers

The switching rates of the digital ICs in a GPS device can degrade GPS performance if they have harmonics that fall spectrally close to the GPS L1 band (1,575 MHz). If coupled into the GPS signal path through the power supply or ground, harmonic content from clocks or other switching sources can overload the GPS front end, thereby masking the GPS signals and making a position fix impossible. Alternatively, it can degrade the accuracy of the GPS tracker by appearing as a legitimate, but misleading, GPS signal.

Two of the WiMedia switching rates could potentially cause problems to GPS based on the spectral location of their harmonics. The first is the OFDM symbol rate of 3.2 MHz. Its 492nd harmonic lands at 1,574.4 MHz, which is definitely contained in the GPS L1 band. As the RF output stage switches according to the OFDM symbol rate, harmonic content could be conducted in the ground plane and/or power supply rails. Another possible jammer is the 528 MHz sampling clock used in the IFFT device. Its third harmonic at 1,584 MHz is roughly 9 MHz away from the center of GPS L1, but it is still contained in the 20.46 MHz-wide SPS signal bandwidth

To combat the possible conducted jamming caused by these harmonics, isolating the ground and power planes of the GPS and UWB radios could be effective [58]. The ground planes should be stitched by many vias at close intervals to provide as little inductance as possible between stacked PCB ground layers. Furthermore, the GPS and UWB chipsets should have unique power supply rails with plenty of decoupling capacitors placed close to the ICs [58]. To prevent electric fields from radiating from the

PCB traces, and to improve resilience against interference, shielding cans should be placed over the UWB and GPS chipsets.

7.2 Selecting a UWB Antenna

Printing a UWB antenna on the circuit board would incur the least material cost of all the antennas that could be used with a UWB system, and it could likely provide adequate performance [23]. However, selecting a viable design for commercial production could be difficult due to the wide-band requirements of UWB and the extensive amount of intellectual property claimed in this field. If a PCB antenna is ruled out, then a chip-type antenna is the next best option. The chip antenna has a small size, an omni-like gain pattern [23], and is easily mounted on a PCB.

Of the three chip antennas evaluated in this thesis, it is difficult to select the best antenna with the limited data we have collected. The sampled antennas offered similar throughput performance when used with the Belkin UWB system, but they performed worse than the PCB antenna that came with the UWB system. More real-world testing is needed in a variety of environments in order to choose an antenna. If the appropriate facilities exist, an antenna efficiency measurement would also be valuable.

7.3 Placing the UWB Antenna

A PCB antenna or a chip-type antenna typically requires a cutout area in the ground plane for proper tuning. The datasheet for the Johanson antenna recommends a cutout of 14.5 mm by 20.7 mm, and the datasheet for the Pulse antenna recommends a cutout of 13.4 mm by 20.0 mm. The antenna and cutout should be located at a corner of the PCB as far away from metallic structures as possible for best performance.

Additionally, the UWB antenna should be placed as far away from the GPS antenna as possible to minimize coupling. An example of a PCB layout is given in Figure 7-1. Components needed for impedance matching such as capacitors, inductors, and baluns have been omitted for simplicity.

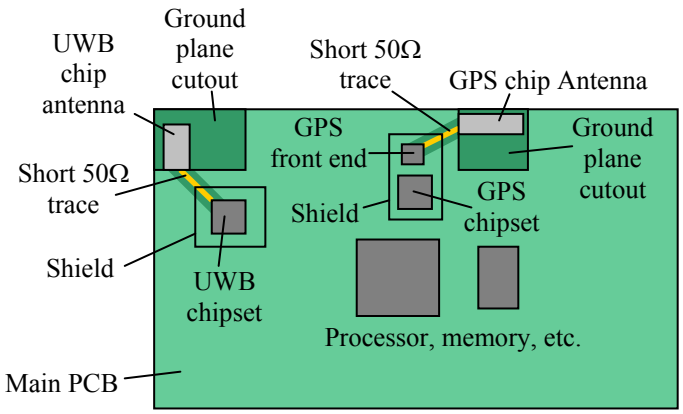

Figure 7-1: Example PCB layout for a PND with UWB and GPS radios.

7.4 High-Frequency Routing Considerations

Due to the reasonable cost and good mechanical properties of FR-4 material, many automotive and high-end consumer electronic products utilize this material as a PCB substrate. FR-4 has decent electrical properties for frequencies below about 2 GHz, however it becomes quite lossy at UWB frequencies. Microstrip traces carrying UWB RF signals should be tuned to the appropriate impedances on the line, and they should be as short in length as possible to minimize loss. Additionally, abrupt routing angles should be avoided to minimize reflections.

Chapter 8

Conclusions and Future Work

We have presented evidence suggesting that UWB and GPS radios could be integrated into a commercial product. UWB and GPS coexistence is not guaranteed, but following careful design considerations can increase the likelihood of success. Also, we have evaluated the data throughput of a commercial UWB device and the distances over which it can be operated.

8.1 Conclusions

In Chapter 2, we presented the basics of GPS and UWB. GPS is a mature positioning and timing technology that is relied upon worldwide for safety-critical applications. Due to the broadcast power limitations of the satellites, terrestrial receivers must be able to sufficiently reject interference in order to utilize weak GPS signals. UWB, as a radio technology, is old in concept but young in terms of being standardized. It promises high data rates, low power, and coexistence with incumbent wireless services.

The sensitivity of GPS combined with the unknown effect of UWB emitters raises concerns about the ability of GPS and UWB radios to coexist in a mobile product.

In Chapter 3, we measured the radiated emissions of an MB-UWB device in the GPS L1 band, both from its antenna and its circuitry. We found that the former contributes little interference while the latter contributes appreciable interference at a close distance of 1 cm. In an anechoic chamber, the GPS CNR is degraded only about 1 dB when the UWB system is powered and located 10 cm from the GPS receiver. Most of the interference originates from the circuitry.

In Chapter 4, we evaluated three chip-type UWB antennas using return loss and gain pattern measurements. Based on return loss, it is easy to determine the WiMedia band groups for which each antenna is designed to operate. Due to the small size of the antennas, the gain patterns are roughly omni-directional. This is good, since a handheld UWB product could be held in virtually any orientation. We were observed that each antenna exhibits some degree of polarization sensitivity.

In Chapter 5, we covered the basics of UWB channel modeling. Large scale path loss can be estimated using the common log-distance model. Depending on the multipath characteristics of the physical environment, the path loss exponent of a channel can be lower than that of free space. MB-UWB effectively collects multipath energy, so using antennas with broad patterns can improve system performance over that which can be obtained using directional antennas—especially in NLOS links. Additionally, we found that the dispersive nature of the indoor channel relaxes the requirement of co-polarized antenna orientations. UWB inherently resists fading, unlike narrowband systems, so less transmit power overhead is needed to maintain an adequate link margin. We created a

theoretical link budget indicating that a WiMedia UWB system should be capable of operating at distances up to ten meters.

In Chapter 6, we operated the UWB system with the three sample antennas in a laboratory environment to determine maximum data throughput and distance over which the system can be operated. The maximum data rate that we observed was about 20 Mbps, which is a substantial improvement over the rates offered by existing WPANs. However, it is disappointingly lower than the maximum estimated throughput of 420 Mbps for WiMedia systems or even the theoretical maximum rate of 80 Mbps for systems implementing the legacy wired USB protocol. With a throughput link efficiency of only 4% at the highest data rate profile, we expect that there is plenty of room for improvement in future UWB products.

A theoretical UWB link budget suggests that a TX/RX separation distance of ten meters is possible, but our testing showed a maximum of only five meters. Without access to the internal signal strength measurements of the UWB system, we are unable to determine the cause of the reduction in range. The reduction could be due to the path loss exponent or the variance of the fading being greater than expected. Alternatively, it could be due to large implementation loss in the UWB chipset.

Operating the system with the sampled UWB antennas showed similar throughput for each antenna. We are unable determine which antenna performed the best. However, it was clear that the antenna supplied with the UWB system outperformed the three sample antennas. We believe that measuring the efficiency of the antennas could possibly reveal an association with the system's data throughput.

In Chapter 7, we suggested ways to help integrate UWB and GPS radios into a single handheld product. GPS is definitely the more sensitive receiver of the two, so minimizing interference from the UWB chipset is the primary goal. Two switching frequencies used in WiMedia UWB were identified that could cause conducted GPS jamming. Careful PCB routing techniques and the liberal use of bypass capacitors on the power supply rails are essential to maintain good GPS performance. We recommend using an antenna printed on the PCB or a chip-type UWB antenna due to their small sizes and broad gain patterns. The antenna should be located at a corner of the PCB with a ground plane cutout area as recommended by the manufacturer in such a fashion that it is placed away from the GPS antenna to minimize coupling.

8.2 Future Work

We attempted to cover a broad range of aspects related to UWB and GPS performance in this research. Due to time and equipment restrictions, some areas could not be investigated as thoroughly as we wished. The following sections are opportunities for future work.

8.2.1 GPS Performance with UWB

We measured the degradation of GPS CNR caused by the UWB device in an anechoic chamber with a synthesized GPS signal. While this experiment provides some understanding of how GPS sensitivity is affected, a more realistic test is necessary. Real GPS performance is not characterized by CNR but by the accuracy of the position solution to an end user. Operating the GPS and UWB devices outside with actual GPS signals could provide more useful results. A more challenging test for GPS could be to

operate it during the signal coarse/acquisition phase, when higher a CNR is required than is under normal tracking [12]. Multiple UWB sources could be used to determine how the interference compounds. Additionally, GPS devices utilizing different tracker chips could be tested to determine their sensitivity to UWB interference.

8.2.2 UWB Antenna Evaluation

In our evaluation of the three UWB antennas, we were unable to determine decisively which antenna performed best. Measuring the radiation efficiency of the antennas would likely be useful. When the antennas were tested with the UWB system, each antenna yielded similar data throughput rates. We recommend that more data throughput testing be conducted with these antennas in various environments such as indoors, outdoors, and in an anechoic chamber. Our polarization sensitivity results with the UWB antennas were counter-intuitive, because they were greater in the laboratory than they were in the anechoic chamber. We expected less polarization sensitivity in the lab due to rich multipath content. Therefore, we recommend more extensive testing with careful attention being paid to minimize the effect of radiation from the measurement cables. Perhaps further testing with antenna polarization sensitivity or radiation efficiency could reveal a correlation with data throughput performance in a UWB system.

8.2.3 Evaluation of Other UWB Devices

The UWB device that we evaluated was the first UWB device to be sold in the United States. Since March 2007, other products have been released. It would be useful to evaluate the radiated emissions of these newer devices to gain a more comprehensive understanding of how UWB affects GPS. Additionally, the data throughput and range of

these devices could be assessed to better determine the real-world performance of MB-UWB.

In addition to measuring the radiated emissions, it would be useful to quantify the spectral content at GPS L1 that exists at the UWB RF output port in a conducted fashion. To accomplish this, a high-gain LNA with a low noise figure would be needed to overcome the noise figure of the following spectrum analyzer. To protect the LNA from being forced into compression by signals outside the GPS band (such as the transmissions in the UWB band), a low-loss GPS L1 pre-select filter should be inserted between the UWB output port and the LNA.

8.2.4 Antenna Sharing for UWB and 2.4 GHz Applications

As consumer electronic devices are designed to be smaller and smaller, antenna sharing is becoming more common as a way to save PCB space and component cost. Sharing an antenna between UWB and 2.4 GHz radios such as WiFi is a possibility that merits further investigation. If Bluetooth includes UWB in a future implementation, then compliant chipsets will likely not require any external multiplexing circuitry.

8.3 UWB Market Potential

Despite taking a long time to reach widespread adoption, early UWB products have demonstrated that UWB can offer higher wireless connectivity speed to mobile devices than existing WPANs can provide, all while coexisting theoretically across other wireless services. UWB still has potential to become a widespread utility. The USB Implementers' Forum has selected the WiMedia Common Radio Platform as the backbone of its CW-USB standard. In March 2009, WiMedia officially transferred

ownership of its MB-OFDM specification to the USB-IF and the Bluetooth SIG as the next step toward large scale deployment [3]. This was done to allow the two industry groups to refine the technology as needed. Although the Bluetooth 3.0 + HS release in April 2009 did not include UWB as originally anticipated, chances are good that a future version of Bluetooth will include UWB, which could be the key to mass market adoption.

Appendix A – FCC Spectral Masks for UWB

The FCC specifies emission limits for different types of UWB systems. For UWB systems operating principally between 1,990 MHz and 10,600 MHz, the types are:

- Indoor
- Handheld
- Medical Imaging
- Surveillance
- Through-Wall Imaging
- Ground-Penetrating Radar.

The Handheld and Indoor types are the only types that can be used by general civilians without a license; the rest are restricted for use by medical or government-approved entities. A handheld GPS product with UWB would fall into the Handheld classification. An Indoor UWB system must depend upon an AC mains connection to operate. Table A-1 lists the EIRP limits per 1 MHz for UWB operating principally between 1,990 MHz and 10,600 MHz.

Table A-1: FCC EIRP limits per 1 MHz for intentional UWB [20].

Frequency (MHz)	Indoor EIRP (dBm)	Handheld EIRP (dBm)	Medical Imaging EIRP (dBm)	Surveillance EIRP (dBm)	Through-Wall Imaging EIRP (dBm)	Ground Penetrating Radar EIRP (dBm)
960-1,610	-75.3	-75.3	-65.3	-53.3	-46.3	-65.3
1,610-1,990	-53.3	-63.3	-53.3	-51.3	-41.3	-53.3
1,990-3,100	-51.3	-61.3	-51.3	-41.3	-41.3	-51.3
3,100-10,600	-41.3	-41.3	-41.3	-41.3	-41.3	-41.3
Above 10,600	-51.3	-61.3	-51.3	-51.3	-51.3	-51.3

Appendix B – UWB Chipsets

Table B-1 lists the UWB chipsets known to be available at the time of this writing. WiQuest, the former market leader (estimated 85% share), filed for bankruptcy in late 2008, so its products are not included [59]. When known, information such as IC package and interface type is included.

Table B-1: Current UWB chipsets.

Chipset PHY	Chipset MAC	PHY Spec.	MAC Spec.	Band Groups	IC Package(s)	Interface(s)
Alereon (alereon.com)						
AL5100	AL5300	1.2	1.0	1, 3, 4, 6		PCIe 1.1, CF+, SDIO, USB 2.0 host/device
AL5100	AL5350	1.2	1.0	1, 3, 4, 6		PCIe 1.1
Realtek Semiconductor (realtek.com)						
RTU7010	-	1.1	-	1		GPIO
RTU7012	-	1.2	-	1, 3		GPIO
-	RTU7300	-	1.0	-		USB 2.0, SPI, I2C
-	RTU7305	-	1.0	-		PCIe 1.1, SPI
RTU7105		1.1	1.0	1, 3		USB 2.0, SPI, I2C, SDIO 1.2
Samsung (samsung.com / wimedia.org)						
S3CR650X		1.1		1		
Staccato Communications / Artimi (staccatocommuncations.com / artimi.com)						
A-10	A-150	1.1?	1.0	1	7x7mm QFN / 10x10mm LFBGA	
A-200		1.2	1.0	1, 3, 6	10x14mm BGA	
SC3501		1.1	1.0	1	7.5x7.5mm WCSP	USB 2.0
SC3502		1.1	1.0	1	7.5x7.5mm WCSP	USB 2.0 host/device
SC3503		1.1	1.0	1	7.5x7.5mm WCSP	SDIO 1.1
SC4501		1.2	1.0	1, 3, 6	5x5mm WCSP	SDIO 2.0
SC4502		1.2	1.0	1, 3, 6	5x5mm WCSP	USB 2.0
SC4503		1.2	1.0	1, 3, 6	5x5mm WCSP	PCIe 1.1
Tzero Technologies (tzerotech.com)						
TZR7200	TZB7200	1.2	1.0	1	7x7mm QFN / 19x19mm fpBGA	PCI, UART, GPIO, I2C, JTAG
Wisair Ltd. (wisair.com)						
WSR601		1.1	1.0	1	13x13mm TFBGA	USB 2.0, SDIO 2.0

Appendix C – UWB-Enabled Products

Most of the UWB-enabled products to-date have featured WiQuest chipsets. WiQuest filed for bankruptcy in late 2008, and we are unsure which chipsets are being utilized at this time. According to WiMedia's website, the current WiMedia-certified products are:

- Wireless USB Hubs, Adapters, and Docking Stations
    - Belkin – 4-Port Wireless USB Hub (F5U302)
    - D-Link – Wireless USB Adapter (DUB-9240)
    - Cables Unlimited – Wireless USB Kit with TX and RX with base
    - Olidata – Wireless USB Adapter Set
    - Kensington – Wireless USB Docking Station
    - Imation – Apollo Pro WX
- Wireless USB-Enabled Laptops
    - Dell – Inspiron series, models 1520, 1525, and 1720
    - Dell – XPS series, models M1330, M1530, and M1730
    - Lenovo – Thinkpad T61/T61P
    - Toshiba – R400 with Wireless
- Video Streaming
    - Monster Cable – Wireless Digital Express HD
    - Gefen – Wireless HDMI Extender
    - Hitachi – Wooo UT-series HDTVs, models V-32, V-37, and V-42

REFERENCES

[1] U.S. Federal Communications Commission, "FCC Revision of part 15 of the commission's rules regarding ultra-wideband transmission systems: first report and order," technical report, Feb. 2002.

[2] WiMedia Alliance, "UWB – Best Choice to Enable WPANs," white paper, Jan. 2008.

[3] G. Fleishman, "UWB group shutters, sends tech to Bluetooth, USB groups," ARS Technica, 16 Mar. 2009, http://arstechnica.com/hardware/news/2009/03/ultrawideband-groups-disbands-doesnt-despair.ars, last accessed 14 May 2009.

[4] ECMA International, "ECMA-368: high rate ultra-wideband PHY and MAC standard."

[5] P. A. Dafesh, P. Hanson, R. Yowell, T. Stansell, and D. Alcocer, "A portable UWB to GPS emission simulator," in *Position Location and Navigation Symposium 2004*, 26-29 Apr. 2004, pp. 405-413.

[6] M. Luo, D. Akos, S. Pullen, and P. Enge, "Interference to GPS from UWB transmitters," presented at Institute of Navigation's GPS conference, Salt Lake City, UT, USA, Sep. 2000.

[7] D. Månsson, R. Thottappillil, T. Nilsson, O. Lundén, and M. Bäckström, "Susceptibility of civilian GPS receivers to electromagnetic radiation," *IEEE Transactions on Clectromagnetic Compatibility*, vol. 50, no. 2, pp. 434-437, May 2008.

[8] D. A. Cummings, "Aggregate ultra wideband impact on global positioning system receivers," *Radio and Wireless Conference 2001*, Waltham, MA, USA, pp. 101-104, 19-22 Aug. 2001.

[9] R. Giuliano and F. Mazzenga, "On the coexistence of power-controlled ultrawide-band systems with UMTS, GPS, DCS1800, and fixed wireless systems," *IEEE Transactions on Vehicular Technology*, vol. 54, no. 1, Jan. 2005.

[10] R. Aiello and A. Batra, "Ultra wideband systems: technologies and applications," *Newnes Publication*.

[11] WiMedia Alliance homepage, wimedia.org.

[12] D.S. Anderson, E.F. Drocella, S.K. Jones, and M.A. Settle, "Assessment of compatibility between ultrawideband (UWB) systems and global positioning system (GPS) receivers," *NTIA Special Publication 01-45*, Feb. 2001.

[13] A. Swami, B. Sadler, and J. Turner, "On the coexistence of ultra-wideband and narrowband radio systems," *2001 Military Communications Conference*, vol. 1, pp. 16-19, 2001.

[14] M. Hämäläinen, V. Hovinen, R. Tesi, J.H.J. Iinatti, and M. Latva-aho, "On the UWB system coexistence with GSM900, UMTS/WCDMA, and GPS," *IEEE Journal on Selected Areas in Communications*, vol. 20, no. 9, pp. 1712-1721, Dec. 2002.

[15] Y.T. Morton, M.P. French, Q. Zhou, J.B.Y. Tsui, D.M. Lin, M.M. Miller, and D. Janning, "Software approach to access UWB interference on GPS receivers," *IEEE Aerospace and Electronic Systems Magazine*, vol. 20, no. 1, pp. 28-33, Jan. 2005.

[16] R.A. Scholtz, R. Weaver, E. Homier, J. Lee, P. Hilmes, A. Taha, and R. Wilson, "UWB radio deployment challenges," *The 11th IEEE International Symposium on Personal, Indoor, and Mobile Communications, 2000*, vol. 1, pp. 620-625, 18-21 Sep. 2000.

[17] A. Isola, M. Hämäläinen, J. Iinatti, and E. Airos, "UWB coexistence with GPS and aggregate UWB noise rise in the selected radio bands," *IEEE Military Communications Conference 2007*, Orlando, FL, USA, pp. 1-7, 29-31 Oct. 2007.

[18] T. Van Slyke, W.B. Kuhn, and B. Natarajan, "Measuring interference from a UWB transmitter in the GPS L1 band," *Proc. 2008 IEEE Radio and Wireless Symposium*, Orlando, FL, USA, pp. 887-890, 22-24 Jan. 2008.

[19] U.S. Department of Defense, "Global positioning system standard positioning service performance standard, 4th edition," Sep. 2008.

[20] U. S. Federal Communications Commission, "Code of federal regulations title 47, part 15."

[21] R.J. Fontana, "Recent system applications of short-pulse ultra-wideband (UWB) technology," *IEEE Transactions on Microwave Theory and Techniques*, vol. 52, no. 9, pp. 2087-2104, Sep. 2004.

[22] J.T. Conroy, J.L. LoCicero, and D.R. Ucci, "Communication techniques using monopulse waveforms," *IEEE Militar Communications Conference Proceedings, 1999*, Atlantic City, NJ, USA, pp. 1181-1185, 10 Oct 2008 – 03 Nov 2008.

[23] I. Oppermann, M. Hämäläinen, and J. Iinatti, "UWB theory and applications," John Wiley & Sons, Ltd, 2004.

[24] G.R. Aiello and G.D. Rogerson, "Ultra-wideband wireless systems," *IEEE Microwave Magazine*, vol. 4, no. 2, pp. 36-47, Jun. 2003.

[25] R.M. Buehrer, W.A. Davis, A. Safaai-Jazi, and D. Sweeney, "Characterization of the ultra-wideband channel," *2003 IEEE Conference on Ultra Wideband Systems and Technologies*, pp. 26-31, 16-19 Nov. 2003.

[26] M.Z. Win and R.A. Scholtz, "On the energy capture of ultrawide bandwidth signals in dense multipath environments," *IEEE Communications Letters*, vol. 2, no. 9, pp. 245-247, Sep. 1998.

[27] Agilent Technologies, "89600 vector signal analysis software option BHB: multiband-OFDM modulation analysis," technical overview and demonstration guide.

[28] WiMedia Alliance, "WiMedia ultra-wideband: efficiency consideratios of the effects of protocol overhead on data throughput," white paper, Jan 2009.

[29] A. Batra and J. Balakrishnan, "Improvements to the multi-band OFDM physical layer," *3rd IEEE Consumer Communications and Networking Conference, 2006*, vol. 2, pp. 701-705, 8-10 Jan. 2006.

[30] A. Batra, J. Balakrishnan, G.R. Aiello, J.R. Foerster, and A. Dabak, "Design of a multiband OFDM system for realistic UWB channel environments," *IEEE Transactions on Microwave Theory and Techniques*, vol. 52, no. 9, Sep. 2004.

[31] D. Leenaerts, R. van de Beek, J. Bergervoet, H. Kundur, and G. van der Weide, "WiMedia UWB technology: 480Mb/s wireless USB," *IEEE International Workshop on Radio-Frequency Integration Technology, 2007*, pp. 8-12, 9-11 Dec. 2007.

[32] M.Z. Win and R.A. Scholtz, "On the robustness of ultra-wide bandwidth signals in dense multipath environments," *IEEE Communications Letters*, vol. 2, no. 2, pp. 51-53, Feb. 1998.

[33] S.M. Yano, "Investigating the ultra-wideband indoor wireless channel," *IEEE 55th Vehicular Technology Conference, 2002*, vol. 3, pp. 1200-1204, Aug. 2002.

[34] Intersil, "Tutorial on basic link budget analysis," Application Note AN9804.1, Jun. 1998.

[35] M.Z. Win and R.A. Scholtz, "Characterization of ultra-wide bandwidth wireless indoor channels: a communication-theoretic view," *IEEE Selected Areas in Communications*, vol. 20, no. 9, Dec. 2002.

[36] D. Cassioli, M.Z. Win, and A.F. Molisch, "The ultra-wide bandwidth indoor channel: from statistical model to simulations," *IEEE Journal on Selected Areas in Communications*, vol. 20, no. 6, pp. 1247-1257, Aug. 2002.

[37] J.R. Foerster, "Interference modeling of pulse-based UWB waveforms on narrowband systems," *IEEE 55th Vehicular Technology Conference, 2002*, vol. 4, pp. 1931-1935, Aug 2002.

[38] L. Liu and X. Dong, "WiMedia UWB Product Testing Report," available online http://www.ece.uvic.ca/~xdong/WiMedia_testing_report.pdf, last accessed 14 May 2009.

[39] Agilent Technologies, "Fundamentals of RF and microwave noise figure measurements," *Application Note 57-1*.

[40] J. Reed, "An introduction to ultra wideband communication systems," Prentice Hall, Englewood Cliffs, NJ, USA, 2005.

[41] X. Luo, L. Yang, and G.B. Giannakis, "Designing optimal pulse-shapers for ultra-wideband radios," in *Proc. 2003 IEEE Conference on Ultra Wideband Systems and Technologies*, Newark, NJ, USA, pp. 349-353, 16-19 Nov. 2003.

[42] M.Z. Win and R.A. Scholtz, "Impulse radio: how it works," *IEEE Communications Letters*, vol. 2, no. 2, pp. 36-38, Feb. 1998.

[43] T.P. Montoya and G.S. Smith, "A study of pulse radiation from several broadband loaded monopoles," *IEEE Transactions on Antennas and Propagation*, vol. 44, no. 8, pp. 1172-1182, Aug. 1996.

[44] J.A. Dabin, N. Ni, A.M. Haimovich, E. Niver, and H. Grebel, "The effects of antenna directivity on path loss and multipath propagation in UWB indoor wireless channels," in *Proc. 2003 IEEE Conference on Ultra Wideband Systems and Technologies*, Newark, NJ, USA, pp. 305-309, 2003.

[45] Y. Dakeya, T. Suesada, K. Asakura, N. Nakajima, and H. Manhdai, "Chip multilayer antenna for 2.45 GHz-band application using LTCC technology," in *Proc. 2000 IEEE MTT-S International Microwave Symposium*, Boston, MA, USA, vol. 3, pp. 1693-1696, 11-16 Jun. 2000.

[46] S. Venkatesh, J. Ibrahim, and R.M. Buehrer, "A new 2-cluster model for indoor UWB channel measurements," in *Proc. 2004 IEEE Antennas and Propagation Society International Symposium*, vol. 1, pp. 946-949, 20-25 Jun. 2004.

[47] S.S. Ghassemzadeh, R. Jana, C.W. Rice, W. Turin, and V. Tarokh, "A statistical path loss model for in-home UWB channels," in *Proc. 2002 IEEE Conference on Ultra Wideband Systems and Technologies*, pp. 59-64, Aug. 2002.

[48] A.F. Molisch, J.R. Foerster, and M. Pendergrass, "Channel models for ultrawideband personal area networks," *IEEE Wireless Communications*, vol. 10, no. 6, pp. 14-21, Dec. 2003.

[49] L.A. Rusch, C. prettie, D. Cheung, Q. Li, and M. Ho, "Characterization of UWB propagation from 2 to 8 GHz in a residential environment," *IEEE J. Select. Areas Commun.*,

[50] D.R. McKinstry, "Ultra-wideband small scale channel modeling and its application to receiver design," Master's Thesis, Dept. of Electrical and Computer Engineering, Virginia Tech, 2003.

[51] B.M. Donlan, S. Venkatesh, V. Bharadwaj, R.M. Buehrer, and J. Tsai, "The ultra-wideband indoor channel," in *Proc. 2004 IEEE 59th Vehicular Technology Conference*, vol. 1, pp. 208-212, 17-19 May 2004.

[52] T.S. Rappaport, "Wireless communications: principles and practice," Prentice Hall, Upper Saddle River, NJ, USA, 2002.

[53] A.F. Molisch *et al.*, "IEEE 802.15.4a channel model – final report," Technical Report Document IEEE 802.15-04-0662-02-004a, 2005.

[54] S. Zhao, H. Liu, and S. Mo, "Performance of a multi-band ultra-wideband system over indoor wireless channels, in *Proc. First IEEE Consumer Communications and Networking Conference 2004*, pp. 700-702, 5-8 Jan. 2004.

[55] A. Saleh and R. Valenzuela, "A statistical model for indoor multipath propagation," *IEEE Journal on Selected Areas in Communications*, vol. 5, no. 2, pp. 128-137, Feb. 1987.

[56] J. Kunisch and J. Pamp, "Measurement results and modeling aspects for the UWB radio channel," in *Proc. 2002 IEEE Conference on Ultra Wideband Systems and Technologies*, pp. 19-23, Aug. 2002.

[57] A.F. Molisch, J.R. Foerster, and M. Pendergrass, "Channel models for ultrawideband personal area networks," in *Wireless Communications*, vol. 10, no. 6, pp. 14-21, Dec. 2003.

[58] S.H. Hall, G.W. Hall, and J.A. McCall, "High-speed digital system design—a handbook of interconnect theory and design practices," John Wiley and Sons, New York, NY, USA, 2000.

[59] R. Merritt, "Wireless USB startup WiQuest folds," *EE Times*, 31 Oct. 2008, available online http://www.eetimes.com/news/latest/showArticle.jhtml?articleID=211800631, last accessed 14 May 2009.